Synthesis and Characterization of Bioactive Hydrogels as a Matrix for Tissue Repair

A Thesis Submitted in Partial Fulfillment

of the Requirements for the Degree of Master of Science (M.Sc.)

in Biomedical Chemistry

Presented to FB 09 - Faculty of Chemistry, Pharmaceutical Sciences, Geography and Geosciences

Johannes Gutenberg University Mainz

by

Yanira Zeyn

Mainz, April 2020

Period of work: 01.10.2019 to 16.04.2020

Prepared at: Max Planck Institute for Polymer Research

Department Synthesis of Macromolecules

Primary Reviewer: **Prof. Dr. Tanja Weil**, MPI-P Mainz

Secondary Reviewer: **Prof. Dr. Pol Besenius**, JGU Mainz

Submitted on April 16, 2020

Eigenständigkeitserklärung

Ich, Yanira Zeyn, Matrikelnummer 2710264, versichere, dass ich meine Masterarbeit selbstständig verfasst und keine anderen als die angegebenen schriftlichen und elektronischen Quellen sowie andere Hilfsmittel benutzt habe. Alle Ausführungen, die anderen Schriften wörtlich oder sinngemäß entnommen wurden, habe ich kenntlich gemacht.

Mainz, 16.04.2020 Y. Zeyn

_____ _____

(Ort, Datum) (Unterschrift)

Acknowledgement

First of all, I want to thank Prof. Dr. Tanja Weil for giving me the great opportunity to do my master's thesis at the Max Planck Institute for Polymer Research. In addition, I would like to express my sincere thanks to Prof. Dr. Pol Besenius for being the second reviewer of my thesis. Moreover, a special thank-you is addressed to my supervisor Dr. Christopher Synatschke, who always supported me and helped me whenever possible.

I would like to express my special gratitude to my PhD supervisor, Adriana Sobota, who always had a helping hand, taught me a lot and was patient with me anytime. An additional personal thank-you goes to Michael Müller, who always gave me helpful advices and supported me in solving problems. Special thanks also to everybody in my office 0.119 who welcomed me in their office and invited me to stay during my master's thesis. I would like to express additional thanks to Maksymilian Żegota who always helped me in solving HPLC and LC-MS problems. Also, thanks to Jasmina Gacanin, on whose work this project is based, who always gave me competent advices. Next, I want to thank Jana Hedrich for helping me with the cell culture of HUVECs and the bioassays. At last, a thank-you goes to Lucas Gunkel, who helped me with his physical and chemical knowledge.

I want to thank everybody who made my experience at the MPI-P so special and funny and created a pleasant working atmosphere where I always felt comfortable.

Lastly, I want to thank my family and friends with all my heart who I always can rely on and always support me in every possible way.

German Summary

Das Projekt basiert auf einem, vor kurzem veröffentlichten, Hybrid-Hydrogel (*Gacanin, J. et al., 2019*[1]), das aus einem Protein (Humanes Serum Albumin) besteht, welches mit einem selbst-assemblierenden Peptid (Depsi-Maleimid, Maleimid-KIKI(COO-)SQINM) und Polyethylenglykol-Ketten konjugiert ist.

Das Hauptziel des Projekts war es, dem zuvor beschriebenen Peptid-Protein-Hybrid-Hydrogel eine bioaktive Komponente hinzuzufügen, um ein biokompatibles Material für das *Tissue Engineering* zu erzeugen. Dafür wurde zuerst das Depsi-Maleimid synthetisiert und aufgereinigt. Zusätzlich wurden fünf angiogenesefördernde Sequenzen, die durch Literaturrecherche erhalten wurden, synthetisiert und dabei ein Cystein entweder am N- oder C-Terminus zur Kopplung an die Maleimidfunktion des Depsi-Peptids angebracht. Da Nebenreaktionen mit dem Fmoc-Cys(Trt)Wang-Harz bei der Synthese beobachtet wurden, wurden vier der fünf verwendeten Sequenzen gekauft. Des Weiteren waren die anschließend durchgeführten Kopplungen der bioaktiven Peptide (BAP) an das Depsi-Maleimid erfolgreich und es wurden gute Ausbeuten erhalten. TEM-Messungen bestätigten die Fibrillenbildung der gekoppelten Depsi¬Maleimid-BAPs, wobei sich die Dicke und Länge der Fibrillen unterschied. Zusätzlich gab der ThT (Thioflavin T) Test Hinweise darauf, dass die meisten der BAP-Konjugate auch Amyloidstrukturen bilden. Darüber hinaus assemblierten die bioaktiven Peptide IKVAVC und CRKRLQVQLSIRT sogar ohne Konjugation an Depsi-Maleimid zu fibrillartigen Strukturen.

Anschließend wurde der Protein-Peptid-Hybrid (dcHSA-PD) anhand des bereits veröffentlichten Protokolls synthetisiert.[1] Die Synthese ergab zwei dcHSA-PD mit leicht unterschiedlichen PEGylierungsraten und einem niedrigeren Depsi-Maleimid-Kopplungserfolg als im entsprechenden Protokoll.

Darüber hinaus wurden *in vitro* Tests durchgeführt, um das Potenzial der BAPs bzw. Depsi¬Maleimid-BAPs in Bezug auf Angiogeneseförderung und die Zellkulturkompatibilität zu untersuchen. Hier wurde zum ersten Mal beobachtet, dass das Peptid CRKRLQVQLSIRT bei den benötigten Konzentrationen unlöslich war. Der CellTiter Glo-Cell Viability Assay zeigte, dass die BAPs keine toxischen Effekte auf A549-Zellen haben, wenn sie über 24 h dem Peptid ausgesetzt waren. Im Vergleich dazu zeigte sich bei Zugabe einiger gekoppelter Depsi-Maleimid-BAPs eine Abnahme der Zellviabilität, insbesondere bei dem IKVAVC-Depsi-Maleimid. Jedoch war keine Abweichung von der Kontrolle statistisch signifikant.

Des Weiteren wurde ein Protokoll für den *HUVEC Tube Formation Assay* auf Matrigel erarbeitet und dabei auf angiogenesefördernde Effekte von verschiedenen Konzentrationen der BAPs getestet. Es wurde festgestellt, dass IKVAVC die durchschnittliche *Tube Formation* am stärksten erhöhte. Erwähnenswert ist zudem, dass keins der BAPs die *Tube Formation* verringerte, sie aber, abgesehen von hohen Konzentrationen sGliafin, größtenteils verstärkte. Anschließend wurde der Test unter Verwendung von Depsi-Maleimid-BAPs wiederholt. Hier verringerten hohe Konzentrationen des konjugierten IKVAVC die *Tube Formation* drastisch. Insbesondere die konjugierten Peptide IKVAVC und CRKRLQVQLSIRT lagerten sich auf dem Matrigel zu aggregat- bzw. gelartigen Strukturen zusammen, die ein Grund für die geringere Ausdifferenzierung der Zellen sein könnten.

Zuletzt wurde der *HUVEC Tube Formation Assay* unter Verwendung des dcHSA-PD-Hydrogels anstelle von Matrigel durchgeführt, wobei das Hydrogel zusammen mit den Depsi-Meleimid-BAPs co-assembliert wurde. Es stellte sich heraus, dass die HUVECs sich an das Hydrogel anlagerten, sich aber selbst nach 24 h keine Veränderung der Morphologie zeigte, wie dies in den auf Matrigel durchgeführten Tests beobachtet wurde. Daher wurde die Inkubationszeit auf 8 Tage verlängert. Jedoch auch nach der verlängerten Inkubationszeit konnte keine *Tube Formation* der HUVECs beobachtet werden und zudem konnten nur sehr wenige Zellen gefunden werden, die sich an das Gel angeheftet haben.

Zusammenfassend kann festgestellt werden, dass die Synthese des Hydrogels und Depsi-Maleimids anhand des Protokolls von *Jasmina Gacanin* reproduziert werden konnten, wobei die wesentlichen Eigenschaften erhalten blieben. Das System konnte zudem um eine bioaktive Komponente in Form von angiogenesefördernden Peptidsequenzen erweitert werden. In Zukunft sollte die weitere Forschung auf eine Anpassung der optischen Eigenschaften des Hybrid-Hydrogels fokussiert werden, sowie eine Anpassung des *in vitro* Testsystems (von 2D auf 3D).

List of Contents

I. List of Abbreviations

2D	Two dimensional
3D	Three dimensional
4-DMAP	4-Dimethylaminopyridine
ACN	Acetonitrile
Ala	Alanine
Arg	Arginine
Asn	Asparagine
ATP	Adenosine triphosphate
ATPase	Adenosine triphosphatase
BAP	Bioactive peptide
bFGF	Basic fibroblast growth factors
BME	Basement membrane extract
Boc	Tert-butyloxycarbonyl protecting group
CCD	Charge coupled device
CD	Circular dichroism
CHCA	α-Cyano-4-hydroxycinnamic acid
cHSA	Cationized human serum albumin
CILKNLSRSR	Cys-Ile-Leu-Lys-Asn-Leu-Ser-Arg-Ser-Arg peptide
CLSM	Confocal laser scanning microscope
con	Control
CRKRLQVQLSIRT	Cys-Arg-Lys-Arg-Leu-Gln-Val-Gln-Leu-Ser-Ile-Arg-Thr
Cys	Cysteine
DCC	*N,N*'-Dicyclohexylcarbodiimide
dcHSA	Denatured cationized human serum albumin
dcHSA-PD	dcHSA-PEG(2000)$_n$-Depsi-Maleimide$_m$
DCM	Dichloromethane
DIC	*N,N*'-Diisopropylcarbodiimide
DIPEA	*N,N*-Diisopropylethylamine
D_{MAL}	Depsi-Maleimide
D-Mal	Depsi-Maleimide
DMF	Dimethylformamide

DMSO	Dimethyl sulfoxide
DNA	Deoxyribonucleic acid
$E1_{cb}$	Elimination unimolecular conjugate base
ECM	Extracellular matrix
EDA	Ethylenediamine
EDP	Elastin-derived peptide
ESI	Electrospray ionization
Fmoc	9-Fluorenylmethoxycarbonyl protecting group
FRAP	Fluorescence recovery after photobleaching
GDNF	Glial cell line-derived neurotrophic factor
GF	Growth factor
Gln	Glutamine
Gly	Glycine
HET-CAM	Hen's egg test on chorioallantoic membrane
HIF	Hypoxia-inducible factors
HOBt	Hydroxybenzotriazole
HPLC	High-performance liquid chromatography
HSA	Human serum albumin
HUVEC	Human umbilical vein endothelial cell
IKVAVC	Ile-Lys-Val-Ala-Val-Cys peptide
Ile	Isoleucine
IR	Infrared
KIKISQINM	Lys-Ile-Lys-Ile-Ser-Gln-Ile-Asn-Met peptide
LC	Liquid chromatography
LE	Locally excited
LED	Light-emitting diode
Leu	Leucine
Lys	Lysine
m/z	Mass-to-charge ratio
MALDI-TOF	Matrix-assisted laser desorption/ionization
Met	Methionine
MS	Mass spectrometry
NHS ester	*N*-hydroxysuccinimide ester

NP-HPLC	Normal-phase high performance liquid chromatography
PA	Peptide amphiphiles
PB	Phosphate buffer
Pbf	2,2,4,6,7-Pentamethyldihydrobenzofuran-5-sulfonyl PG
PBS	Phosphate-buffered saline
PcP	Polypeptide copolymers
PEG	Polyethylene glycol
PG	Protecting group
PMT	Photomultiplier tubes
Pro	Proline
RP-HPLC	Reversed-phase high performance liquid chromatography
rpm	Revolutions per minute
SAP	Self-assembling peptide
Ser	Serine
sGliafin	CILKNLSRSR peptide
SPPS	Solid phase peptide synthesis
SVEC4-10	SV40 transformed endothelial cells
SVVYGLRC	Ser-Val-Val-Tyr-Gly-Leu-Arg-Cys
tBu	tert-Butyloxycarbonyl protecting group
TCCD	Two color coincidence detection
TCEP	Tris(2-carboxyethyl)phosphine
TEM	Transmission electron microscope
TFA	Trifluoroacetic acid
Thr	Threonine
ThT	Thioflavin T
TICT	Twisted intramolecular charge transfer
TIPS	Triisopropylsilane
TRLEC	Transformed rat lung endothelial cells
Trt	Trityl
Tyr	Tyrosine
Val	Valine
VEGF	Vascular endothelial growth factor
VGVAPGC	Val-Gly-Val-Ala-Pro-Gly-Cys

II. List of Figures

III. List of Schemes

IV. List of Tables

1. Introduction

Amino acids are the fundamental building blocks of proteins as well as peptides and therefore, are essential to any organism in the world and play an important role in nature. Different kinds of interactions between peptide chains allow peptides to self-assemble into higher order structures. The studies of self-assembling peptides are important to understand the biology of proteins and also to generate biocompatible materials controlled by the different properties of the amino acids and peptide modifications.[2] In this work, the aim is to use the recently published peptide-protein hybrid hydrogel (*Gacanin, J. et al., 2019*)[1] and modify it by co-assembly with self-assembling peptides that are coupled to angiogenesis promoting peptide sequences to generate a bioactive hydrogel. This should lead to a mimic of the extracellular matrix (ECM) and address endothelial cells to increase angiogenesis for biomedical application like tissue repair.

This work starts in chapter 2. with the explanation of the theoretical background of self-assembling peptides as well as hydrogels and their advantages by usage in biomimetic materials. In addition, the mechanism of angiogenesis is explained and its importance in tissue engineering. Furthermore, the applied methods are described. Afterwards, in chapter 3., the motivation of this work is illustrated, followed by chapter 4., where the results are presented and discussed. Then, the work is concluded and the outlook illustrated in chapter 5. At last, experimental procedures are described in chapter 6., followed by the list of references (chapter 7.) and the appendix (chapter 8.).

2. Theoretical Foundations

2.1. Theoretical Background

2.1.1. Peptides

In general, peptides consist of amino acids that are made of a carboxylic acid, an amine and a characteristic side chain. There are 20 natural amino acids whereby each amino acid has specific properties. Due to their side chain and its unique structure, the amino acids can be categorized into e.g. hydrophobic/hydrophilic or positively/negatively charged.[2]

The structure of a peptide is composed of amino acids that are linked via amide bonds.

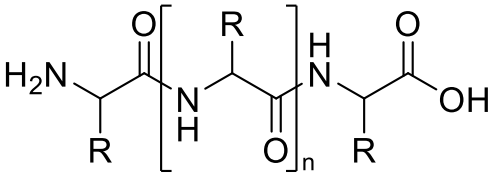

Figure 1: Basic structure of a peptide.

The linear amino acid chain, as can be seen in Figure 1, is called primary structure.

A special characteristic of peptides is that the formation of hydrogen bonds within peptide chains allow them to arrange themselves in three dimensional structures. This formation is called the secondary structure and is defined as the spatial arrangement of the amino acids from linear chains that are close to each other. The type of the secondary structure is determined by the amino acid sequence.[3]

Furthermore, the secondary structure consists preferentially of α-helices and β-sheets, which are defined by a regular pattern of hydrogen bonds between the amide hydrogen and the oxygen of another amino acid that are close in the primary structure. Exemplarily, two types of β-sheets are shown in Figure 2. An antiparallel β-sheet consists of two amino acid chains that arrange themselves parallel to each other, but chain directions differ. Regarding the parallel β-sheet, the directions of the chains are identical.[3]

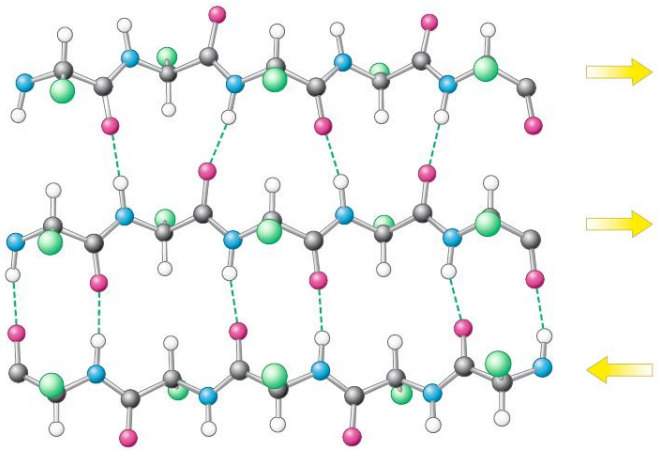

Figure 2: Mixed β-sheet. The lower structure shows an antiparallel β-sheet. The upper peptide chains form a parallel β-sheet. The arrows hereby indicate the direction of the peptide chain from N- to C-terminus. Green: residues, red: oxygen, blue: nitrogen, white: hydrogen (by Stryer et al., 2018).[3]

Secondary structures can arrange themselves in 3D structures. As proteins are naturally in aqueous solution, polypeptide chains fold spontaneously so that their hydrophobic side chains are hidden inside of the protein and the polar, charged residues remain on the surface. The overall arrangement of the polypeptide chain of a protein is called tertiary structure. The tertiary structure is defined as the spatial arrangement of amino acids that are far apart within the linear sequence, as well as the pattern of disulfide bridges. Some proteins contain more than one polypeptide chain. The arrangement of these protein subunits is called quaternary structure.[3]

2.1.2. Self-assembling Peptides

Numerous peptides have been developed to mimic natural self-assembling structures. The formation of 3D structures is decisive if self-assembly is triggered by external stimuli. These stimuli can be e.g. a change in pH, temperature, ionic strength or photoactivation. Self-assembling peptides (SAP) can be designed to form different kinds of secondary structures like α-helices or β-sheets or to mimic a protein structure like collagen. Furthermore, the different characteristics of the peptide side chains and their ability to be chemically modified generates various perspectives for SAP design. For instance, peptides can be designed by using a sequence with alternating hydrophilic and hydrophobic residues to gain a β-sheet structure after self-assembly (Figure 3).[4]

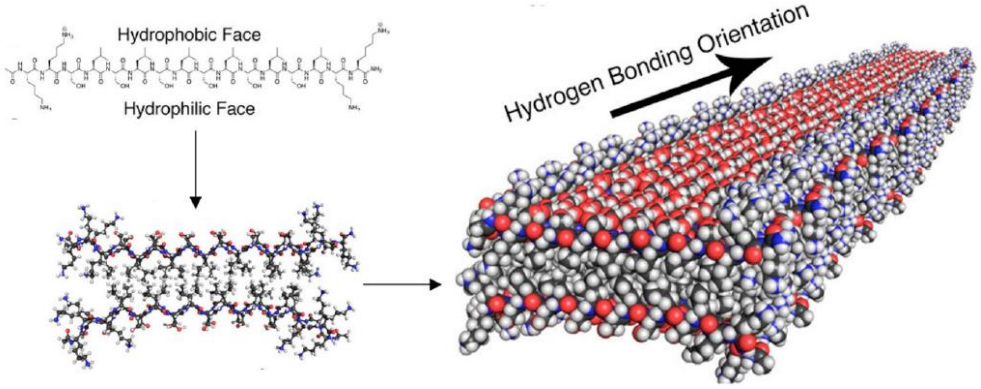

Figure 3: β-sheet formation and self-assembly of a peptide with alternating charges of the side chains (Chen, J. et al. (2019), Copyright © 2017 American Chemical Society).[4]

If the previously mentioned technique is used to design self-assembling peptides, there are four different types of charged amino acid alternation that ensure ionic complementary: 1. "- +", 2. "- - + +", 3. " - - - + + +" and 4. "- - - - + + + +". For example, the well-studied RADA-16 peptide (sequence RADARADARADARADA) is allocated to type 1 and forms highly stable β-sheets that assemble into nanofibrils even under acidic conditions, whereby fibril formation is enhanced by increasing pH or salt concentration.[5]

Not only β-sheet forming peptides are important in the development of biologically active materials, but also α-helix forming peptides that can assemble into superhelical bundles, the so-called coiled coils. The coiled coil motif is a common ubiquitous protein structure motif in nature, e.g. the leucin zipper consists of two α-helices assembling into a coiled-coil[6]. Therefore, the peptide sequence needs to consist of seven amino acids in repetition $(abcdefg)_n$ (Figure 4). Typically, the amino acid residues *a* and *d* are non-polar and therefore build the inner region of the coiled coil where they are stabilized by hydrophobic interactions. Additionally, *e* and *g* are polar or charged and stabilize the structure via interstrand electrostatic interactions. The remaining residues *b*, *c* and *f* are used to enhance the solubility of the peptide as well as controlling oligomer aggregation.[7]

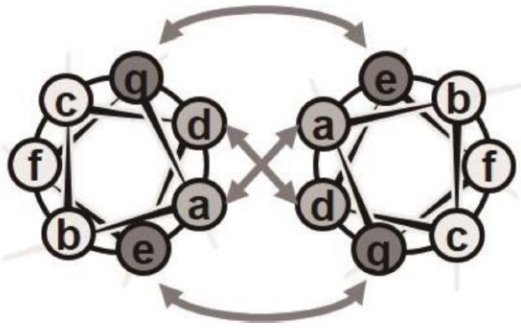

Figure 4: Schematic structure of a coiled coil. The arrows show the interactions between the amino acid residues. (Wu et al., 2017).[7]

Another category of self-assembling peptides are amphiphilic peptides. Peptide amphiphiles (PA) are peptides containing hydrophobic segments, e.g. lipid chains. The *Stupp* laboratory reports PAs that have the ability to assemble into various structures like fibrils that are able to form hydrogels and therefore have the potential to mimic extracellular matrices.[8] Thereby, the peptides consist of an aliphatic residue connected to a β-sheet forming peptide sequence. This sequence is followed by charged residues to enhance the solubility of the peptide. Then, a spacer region can be added to give the PA the ability to be chemically modified. In aqueous solution, the hydrophobic aliphatic tail of the peptide collapses and hydrogen bond formation of the peptides lead to fiber formation. PAs gained a high interest in research due to their biodegradability, biocompatibility and their ability to activate biological pathways when modified with bioactive molecules.[8]

In addition, also short peptides containing aromatic systems are suitable for self-assembling systems. Due to their π-π stacking interactions, Fmoc-modified di- or tripeptides can build up nanometer-sized fibers at physiological pH.[9] Thereby, variations in chirality (L- or D-peptides) can have an impact on hydrogelation and are an additional opportunity for building durable supramolecular architectures. These kinds of short self-assembling peptides are usable for design of biomaterials.[10]

A recently reported β-sheet forming SAP by *Gacanin, J. et al. (2019)*[1] is used in this work. It is a *Depsi* peptide (Maleimide-KIKI(COO-)SQINM, D-Mal, Figure 5: **1**), i.e. a peptide that contains an intrastrand serine ester bond instead of a peptide bond and additionally, is functionalized with a maleimide group at the *N*-terminus. This kinked peptide is soluble in acidic conditions. If the pH is changed to neutral, an *O,N*–acyl migration occurs, and the peptide linearizes (Figure 5: **2**). At neutral pH, the linear peptide forms cross β-sheets that assemble into amyloid structures.[1,11]

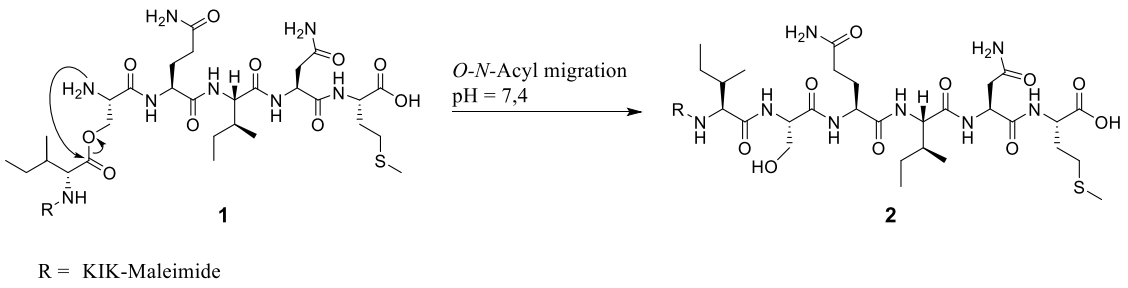

Figure 5: O,N intramolecular acyl migration of the D-Mal.

Furthermore, amyloid structures are often connected with the Alzheimer's disease, whereby wrongly folded peptides aggregate into amyloid fibrils and form *plaques* inside of the brain. Nevertheless, amyloid fibrils are suitable material structures for biomedical applications due to their excellent molecular support in nano- and bulk materials.[11,12]

Moreover, having the self-assembling D-Mal peptide as a scaffold is anticipated to provide biodegradability and biocompatibility, gives the hydrogel self-healing properties as well as the possibility of controlled gelation.[1] In this work, the D-Mal is coupled to a denatured and modified protein backbone to generate stable and self-healing hydrogels in neutral aqueous solution. The self-assembly of the D-Mal thereby is the prerequisite for certain characteristics of the hydrogel, like pH inducible gelation.

2.1.3. Hydrogels

Hydrogels are chemically or physically cross-linked polymers that make up three-dimensional structures. Due to their partly hydrophilic character, they swell in water and retain a high amount of liquid inside of the polymeric structure.[13] The components of hydrogels can consist of different natural or synthetic structures, e.g. polysaccharides[14], peptides[15] or polyacrylic acid and polyvinylalcohol[16].

The classification of hydrogels is conducted considering the cross-link type (physically or chemically, e.g. covalent bonds) or alternatively considering their ability to embed chemicals or cells. Furthermore, the design of hydrogels includes great possibilities for modifications that can have an impact on the physical properties, for instance *in situ* gelling gels or stimuli-responsive materials that can be used for injection.[15]

Since several years, hydrogels and polymers are used in medicine and biology, e.g. for clinical applications in regenerative medicine and tissue engineering. Especially peptides are promising materials as they are able to self-assemble and can therefore act as hydrogelators. Their characteristic to be biocompatible and ability to gel under physical conditions gives them great potential for biomedical applications.[15]

In general, hybrid monomers like peptide-protein hybrids enhance the stability of the gel by adding more covalent bonds. Hybrid hydrogels thereby keep the strain resistance of the polymer hydrogel and gain self-healing properties of self-assembling peptides. In addition, the peptides can modify the mechanical properties of the hydrogel or act as recognition sequences for cells to activate a biological response. Especially β-sheet forming peptides have been used as cross-linker in polymer hydrogels.[17]

The protein backbone used in this work is the HSA (Human Serum Albumin). The preparation of the polypeptide backbone was performed according to a recently published protocol[1]. It is first cationized to increase the amount of primary amines to facilitate cellular membrane interactions.[1] Then, the PEGylation increases the amount of water to be stored in the hydrogel and additionally, non-specific protein absorption and immunogenicity are decreased.[18] The denaturation of the PEGylated cHSA (cationized HSA) is performed by addition of urea buffer and tris(2-carboxyethyl)phosphine (TCEP). Urea establishes hydrogen bonds to polarized areas, such as peptides, as a result destabilizing the globular structure and denature the tertiary and secondary structure.[19] TCEP is used to reduce disulfide bridges of cysteines within the protein irreversibly.[20] The previous described kinked D-Mal peptide (chapter 2.1.2.) is coupled to the hydrogel the to give it pH controllable and recovering properties.[1]

Some works have been published using HSA as a scaffold. For example, single stranded DNA has been coupled to the PEGylated dcHSA (denatured cHSA) resulting in a biocompatible hydrogel. In addition, proteins can be immobilized within the hydrogel and be released by controlled enzymatical degradation of the DNA.[18] In addition, the dHSA can be used for synthesis of PcP (Polypeptide Copolymers). These PcPs can be used for different applications, e.g. as coatings for the stabilization of nanoparticles and therefore for developing biosensors and in vivo pH reporters.[21]

As described in the work of *Gacanin, J. et al. (2019)*[1] , the dcHSA-PEG(2000)$_n$-D-Mal$_m$ (dcHSA-PD) hydrogel is stable in PBS and cell serum over days and enhances migration of HUVECs into the gel, whereby a high viability of the cells was observed even after 7 days. In addition, it has fast

self-healing properties whereby the gel regenerates after exposure to high shear force.[1] According to its properties, the dcHSA-PD hydrogel has the potential to be used as a regenerative scaffold in biomedicine.

The ability of the D-Mal to self-assemble into cross-linked β-sheet amyloid fibrils allows an external addition of free D-Mal peptide to modify the properties of the dcHSA-PD hydrogel, whereby the maleimide modification of the D-Mal is the fundamental prerequisite for modifying the Depsi peptide.

2.1.4. Angiogenesis

2.1.4.1. Angiogenesis in Tissue Engineering

The phenomenon of angiogenesis describes the sprouting of new capillaries from existing blood vessels. In both cases, the cells of the surrounding tissue (mesenchyme) differentiate either into smooth muscle cells (larger vessels) or pericytes (capillaries).[22]

In general, angiogenesis is a very complex step-by-step process and plays an important role in tissue regeneration and would healing. It starts with the expansion of existing vessels and their increase in permeability, whereby surrounding tissues release proteases to digest parts of the basement membrane and the stroma (supportive scaffold of the connective tissue). This leads to enhanced migration of the activated proliferating endothelial cells and therefore to the formation of lumen, whereby cells differentiate under the influence of the local environment.[22]

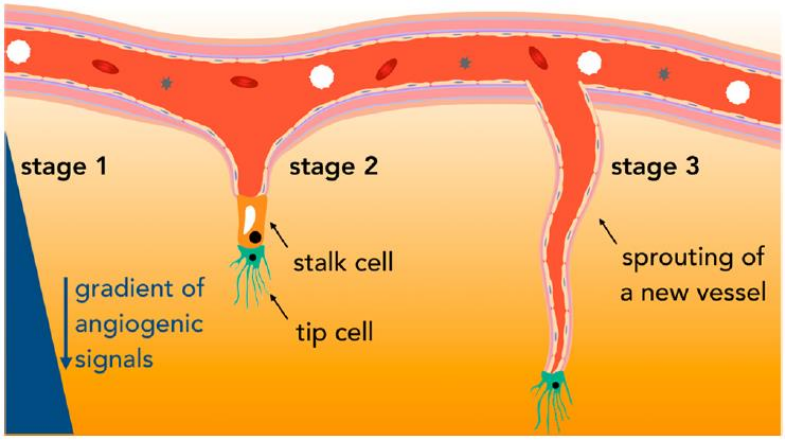

Figure 6: Schematic depiction of the process of angiogenesis (by Sarkar, B. et al., 2018).[23]

The process of angiogenesis is mainly initiated by hypoxia, whereby hypoxia-inducible factors (HIFs) are important for the cellular response. HIFs are activated in hypoxic conditions and upregulate the transcription of VEGF (Vascular endothelial growth factor), which promotes angiogenesis. Specialized endothelial cells, the stalk and tip cells (Figure 6) receive signals from the surrounding cells and lead vessel formation into direction of the angiogenetic gradient. Generally, the process of angiogenesis is important for regeneration of injured tissues or after infarction and therefore plays a crucial role in the treatment of diseases like ischemia or myocardial infarction.[23]

Due to the necessity of angiogenesis in tissue repair, angiogenesis promoting 3D tissue mimics have a great potential for therapeutic applications. Nevertheless, there are high demands that the artificial material has to comply with because it has to retain a similar biological and structural function. In addition, it needs to be easy, reproduceable and low-cost to produce, as well as provide support and regulate of cell functions.[24] Therefore, three-dimensional acellular scaffolds, that provide bioactive components, e.g. signal sequences or growth factors, are promising materials in tissue engineering. Injection or implantation of these materials can induce spatiotemporal tissue regeneration. An example for a useful application is the support of vascularization after implantation of autologous vascular grafts, which often suffer from postsurgical ischemic necrosis. In addition, the treatment of ischemic pathologies is conceivable using proangiogenic materials.[23]

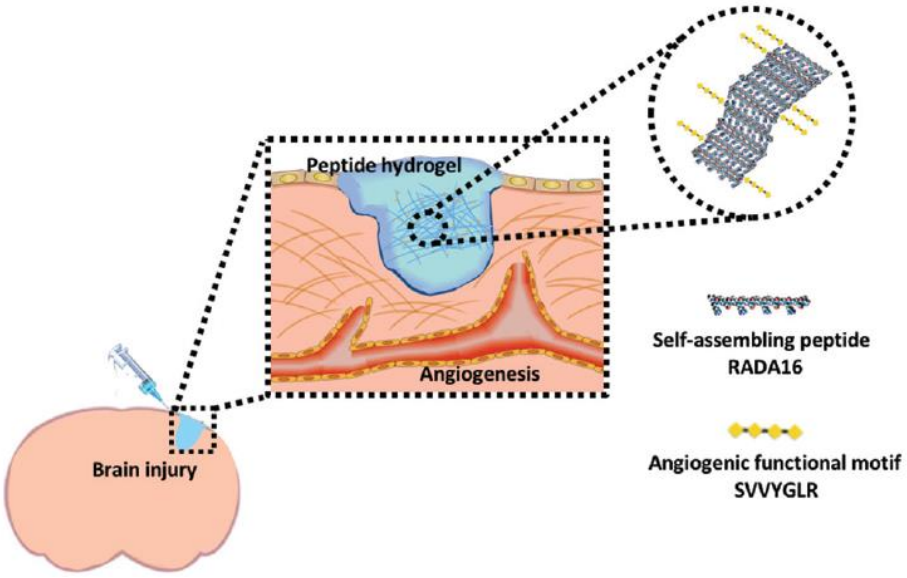

Figure 7: Exemplary application of a hydrogel in tissue engineering (by Wang, T. et al., 2017).[25] Injectable hydrogel consisting of repeated RADA units modified with a BAP (SVVYGLR).

Nowadays, there is a high interest in hydrogels as their mechanical properties are similar to natural tissues. In addition, they can be modified in a broad range with e.g. bioactive components that promote angiogenesis.[24] Exemplarily, a self-assembling peptide hydrogel (RADA16, explained in 2.1.2.) can be injected after brain injury to support the tissue regeneration (Figure 7).[25] An additional example is a hydrogel based on chitosan modified with SIKVAV sequence which is able to enhance re-epithelialization as well as increase of new blood vessel formation *in vivo*.[26]

As the former described dcHSA-PD hydrogel has similar mechanical properties to soft tissues, is injectable, self-healing and provides biocompatibility and biodegradability, it is an auspicious candidate for tissue engineering.[1] In this work, a bioactive component is integrated into the dcHSA-PD hydrogel in the form of angiogenesis promoting sequences that are coupled to the SAP scaffold. The next chapter gives an overview of the chosen bioactive peptide sequences and their source.

2.1.4.2. Angiogenesis Promoting Peptide Sequences

As described in chapter 2.1.4.1., angiogenesis promoting peptide sequences are attached to the free self-assebling peptide scaffold of the dcHSA-PD hydrogel. Only recognition sequences were chosen to be coupled to the SAP due to a possible disturbance in β-sheet formation if large biomolecules like growth factors or ECM proteins would be attached.

Several short peptide sequences have been described in the literature that promote angiogenesis, for example RKRLQVQLSIRT.[27] Figure 8Figure 5 shows exemplarily how vascular formation can be stimulated by bioactive peptides including HUVEC tube formation assay and HET-CAM assay.

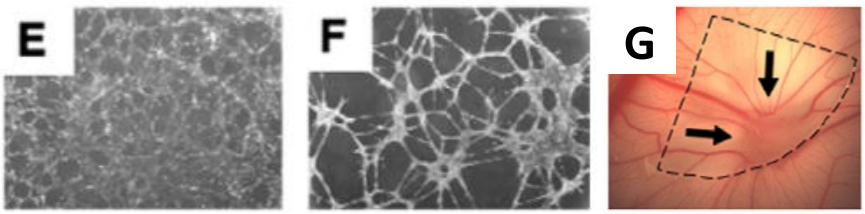

Figure 8: Microphotographs (E, F) and photograph (G) of tube formation after addition of the peptide sequence AG73 (RKRLQVQLSIRT). It induces endothelial tube formation after 6 h (E) and 24 h (F) and shows angiogenetic activities in HET-CAM assay (G) (by Mochizuki, P. et al. ,2007).[27]

In HET-CAM (Hen's egg test on chorioallantoic membrane) assays (Figure 8, **G**) fertilized chicken eggs are used and the CAM is revealed. Thereby, the revealed veins can be used for testing e.g. drugs or antibodies by intravenous injections. Also, cytokine induced angiogenesis can be investigated by application of the substance on the surface and studying if an increase in blood vessel formation can be observed over time.[28]

The process of literature research and the criteria for selection of the BAPs are described in chapter 4.1.3.1. and further information of the tube formation assay is given in chapter 2.2.6.

2.2. Methods

2.2.1. Solid Phase Peptide Synthesis (SPPS)

Solid Phase Peptide Synthesis is a method for the synthesis of peptide chains using protected single amino acids. It was first described by *R. B. Merrifield* in 1963.[29]

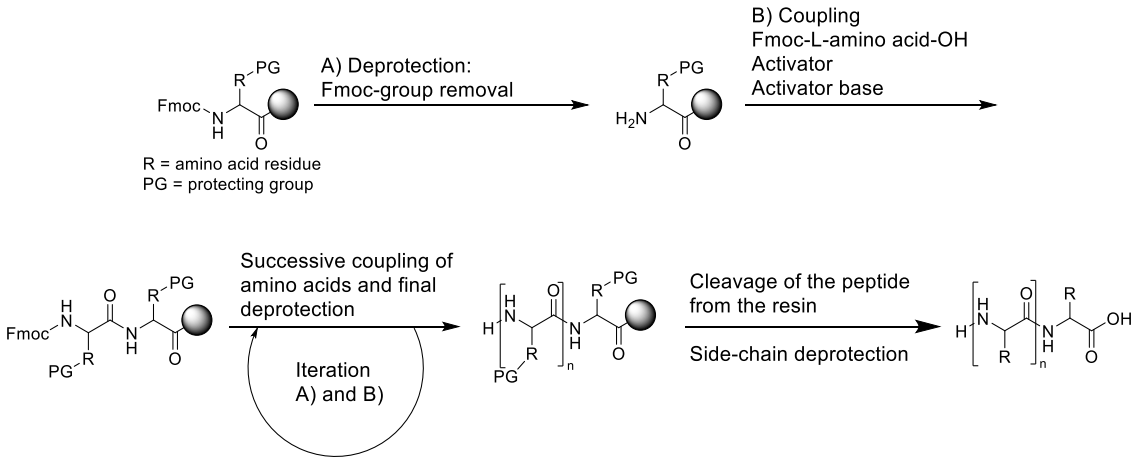

Scheme 1: SPPS-method using the Fmoc-based strategy.

The method is based on the successive coupling of amino acids on a solid phase. The solid phase is a polystyrene resin that is linked to a *N*-protected amino acid via a linker, e.g. 4-benzyloxybenzyl alcohol (Wang resin).[30]

The SPPS starts with the deprotection of the first amino acid that is linked to the resin (Scheme 1). Only *N*-protected amino acids are used to prevent amino acids from undergoing couplings with identical amino acids in solution. Hence, the protection of the amino group leads to coupling reactions only with the unprotected amino acids on the solid phase.[30]

When a base labile protecting group, e.g. Fmoc (9-Fluorenylmethyloxycarbonyl), is bound to the amine, the deprotection is performed using a base. Scheme 2 shows the mechanism of the deprotection of Fmoc using piperidine.[30]

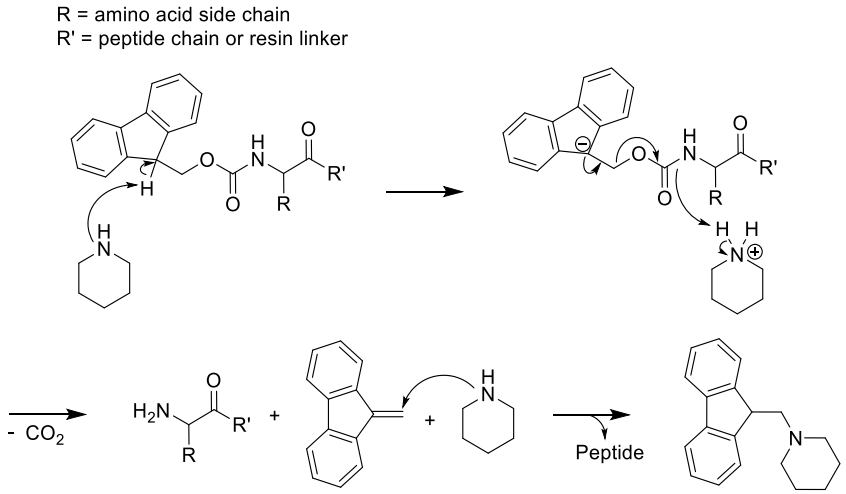

Scheme 2: Mechanism of the deprotection of the Fmoc protecting group.

First, the acidic proton is abstracted. Then, the protecting group undergoes an $E1_{CB}$ elimination leading to the unprotected peptide.

The next step is the coupling of an amino acid to the deprotected one. Due to working under mild conditions, the amino acid needs to be activated for coupling. Therefore, coupling reagents are necessary. Scheme 3 shows exemplarily the mechanism of a coupling reaction with additives. To activate the carboxylic acid, reagents like DCC (*N,N*'-Dicyclohexylcarbodiimide) or DIC (*N,N*'-Diisopropylcarbodiimide, Scheme 3, **2**) are suitable. Besides, if DIC or DCC are used to form an active ester with a carboxylic acid (Scheme 3, **3**), undesirable side reactions can occur. A [1,3]-rearrangement at the *O*-acylisourea can occur and react irreversibly to *N*-acylisourea. Therefore, additives like HOBt (hydroxybenzotriazole) or Oxyma (Ethyl cyanohydroxyiminoacetate, Scheme 3, **4**) are added to the reaction. The addition of these reagents prevents the *N*-acylshift by reacting with the activated ester to another active ester (Scheme 3, **5**). The newly formed activated ester is not able to undergo a *N*-acylshift.[30]

Finally, the amine can attack the ketone of the activated carboxylic acid (Scheme 3, **5**) nucleophilic and form an amide bond so the peptide is expanded by one amino acid (Scheme 3, **6**). Now, the steps of the coupling and deprotection can be repeated to receive a longer peptide chain.

Lastly, the peptide can be cleaved in acidic conditions from the resin. Therefore, usually a mixture of TFA (Trifluoroacetic acid), TIPS (Triisopropyl silane) and H_2O is used. The TIPS acts as a carbocation scavenger by acting as a hydride donor. Once the protecting group is cleaved from the peptide, it is scavenged and cannot react with the peptide again.[31]

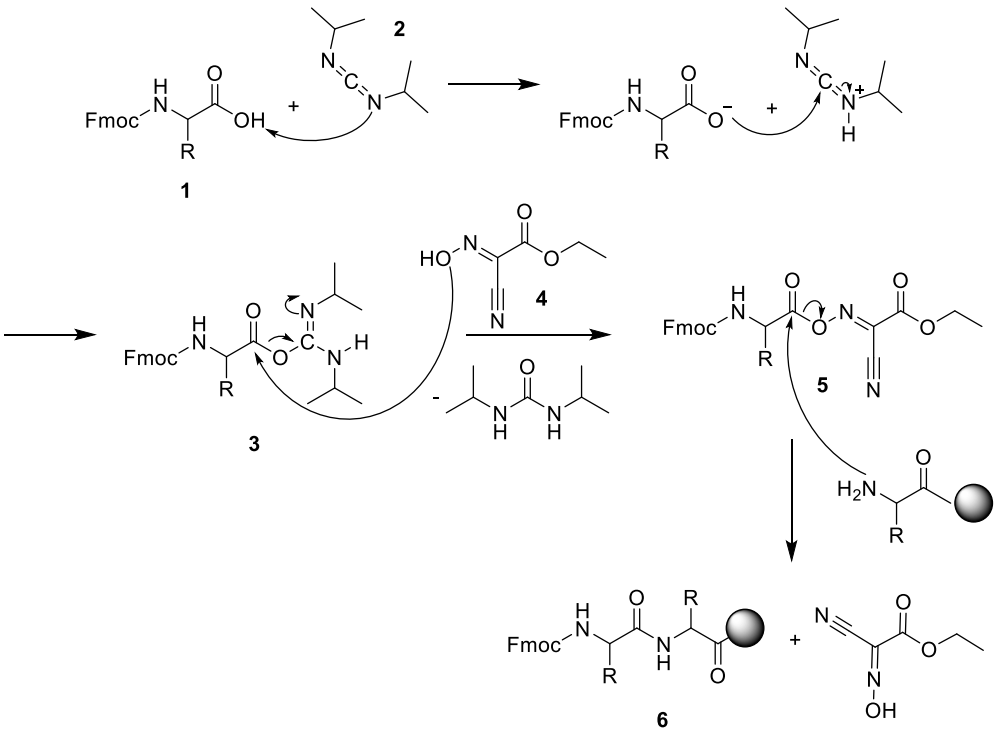

Scheme 3: Mechanism of the amino acid coupling using DIC and Oxyma.

Nowadays, the SPPS can be performed automatically as it is done in this work. This modification of the method enhances the product yields, the reproducibility and controllability. Besides, the reaction times are shorter and the products are more pure.[32]

2.2.2. HPLC and LC-MS

2.2.2.1. HPLC

High Performance Liquid Chromatography (HPLC) is an analytical method used to separate substances from each other, as well as for quantification and identification. This chromatographic method is based on a two-phase system. The mobile phase, that contains the analyte, is pumped through a column that is packed with the stationary phase. Downstream, a detector is connected that detects the elution of the molecules. This time point is called the

retention time (RT). Hereby, the retention time depends on the physical or chemical interactions of the analyte with the stationary phase and the solvents used. [33]

There are different types of HPLC, e.g. normal-phase (NP-) or reversed-phase (RP-) HPLC. In this work, the RP-HPLC method is used to purify peptides.

In comparison to the NP-HPLC, where the stationary phase is polar and the mobile phase non-polar, the stationary phase of the reversed-phase HPLC is non-polar (hydrophobic) and the mobile phase is polar (hydrophilic). By reversing the polarity of the phases, the elution of the substances takes place in reverse order. The separation mechanism of reversed-phase chromatography is based on the distribution of the substances between the alkyl chains on the stationary phase and the solvent of the mobile phase, and in addition on the adsorption of the polar substances on the non-polar stationary phase.[34]

For the stationary phase, silica gel is used which is reacted with dialkyldichlorosilanes containing alkyl chains with 2 to 18 C-atoms. The alkyl chains then build a monomeric layer on the silica gel. The most frequently used stationary phase is the C18-phase, where the silica gel reacted with octadecylsilane.[34]

The mobile phase typically consists of two solvents, e.g. water and acetonitrile. To receive a sufficient separation of molecules, gradient elution can be used. There, the polarity of the solvent mixture is changed during the analysis. If the percentage of the less polar solvent is increased over time, molecules will elute with increasing hydrophobicity.[34]

2.2.2.2. LC-MS

Liquid chromatography–mass spectrometry (LC-MS) combines the separation of molecules (LC, chapter 2.2.2.1.) with a mass spectrometric analysis. In combination with LC, mass spectrometry is predestined for the identification of separated analytes from complex matrices. Hence, detection limits of nano- (ng) or femtogram (fg) can be achieved by LC-MS. While methods like GC-MS are mostly used for low molecular molecules, LC-MS is used for high molecular structures like proteins or peptides.[35]

The separated molecules from the LC column are transferred into a MS ion source. There, the molecules are converted into positively and negatively charged gaseous ions. Furthermore, the charged molecules are separated in an analyzer according to their mass-to-charge ratio (m/z)

and detected with a detector. To avoid collisions between the ionized particles, pumps are used to create a high vacuum in the mass spectrometer.[35]

The interface between LC and MS module plays an important role in this analytical separation process. The analytes need to be transferred from a liquid with a flow rate usually around 1 mL/min into gas phase in high vacuum. Therefore, a drastic reduction of the eluent is required. The most common interface in LC-MS is the ESI (electrospray ionization). Hereby, the liquid is pumped through a metal capillary at around 3 to 5 kV and aerosolized at the tip to form small charged droplets. These droplets are then evaporated rapidly by addition of heat and dry nitrogen. The residual electrical charge is then transferred from the droplet to the molecules. Afterwards, the ionized molecules enter the high vacuum of the mass spectrometer.[36]

In this work, LC-MS is used to identify samples and determine the purity.

2.2.3. Thioflavin-T Assay

Amyloid structures are insoluble proteinogenic aggregates that consist of cross-β sheet structures. Detection of these insoluble structures play an important role in various kinds of diseases, e.g. Alzheimer's disease.[12]

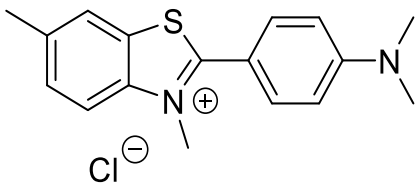

Figure 9: Chemical structure of Thioflavin-T.

Thioflavin-T (ThT) is a fluorescent benzathiole dye that is commonly used for the detection of amyloid-like structures. When ThT binds to amyloid structures, a shift in excitation (385 nm to 450 nm) and emission (445 nm to 482 nm) wavelength occurs which can be measured using a fluorescence detector.[37] The suitable environment of the β-sheet polymers causes a rotational immobilization of the phenyl group of the dye molecule which results in the large red shift of the excitation maximum. Accordingly, a non-fluorescent TICT process (twisted intramolecular charge transfer) competes with a fluorescent LE state (locally excited) in the free molecule. The TICT process between the phenyl group and the benzothiazole group takes place in the excited singlet state. Therefore, a change in the torsion angle from 37 ° to 90 ° occurs. This process

effectively competes with the radiation transition of the LE state and hence, extinguishes the fluorescence. However, when the ThT molecule is bound to an amyloid structure, the rotation is sterically hindered and thereby the quenching of the fluorescent LE state is suppressed. Hence, a higher fluorescence quantum yield can be detected.[38]

The mechanism upon binding of ThT to amyloid fibrils also depends on the charge of the fibrils. As Thioflavin-T is positively charged, positive charged amyloid fibrils may repel the Thioflavin-T. For that reason, ThT is not only specific for amyloid-like structures, but binds to negatively charged nucleic acids as well. [39] Also, highly viscous solvents have an impact on ThT fluorescence. When the torsional relaxation in the molecule is decreased, a higher quantum yield of fluorescence can be observed.[38]

ThT is known to form micelles above a concentration of 5 µM and then induces an increase in fluorescence signal due to its self-fluorescent properties in micelle formation.[40] Therefore, negative controls need to be integrated into a ThT assay where the minimum autofluorescence can be detected (e.g. by adding PBS instead of the investigated sample). In addition, ThT fluorescence correlates linearly with amyloid fibril concentration.[40] Hence, ThT fluorescence intensity can be used for quantification of amyloid fibrils, but side effects as described in the previous paragraph have to be taken into consideration especially if divergent results appear.

For the following experiments, the ThT assay was used to show if the coupling of a short bioactive sequence to a peptide, that is known to form amyloid structures at neutral pH, has an impact on the amyloid fibril formation.

2.2.4. Transmission Electron Microscopy

The TEM (Transmission Electron Microscopy) technique is based on the work of *E. Ruska* and *M. Knoll* in the 1930s. It is a microscopy technique which has basic similarities to light microscopy. In comparison to common light microscopy, a focused, highly accelerated electron beam permeates a sample in high vacuum. Furthermore, the imaged object is enlarged by series-connected electromagnetic lenses. Behind the specimen, an image is created on a luminescent screen or a CCD (Charge Coupled Device) camera, whereby the de Broglie wavelength of the electrons enables a spatial resolution that is improved in comparison to conventional light microscopy. The common resolution of a TEM is usually around 0.1 nm, maximum 0.05 nm if a high resolution device is used.[41,42]

When electrons pass through a specimen, they are partly absorbed and partly scattered in divergent directions. The scattered electrons are collected by a contrast diaphragm which is located in the lower focal point of the objective. In addition, the angle of scattering is dependent of the local thickness and density (atomic number of the scattered atom) of the investigated material. A higher atomic number increases the scattering angle of the electrons that hit the atom. In summary, the higher the atomic number and thickness of the material, the higher is the number of electrons, that are scattered in higher angles. Therefore, the samples need to be ultra-thin, around 0.1 µm. In image formation, the scattered electrons are missing and as a result, darker image areas occur. Hence, staining reagents with higher atomic numbers like uranyl acetate can enhance the contrast of a sample.[41]

In this work, TEM is used to image fibril formation of peptides.

2.2.5. Fluorescence Microscopy

The phenomenon of fluorescence occurs when a molecule is able to be excited with light of a certain wavelength and emit light of a higher wavelength. This process is described by the Jablonski diagram (Figure 10). Thereby, photons of short-wave radiation are absorbed and thus, excite the molecule into an energy-rich, higher vibronic state (coupling of electronic and vibrational state) that is short-lived. There, it quickly undergoes vibrational relaxation and reaches the vibrational ground state of the electronic S_1 state. Thereby, the molecule emits a part of the absorbed energy non-radiatively. The excited molecule then emits the remaining energy due to the striving to get into the most energetically favorable state (thermodynamic laws). During the process of the relaxation of the molecule from high- (S_1) to low-energy (S_0) state, the energy can either be emitted as visible light (fluorescence) or undergo competitive processes, e.g. internal conversion (IC) where the molecule again undergoes non-radiative vibrational relaxation to reach the S_0 state. The yield of the measured fluorescence results from the difference between the other photophysical processes and the fluorescence itself and is called fluorescence quantum yield.[43,44]

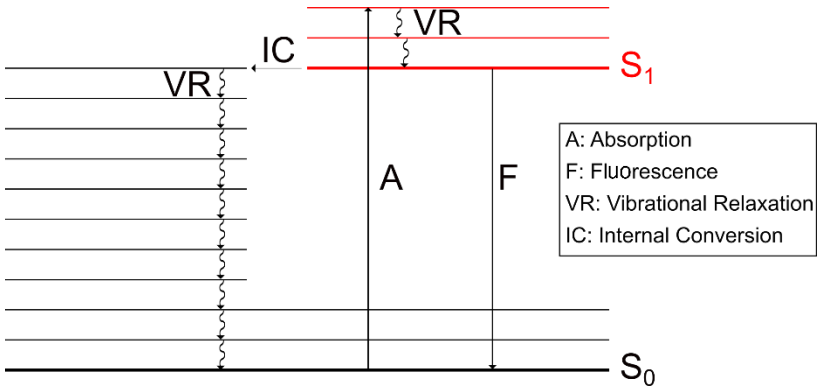

Figure 10 : Jablonski diagram adapted from a template from Jüstel et al., 2019. [45]

A fluorescence microscope often consists of the basic structure of a brightfield microscope. In comparison, the object to be observed is not irradiated, but illuminated by the objective and it is therefore called *Epi*-fluorescence microscope. In addition, the fluorescence microscope has an additional light source, mainly gas discharge lamps, lasers or LEDs. Furthermore, the objective has two functions. It acts as a condenser for focusing the excitation light and it records and transmits the emission (Figure 11). The main part of the microscope is a filter complex, where the emission and excitation filters and a dichromatic mirror (beam splitter) are located. The emission and excitation filters determine the required wavelength and therefore can be set to be permeable for a specific wavelength and bandwidth. Moreover, the function of the dichromatic mirror is to reflect the lower wavelength excitation light at an angle of 45 ° to the sample (blue line, Figure 11) . Additionally, the dichromatic mirror lets the emission light with longer wavelengths pass through to the detector or ocular (green line, Figure 11).[43]

A modification of the epifluorescence microscope is the confocal microscope. This type of microscope can separate focused light signals from the ones out of focus. That is achieved by adding a pinhole in front of the detector at the intermediate image plane that is only permeable for light signals from the focus plane. Furthermore, the sample should not be illuminated in whole at the same time. Therefore, in a CLSM (confocal laser scanning microscope) the specimen is scanned with a focused laser point (e.g. argon or helium-neon laser). Additionally, a second pinhole is built into the CSLM in the beam path of the laser to coordinate the focus of the laser point and the pinhole at the intermediate image plane. Photomultiplier tubes (PMT) then detect the emitted photons of the sample. In addition, the PMT converts the detected photons into electrical signals and amplifies them. These signals can then be converted into digital pictures by special computer programs. If multiple planes along the z-axis are scanned, they can be summed up to a 3D image.[43]

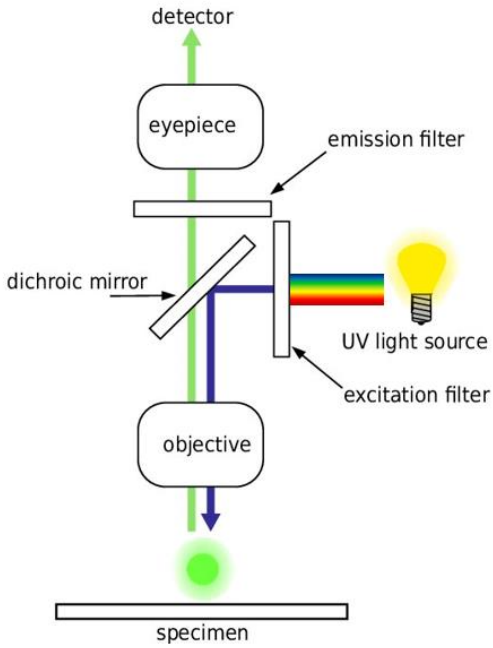

Figure 11: Schematic depiction of a fluorescence microscope (modified according to Schier et al., 2011) [46].

The fluorescence microscopy and confocal microscopy are used in this work to visualize the HUVEC tube formation assays.

2.2.6. Endothelial Cell Tube Formation Assay

In vivo, endothelial cells are located on an extracellular matrix (ECM), called the basement membrane which consists of many structural and functional components like collagen or laminin. In addition, it stabilizes the tube-like structures of the blood vessels. The ability of endothelial cells to differentiate and form tube-like structures on artificial basement membrane extracellular matrices like BME or Matrigel is used for different kinds of *in vitro* tube formation assays (HUVEC tube formation assay, Figure 12, **A**). For example, it can be used to investigate effects of pro- and anti- angiogenic substances (Figure 12, **B** and **C**), or the pathways involved in angiogenesis and wound repair. The process of differentiation of the endothelial cells includes various steps like cell migration and adhesion, tube formation or protease secretion. This process on the basement membrane is highly specific to endothelial cells.[47]

The endothelial tube formation assay can be used for high throughput screening to test different chemicals at the same time or varying concentrations. Additionally, it is rapid and quantitative.

Nevertheless, several aspects have to be taken into consideration before performing a tube formation assay. Crucial for the tube formation assay is the cell density. Too few cells may form incomplete tubule structures, while too many cells can build monolayers. In addition, if primary HUVECs (Human Umbilical Vein Endothelial Cells) are used, it is necessary to use them at early passages. If an assay on angiogenesis promoting substances is about to be performed, basement membrane with reduced growth factors can be used, whereby a pro-angiogenic effect can be observed more clearly.[47]

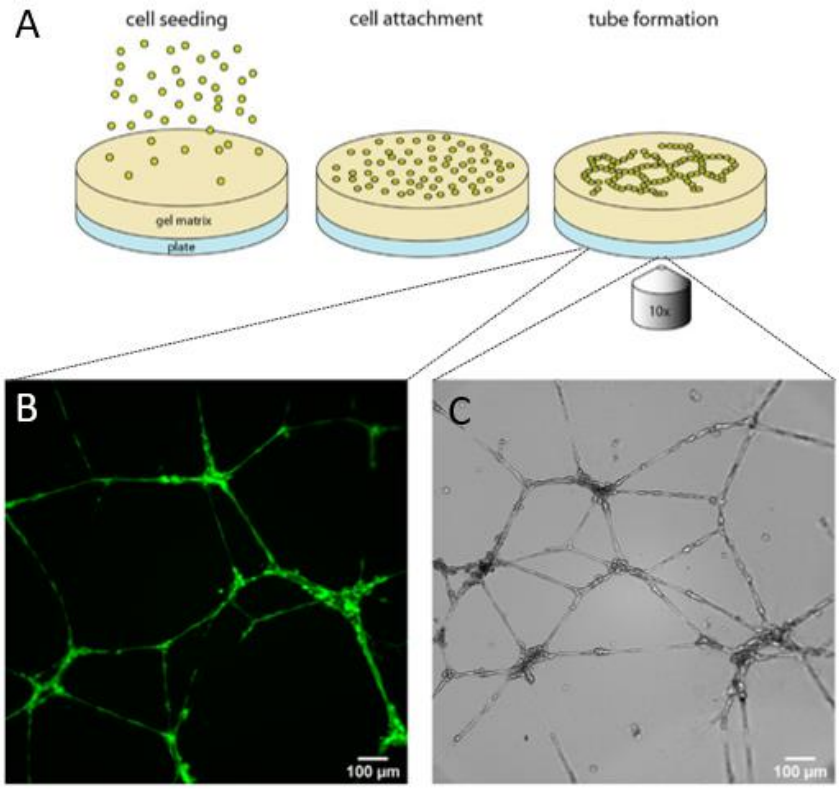

Figure 12: (A) Schematic representation of the procedure of HUVEC tube formation assay (by ibidi GmbH, 2014)[48]). (B) and (C): Tube formation of HUVECs after 16 h with addition of 50 ng/mL bFGF on Matrigel with reduced growth factors. Photographs were taken with a fluorescence microscope (B) After Calcein staining. (C) Brightfield picture. Scalebars represent 100 µm.

To evaluate a HUVEC tube formation assay, controls have to be included. As positive control, to evaluate if the cells are healthy and differentiate properly, the assay can just be performed on matrix like Matrigel without addition of growth factors. This ensures that, if anti-angiogenic effects are observed, they are caused by the investigated substance. As negative control, a substance can be added that is known to be have an inhibiting effect on HUVEC tube formation (e.g. suramine) to make sure tube formation can be inhibited.[49] In this work, the tubes were quantified using a Plugin from ImageJ, called Angiogenesis Analyzer. This software automatically

quantifies the tube formation by detecting nodes, branches, tubes etc.[50] In general, the detection parameters will all show same observable tendencies during experimental time span. One of the most commonly used parameters for quantification is the total tube length because it is the most stable and traceable value.[49] To finally evaluate the assay, total tube lengths can be compared because enhancement of tube formation correlates with pro-angiogenic effects[49].

2.2.7. CellTiter-Glo® Luminescent Cell Viability Assay

The CellTiter-Glo® Luminescent Cell Viability Assay is a testing system to determine cell viability, i.e. the number of viable cells. This method can be used for cell toxicity assays or cell proliferation assays, whereby the CellTiter-Glo® reagents undergo an enzymatic reaction including ATP (Adenosine Triphosphate). The amount of ATP is thereby proportional to the amount of metabolic active cells.[51]

If CellTiter-Glo® mixture is added to cells, they are lysed, and ATP is released. A mutated luciferase enzyme (*Photuris pennsylvanica*, LucPpe2^{m}) then converts the beetle luciferin to the luminescent oxyluciferin. This reaction only occurs in the presence of ATP, Mg^{2+} and molecular oxygen (Scheme 4).[51] The validation of viable cells is thereby given due to the dramatical decrease of ATP in necrotic or apoptotic cells, therefore presence of ATP correlates with number of viable cells at time of detection. In addition, endogenous enzymes are inhibited that are released during cell lysis, e.g. ATPase which is an enzyme that degrades ATP.[51]

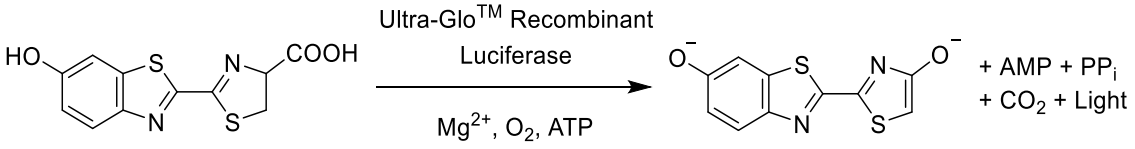

Scheme 4: Chemical equation of the luciferase reaction, created after a template from Promega (2015)[51].

The process of emission in chemiluminescence is identical to fluorescence (see chapter 2.2.5.). Although the chemiluminescence emission spectra in excited state are consistent with the fluorescence or phosphorescence spectra of the product, the process of excitation is decisive for the designation of the phenomenon. Instead of photons, a chemical reaction leads to an excited product and therefore to light emission.[52]

The CellTiter-Glo® Luminescent Cell Viability Assay is used in this work to investigate the impact of the synthesized peptides and their conjugates on cell viability.

3. Motivation

The projects aim is based on a recently published peptide-protein hydrogel (*Gacanin, J. et al., 2019*)[1] which consists of a protein (HSA) conjugated with SAPs (Depsi-Maleimide) and PEG chains.

Especially hydrogels gained a high interest for biomedical applications as they have similar mechanical properties to the natural tissue and can be modified in a broad range with e.g. bioactive components that promote angiogenesis.[24] As the hydrogel used in this work showed to be biocompatible, biodegradable, injectable, self-healing and in addition inducibility by pH trigger to physiological pH, it is an interesting candidate for biomedical applications, especially tissue engineering. Cell assays already confirmed cell compatibility of the above mentioned hydrogel and, additionally, having the HSA protein as a scaffold, suitability for biomedical application is enhanced due to its desirable characteristics in biological environments, e.g. enzymatic degradability and plasma stability.[18] Therefore, it is indicated that the peptide-protein hybrid hydrogel could be able to mimic the extracellular matrix (ECM). Hence, giving the hydrogel additional angiogenesis promoting properties would enhance the potential for successful use in biomedical application.

Our approach is to achieve the bioactivation of the gel by co-assembling the hybrid hydrogel with free Depsi-Maleimide peptide carrying a bioactive group. Thereby, the SAP is integrated into the hydrogel (Figure 13). Here, the projects aim is approached by reproduction of the dc-HSA-PD and Depsi-Maleimide, as well as synthesis of bioactive peptide sequences from literature that have shown to promote angiogenesis in *in vitro* assays. The five chosen bioactive sequences are IKVAV, VGVAPG, SVVYGLR, ILKNLSRSR and RKRLQVQLSIRT. These five BAPs are then conjugated to the SAP. Lastly, the self-assembling system is characterized by TEM and ThT assay to investigate the amyloid character and morphology.

The BAPs and their conjugates are applied in *in vitro* assays to study their bioactivity and possible cell toxic effects. In addition, HUVEC tube formation assays on Matrigel are performed by addition of the respective peptides to investigate angiogenesis promoting. At last, co-assembly of conjugated D_{MAL}-BAPs with the dcHSA-PD into hydrogels and its use as matrix for HUVEC tube formation assays are studied.

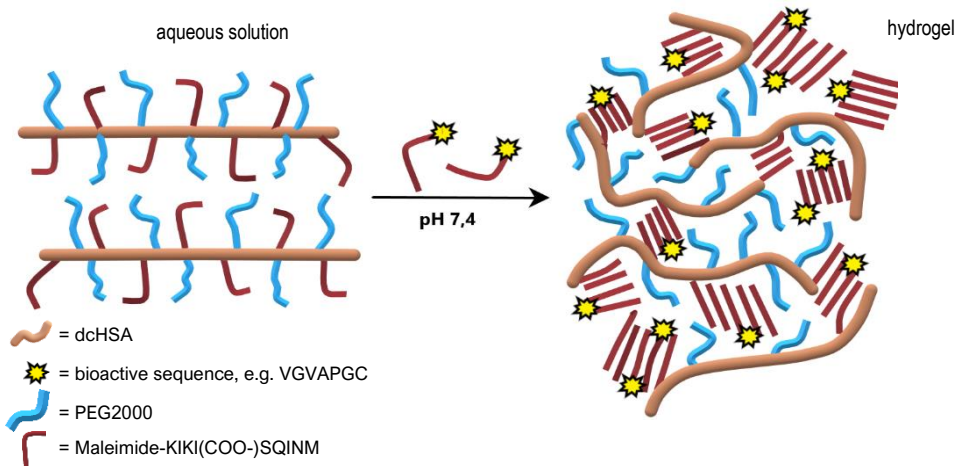

Figure 13: Schematic self-assembly of the dcHSA-PEG(2000)$_n$-D-Mal$_m$ into a hydrogel with addition of free D-Mal modified with bioactive peptide sequences.

An additional approach is to investigate if the hybrid hydrogel can be used as a replacement for Matrigel™, that is an artificial basement membrane-like extracellular matrix. Nevertheless, it is an animal-based product that is associated with ethical concerns because it is extracted from living tissues and, in addition, its components are not completely defined.[53] For this reason, the presented hydrogel is also tested in comparison to Matrigel to investigate its possible suitability as a replacement in addition to its use in tissue engineering.

4. Results and Discussion

4.1. Synthesis and Characterization

4.1.1. dcHSA-PD (dcHSA-PEG(2000)$_n$-D-Mal$_m$)

The synthesis route of the protein backbone dcHSA-PD [dcHSA-PEG(2000)$_n$-D-Mal$_m$] was performed twice according to a protocol by *Gacanin, J. et al.*[1]. The following Scheme 5 gives an overview of the synthesis steps

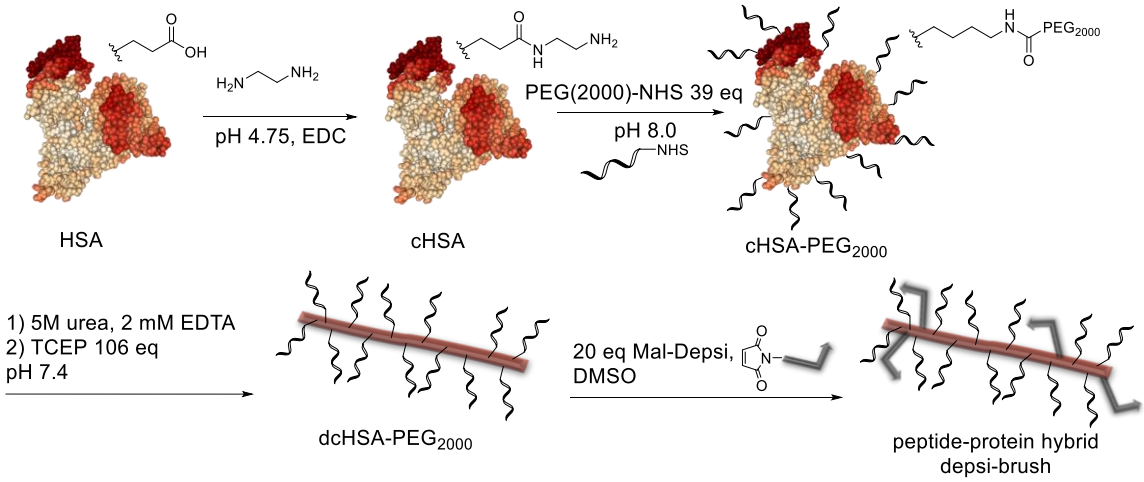

Scheme 5: Synthesis scheme of the peptide-protein hybrid dcHSA-PD [dcHSA-PEG(2000)$_n$-D-Mal$_m$].

According to the published procedure, HSA is initially cationized to enhance the amount of primary amine groups at the protein (Scheme 5, step one). To achieve this, ethylenediamine (EDA) was used to react with carboxyl groups of the amino acid side chains resulting in amide bonds. However, during this thesis, the already cationized material was provided by *Adriana Sobota* and hybrid synthesis was continued from this step.

Next, the protein was PEGylated (Scheme 5, step two) resulting in higher stability of the cHSA (e.g. protection against degradation by proteases) and higher solubility.[1] Therefore, a N-hydroxysuccinimide ester, MeO-PEG(2000)-NHS ester, was used to react with amine groups of the cHSA (e.g. lysine). Hereby, the reaction started with 50.00 mg (0.69 µmol) cHSA and yielded 40.30 mg (0.37 µmol, 54%) cHSA-PEG(2000)$_n$. Regarding the MALDI-TOF-MS measurement of the product, an increase in mass was observed and it was calculated that an average PEGylation of 18 – 19 PEG(2000) chains per cHSA molecule could be achieved (Figure 14).

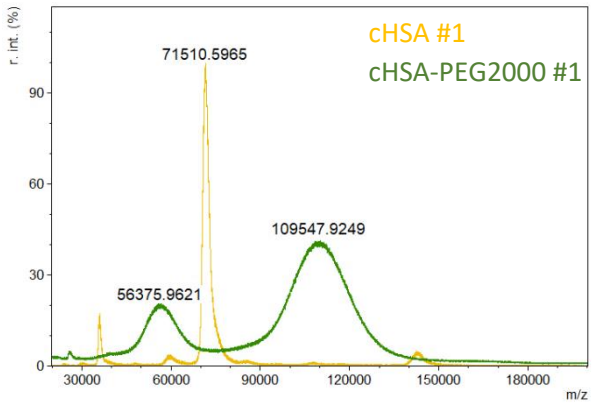

Figure 14: MALDI-TOF-MS spectrum overlay of the cHSA of batch 1 (yellow) and the PEGylated cHSA of batch 1 (green).

Third, the cHSA-PEG(2000)$_{19}$ was denatured with TCEP in urea buffer (Scheme 5, step three) to result in linear protein chains [dcHSA-PEG(2000)$_{19}$]. The denaturation yielded 33.8 mg (0.31 µmol, 84%) regarding dcHSA-PEG(2000)$_{19}$. A second synthesis was performed using cHSA-PEG(2000)$_{23}$ which yielded 56.3 mg (0.48 µmol, 96%) starting with 59.1 mg (0.50 µmol).

Lastly, the D-Mal was coupled to the cysteine residues of the dcHSA-PEG(2000)$_n$ (Scheme 5, step four). The maleimide of the Depsi peptide reacts with the cysteine in a thiol-ene reaction including a Michael addition. The reaction is described in chapter 4.1.3.3. Lastly, the synthesis of dcHSA-PEG(2000)$_{19}$-D-Mal$_{11}$ (dcHSA-PD) yielded 20.1 mg (0.17 µmol, 55%) as a white solid, indicating a coupling of around 11 Depsi peptides per HSA protein. Furthermore, the second batch of dcHSA-PEG(2000)$_{23}$-D-Mal$_{13}$ was synthesized yielding 60.1 mg (0.44 µmol, 92%) containing around 13 Depsi peptides per HSA protein.

The dcHSA-PD were characterized via MALDI-TOF-MS. An increase in mass was observed in both cases (Figure 15).

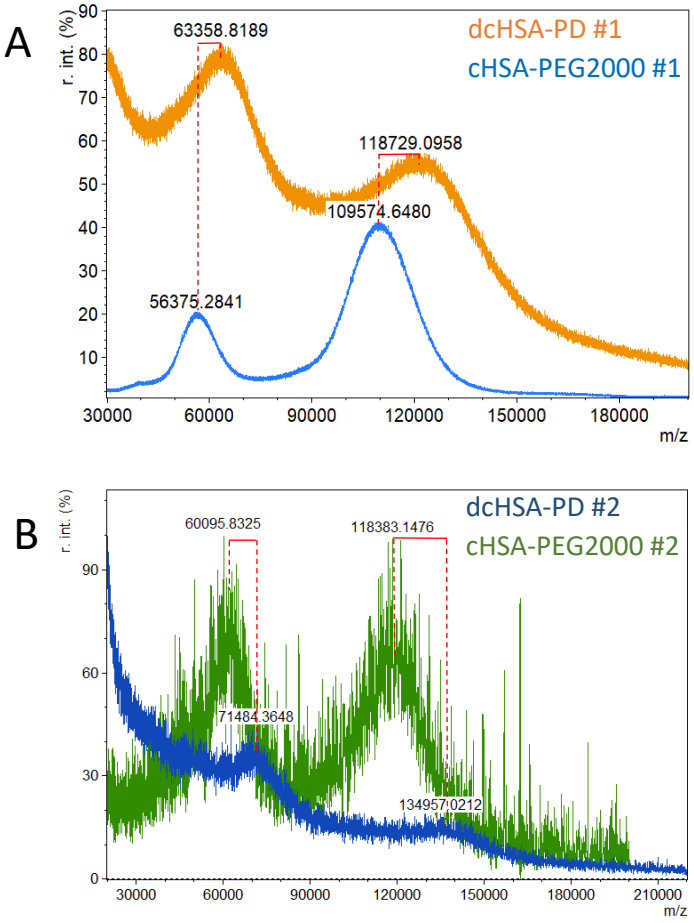

Figure 15: MALDI-TOF-MS spectra of the Depsi-brush from the first synthesis (A) and the second synthesis (B). The red lines show the shift of the peaks and therefore an increase in mass.

The two synthesized batches differ in conjugation rate of PEG chains and D-Mal. Thereby, batch 1 (dcHSA-PEG(2000)$_{19}$-D-Mal$_{11}$) had a lower PEG and D-Mal coupling rate. In comparison, batch 2 (dcHSA-PEG(2000)$_{23}$-D-Mal$_{13}$), where PEG chains were already coupled to the cHSA, a higher D-Mal coupling rate was observed, approximately two more D-Mal per protein backbone. The higher peptide conjugation rate could have resulted from the increased reaction time (48 h instead of 24 h). Nevertheless, the dcHSA-PD was well reproducible.

Compared to the recently described dcHSA-PD[1] where average 22 PEG chains and 20 D-Mal per protein backbone were conjugated, the coupling of D-Mal to the backbone in the here described syntheses was lower. This may result in different mechanical properties of the gels. However, a rheological analysis of batch 2 showed similar self-healing properties as well as shear force resistance (see chapter 8.3.). The different D-Mal coupling rates may arise due to the solvent. Probably, the DMSO was not dry enough and contaminations could have interfered with the

reaction. Additionally, the coupling success was verified by MALDI-TOF-MS whereby a large mass distribution occurred (Figure 15). Especially Figure 15, **B** had to be read out manually which is another source of error.

The following Table 1 gives an overview of the synthesized batches as well as in comparison the dcHSA-PD from literature.

Table 1: Summary of the PEGylation und D-Mal coupling rate, as well as the molecular weight of the synthesized dcHSA-PD batches and, in addition, the dcHSA-PD from literature for comparability.

	dcHSA-PD batch #1	**dcHSA-PD batch #2**	**dchHSA-PD (literature[1])**
Molecular Weight (g/mol)	118729	134957	145000
Average PEGylation / protein	19	23	22
Average D-Mal coupling / protein	11	13	20

4.1.2. Depsi-Maleimide (Maleimide-KIKI(COO-)SQINM)

As mentioned in the chapter above, the Depsi-Maleimde (D-Mal, Maleimide-KIKI(COO-)SQINM) had to be synthesized to be coupled to the dcHSA-PD to act as self-assembling scaffold for the hydrogel. The synthesis instructions were taken from a published protocol by *Gacanin et al.*[1] and adapted by *Adriana Sobota.* The following Scheme 6 shows the synthesis route of the D-Mal in detail.

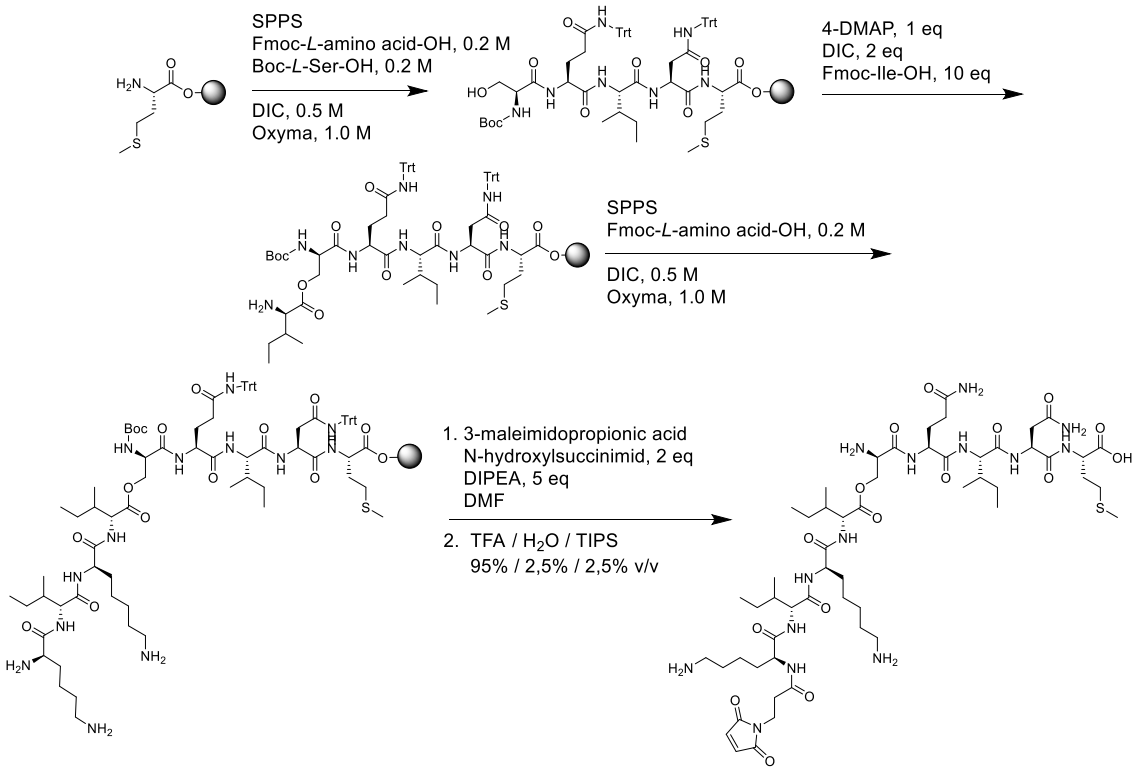

Scheme 6: Schematic representation of the synthesis route of D-Mal.

First, the SQINM sequence was synthesized through successive coupling via solid phase peptide synthesis as described in 6.2.1. The synthesis yielded 37.3 mg (0.03 mmol, 12%) starting with 0.25 mmol. A significant improvement of the yield (98.7 mg, 0.08 mmol, 16%) was achieved after a second Depsi-Maleimide synthesis starting with 0.5 mmol. This occurred most likely due to an increase in reaction time of the maleimide functionalization (48 h instead of 24 h). Finally, the purified and lyophilized Depsi-Maleimide batches were characterized via MALDI-TOF-MS (see chapter 8.1.) and LC-MS (see chapters 6.2.1. and 6.2.2.) and showed a high purity in both cases.

In addition, TEM measurements were carried out with an increased incubation time of 48 h. As anticipated, fibrilization of D-Mal after incubation in PBS could be observed (Figure 16) indicating a successful *O,N* acyl shift at neutral pH.

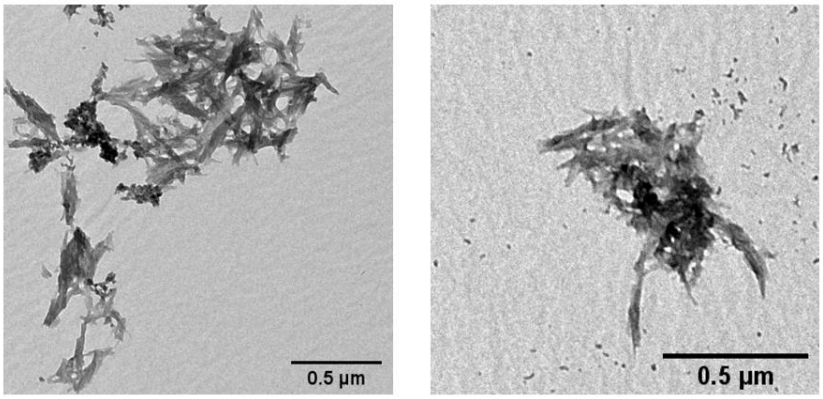

Figure 16: TEM micrographs of D-Mal peptide stained with uranyl acetate after 48 h of incubation time at room temperature in PBS. Scalebars represent 500 nm.

For further characterization of amyloid structure formation, ThT assay was performed. For a better comparability between D-Mal and the BAPs, the results are shown in chapter 4.1.3.

4.1.3. Bioactive Peptide Sequences

After the synthesis of the self-assembling scaffold Depsi-Maleimide, the focus is now shifted to the bioactive peptide sequences. First, the selection process of the BAPs is illustrated, then the synthesis and characterization of the respective sequences is presented. Lastly, the coupling products D_{MAL}-BAPs are analyzed.

4.1.3.1. Literature Research on Bioactive Peptide Sequences

The first sequence found in literature is IKVAV. It is derived from laminin-1, a trimeric basement membrane glycoprotein that is able to activate a variety of cell responses, e.g. cell attachment and cell migration[54], promotion of angiogenesis[55] or tumor metastasis. Furthermore, this motif is very well characterized and previous studies showed that IKVAV enhanced tube formation in HUVEC tube formation assays on Matrigel.[56] In addition, it showed angiogenic effects in *in vivo* studies.[55] Therefore, it is an ideal candidate to promote angiogenesis in the hybrid hydrogels.

Second, the peptide sequence VGVAPG, which is derived from elastin, is an interesting candidate to promote bioactivity. Elastin makes up the main part of elastic fibers that are present in many types of tissues like arteries, skin and lung. If elastin is enzymatically degraded, elastin-derived peptides (EDPs) can induce tissue regeneration processes. This process is supposed to be related to cardiovascular diseases, like e.g. atherosclerotic abdominal aortic aneurysm. It has been

reported that EDPs activate various processes like cell migration and differentiation. In addition, VGVAPG showed angiogenic effects in HET-CAM assays and enhanced tubule formation in HUVEC tube formation assays.[57]

SVVYGLR is a peptide sequence that is derived from osteopontin, an ECM protein that is located in numerous tissues like kidney, skin, bones etc. It is a multifunctional protein that is included in many processes like mediating inflammatory and bone metabolism, showed angiogenic activities[58] and serves as a ligand for a special type of integrins[59]. Furthermore, SVVYGLR enhanced endothelial cell migration and tube formation on collagen gel.[58] In addition, it has been conjugated to a gelatin-poly(ethylene glycol)-tyramine to form bioactive hydrogels which showed enhanced HUVEC activities like tube formation, migration and attachment on the gel surface *in vitro* as well as blood vessel formation *in vivo.*[60]

The bioactive sGliafin sequence (ILKNLSRSR) has been previously used withing our working group by *Thomas Mack*, University of Ulm. It is derived from Glial cell line-derived neurotrophic factor (GDNF) that affects migration, differentiation and proliferation of various neuronal cells.[61] In this work, it was investigated if the sGlaifin sequence is also able to affect endothelial cells.

The last sequence that is tested is the RKRLQVQLSIRT (AG73) peptide. Similar to IKVAV, it is derived from laminin and is recognized by syndecans (transmembrane proteins). This sequence affected endothelial cells *in vitro* whereby it had a positive effect on tube formation on Cultrex BME. Hereby, the endothelial cells formed longer persisting tubes. In *ex vivo* aortic ring and *in vivo* CAM assays, the AG73 showed angiogenesis promoting effects. In addition, it enhances cell migration and in a study, has been conjugated to a chitosan membrane where it triggers angiogenic effects as well, indicating its potential in tissue engineering.[27]

Table 2 gives an overview of the used BAPs and the position of the added cysteine (N- or C-terminus). Regarding peptide VGVAPG, it was indicated that the position of cysteine is not important because it is a repetitive sequence in tropoelastin.[57] Therefore, it was added to the C-terminus. In all other cases, the literature or working group members indicated the position of the linking peptide.

Table 2: Overview of the chosen bioactive peptide sequences with an additional cysteine residue at either N- or C-terminus. The main functions and in literature tested endothelial cell lines are listed as well.

Sequence	Function / Promotion of	Cell type (angiogenesis assay)
IKVAVC	Cell adhesion, cell migration, angiogenesis	HUVEC [56]
VGVAPGC	Angiogenesis, cell migration	HUVEC [57]
SVVYGLRC	Angiogenesis, cell migration, cell attachment	TRLEC [58]
CILKNLSRSR	Migration, differentiation, proliferation (neuronal cells)	-
CRKRLQVQLSIRT	Angiogenesis, cell adhesion	SVEC4-10 [27]

4.1.3.2. Synthesis and Analysis of BAPs

As described in the previous chapter, the most promising sequences from the literature were chosen to be used in further *in vitro* assays. Thereby, four peptides (Table 3, **[1]** – **[3]**, **[5]**) are known to promote angiogenesis in different model systems, while **[4]**, Table 3, is known to primarily stimulate neuronal cells.

All five linear BAPs (**[1]** to **[5]**, Table 3) were synthesized according to chapter 6.2.3. containing a cysteine residue at either the N- or the C-terminus for the thiol-ene Michael addition with D-Mal. After purification and lyophilizing, the peptides appeared as colorless solids. The total yields of the synthesized BAPs are shown in the following Table 3.

Table 3: Yields of the bioactive peptide sequences synthesized via automated SPPS.

Substance #	Sequence	Yield [mg]	Yield [%]
[1]	IKVAVC	5.0	2
[2]	VGVAPGC	13.7	9
[3]	SVVYGLRC	4.0	2
[4]	CILKNLSRSR	29.2	25
[5]	CRKRLQVQLSIRT	40.8	26

Some peptides showed small yields after purification, whereby a large number of signals were observed during purification by HPLC. In order to identify side products which may contribute to the low yields (peptides **[1]** – **[3]**), selected signals from the chromatogram were isolated and analyzed by MALDI-TOF-MS (see chapter 8.1.). Exemplarily, the HPLC chromatogram of IKVAVC and the respective MALDI-TOF-MS spectrum of an IKVAVC side product are shown in the following Figure 17.

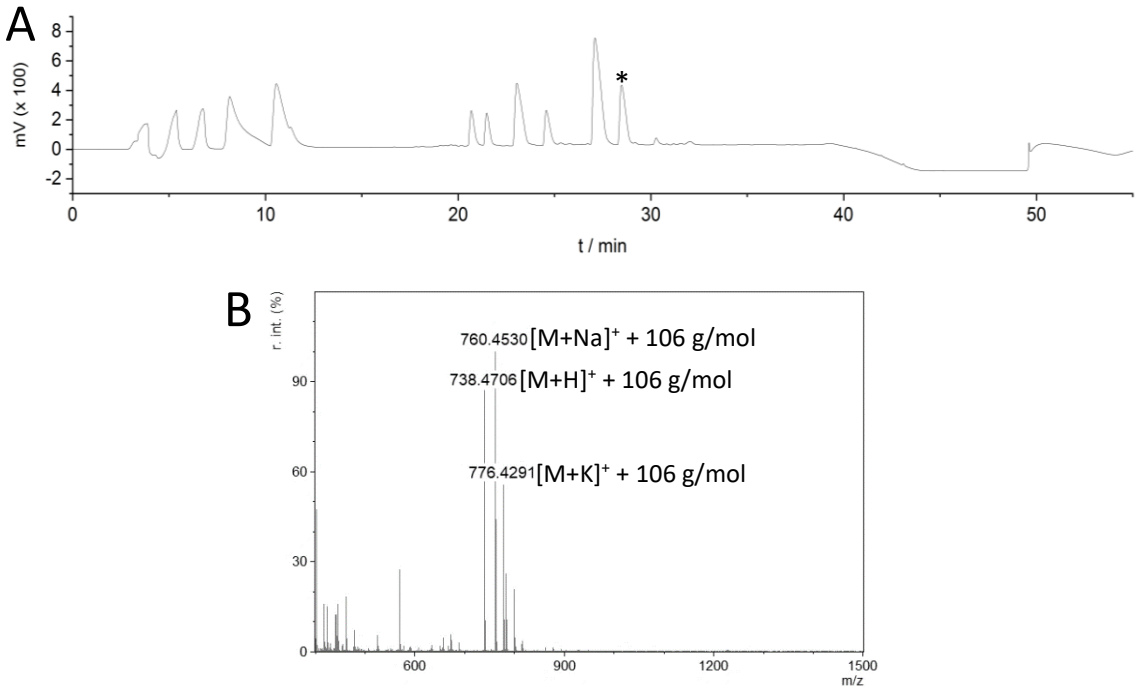

*Figure 17: (A) HPLC chromatogram of crude IKVAVC after cleavage from resin on preparative scale HPLC. (B) MALDI-TOF-MS spectrum of peak at the RT of 29 min (marked with *) collected from preparative HPLC of IKVAVC.*

The HPLC chromatogram in Figure 17 visualizes the large number of side-products. LC-MS (see 6.2.3.1.) confirmed that the collected fraction at a retention time (RT) around 28 min, the highest observable peak in the chromatogram, is assigned to the product. The MALDI-TOF-MS spectrum in Figure 17 is assigned to the peak at a RT of around 29 min. The side product shows an increase in mass of 106 g/mol.

One explanation for the increase in side products are side reactions caused by the Fmoc-Cys(Trt) Wang resin. A rearrangement of the resin linker takes place during the cleavage of the peptide from the resin in the TFA/H_2O/TIPS mixture.[62] The suggested mechanism is shown in the following Scheme 7.

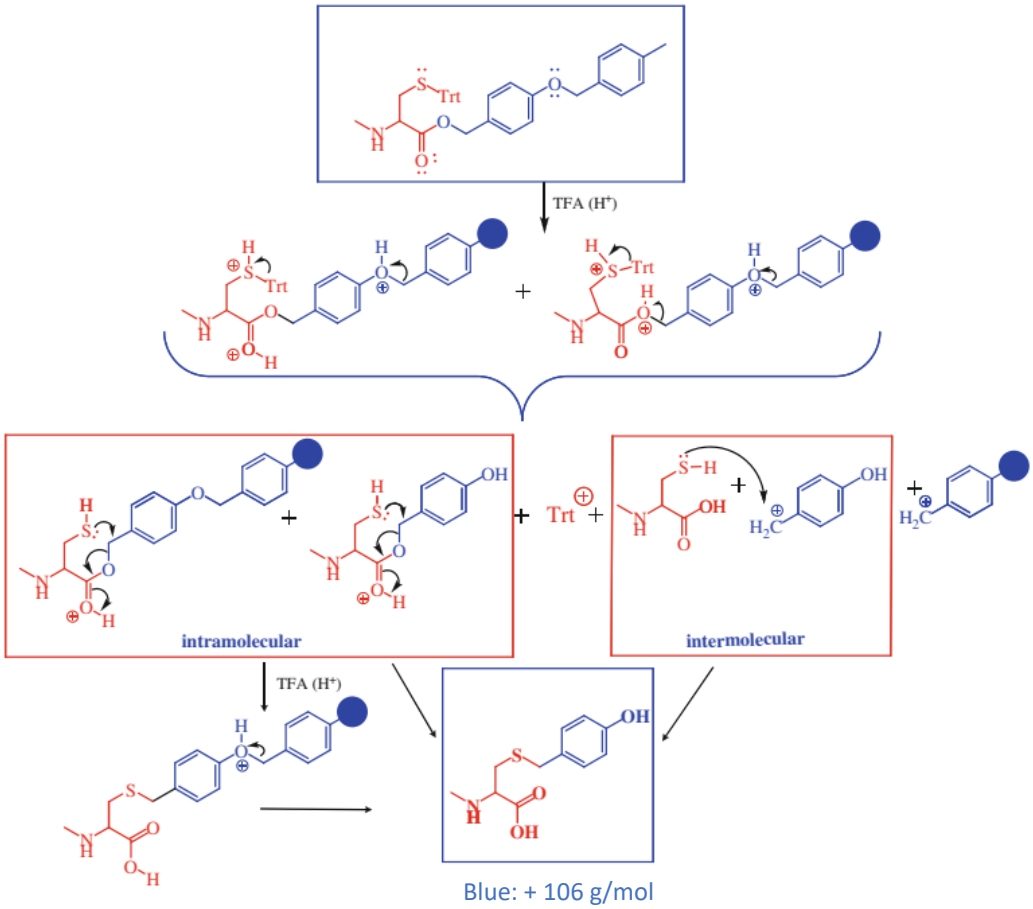

Scheme 7: Possible mechanism of the side reaction of cysteine with the Fmoc-Cys(Trt)-Wang resin resulting in L-[S-(4'-hydroxybenzyl)]cysteine and a mass increase of 106 g/mol (modified according to Stathopoulos, P. et al., 2013)[62].

During cleavage, the benzyl phenyl ether of the resin linker is protonated as well as the thiol of the cysteine and the ester of the C-terminus. Thus, the protecting trityl group is cleaved and the ether and ester bonds are split. Then, the reaction can proceed either through an intramolecular or intermolecular mechanism to result in *L*-[*S*-(4'-hydroxybenzyl)]cysteine. This species increases the molecular weight of the peptide by 106 g/mol. As IKVAVC has a molecular weight of 632 g/mol and the MALDI-TOF-MS spectrum (Figure 17) shows a $[M+H]^+$ peak of 738 g/mol, it is very likely that this side reaction proceeded during cleavage.

The above-mentioned side reaction occurred during every cleavage of a BAP with a C-terminal cysteine. Therefore, the reaction may have potentially been optimized by using a trityl resin instead of the Wang resin. This would likely reduce side reactions due to the more stable composition of the trityl linker. Furthermore, addition of 1,2-ethanedithiol to the cleavage solution is known to reduce side product formation as it acts as an additional scavenger for the *p*-Cresol carbenium ion.[62] Due to cost-benefit reasons, 100 mg of **[1]**, **[2]** and **[3]** were purchased.

In addition, 50 mg of **[5]** were purchased, because at the time of ordering, the CRKRLQVQLSIRT was not purified yet and so the yield was unknown.

Furthermore, a nanostructure analysis was performed using TEM and ThT assay which should reveal if the BAPs are able to assemble into structures without the Depsi-Maleimide motif. If there is a strong tendency towards aggregates, interference with the self-assembly of the Depsi peptide could occur and possibly produce other structures than amyloid fibrils. In addition, the BAP is not necessarily presented on the fibril surface which is expected to be necessary for cells to bind the sequences. Both assays were performed as described in 6.1.5. and 6.1.6.

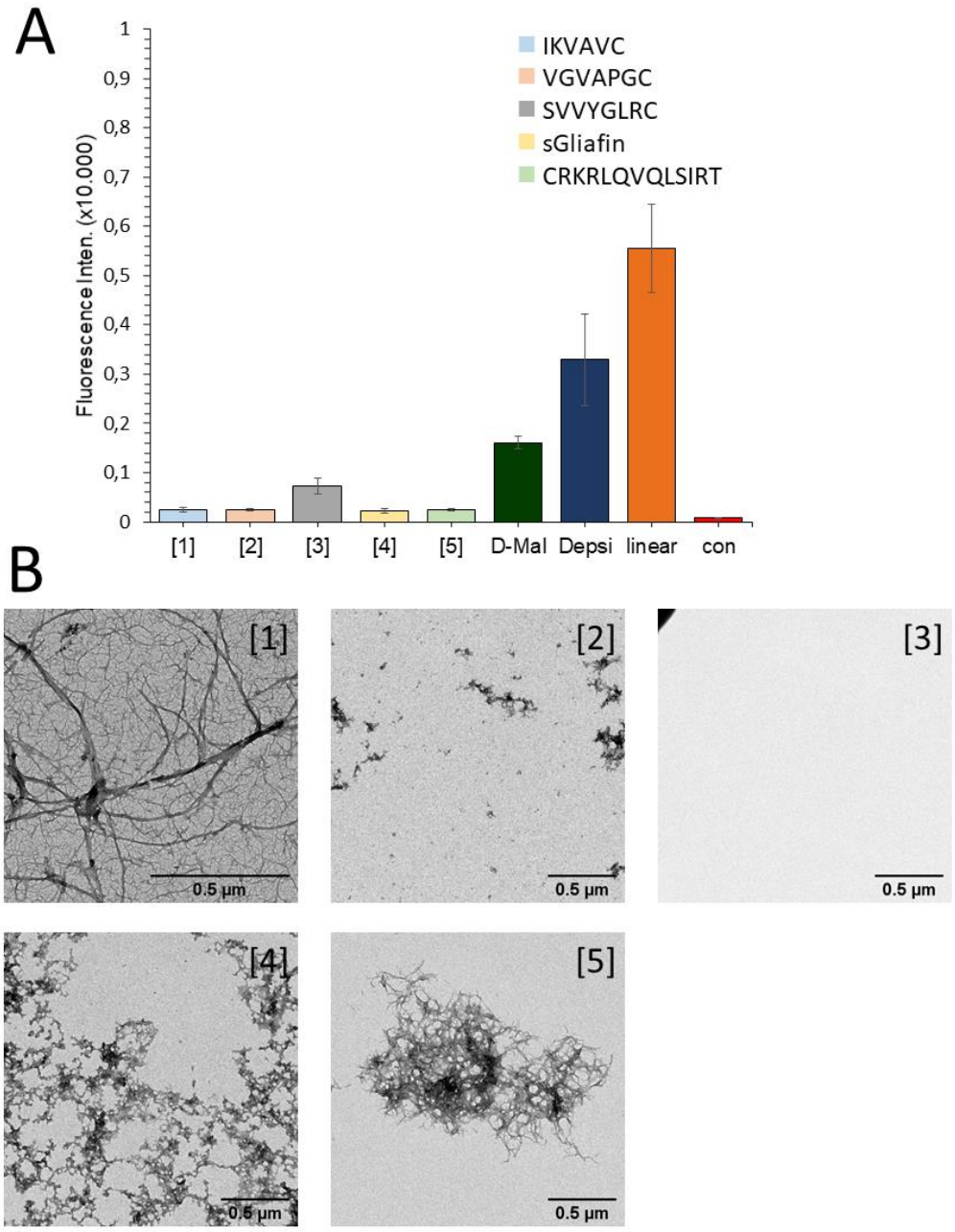

*Figure 18: Results of ThT Assay and TEM micrographs of BAPs (**[1]** – **[5]**). (A) ThT assay, measured after 24 h incubation of the peptides in PBS. In addition, D-Mal, Depsi (D-Mal without maleimide functionalization) and the non-kinked linear KIKISQINM were measured as positive controls. As a negative control (con), only PBS was added. Samples were measured in triplicate and five times per well. (B) Representative TEM pictures after 24 h incubation in PBS of the respective linear BAPs (**[1]** to **[5]**). Scalebars represent 500 nm*

Figure 18, **A** shows the results of the ThT assay. As expected, in most cases the BAPs do not show an increase in ThT fluorescence and therefore no indications of amyloid fibril formation were observed, aside from a slight increase of peptide **[3]**.

If the positive controls (D-Mal to linear, Figure 18, **A**) are taken into consideration, an increasing tendency to interact with Thioflavin T from Depsi-Maleimide to the linear KIKISQINM is visible. This observation is reasonable due to the possible incomplete linearization of the two Depsi peptides therefore showing an, in comparison enhanced, amyloid fibril formation of the linear KIKISQINM. The lower fluorescence intensity of D-Mal in comparison to the unfunctionalized Depsi peptide can be explained by the addition of the maleimide function to the N-terminus of the D-Mal. As the functionalization is not part of the fibril structure, it could interfere with fibrilization und therefore slowing the formation down or interfere with ThT binding to the fiber. However, all three peptides including the self-assembling sequence show an increased ThT fluorescence compared to the background (con) and all BAPs.

To confirm the ThT assay results, TEM measurements were performed (Figure 18, **B**). Fibril structures were observed at **[1]** and **[5]** but no indication for an assembly into amyloid structures was provided by ThT assay. Furthermore, peptide **[1]**, IKVAVC, forms large fibril networks in contrast to peptide **[5]**, which forms networks on single spots on the TEM grid. This observation indicates a formation of super structures of those two peptides that are most likely not amyloid-like. In addition, it is already known that IKVAV-PAs are able to self-assemble.[63] That is why it was expected that IKVAVC would build fibril structures. Moreover, **[2]** and **[4]** aggregate at neutral pH in PBS which is in good agreement with low ThT activity. At last, **[3]** shows neither aggregation nor fibril formation on the TEM grid which is unexpected, due to the signal observed in the ThT assay (Figure 18, **A**). There, a slight fluorescence increase was observed. Possibly, the dissolved peptide interacted with ThT or the formed aggregates did not precipitate on the TEM grid. Since all peptides were measured under the same conditions, the positive ThT assay readout cannot be explained plausibly.

4.1.3.3. Coupling of BAPs to D-Mal and Analysis of D_{MAL}-BAPs

After synthesis of BAPs, a conjugation to D-Mal was performed to yield bioactive fibril forming peptides. For the coupling, the strategy of the thiol-ene reaction proceeding through a Michael-addition pathway was performed. The reaction conditions were adapted from a patent by *Balganesh, M. et al. (1999)*[64] and performed in DMF at room temperature for 48 h on a shaker. The reaction is based on the addition of the nucleophile thiol group to the Michael system of the maleimide group. The mechanism is shown in the following Scheme 8.

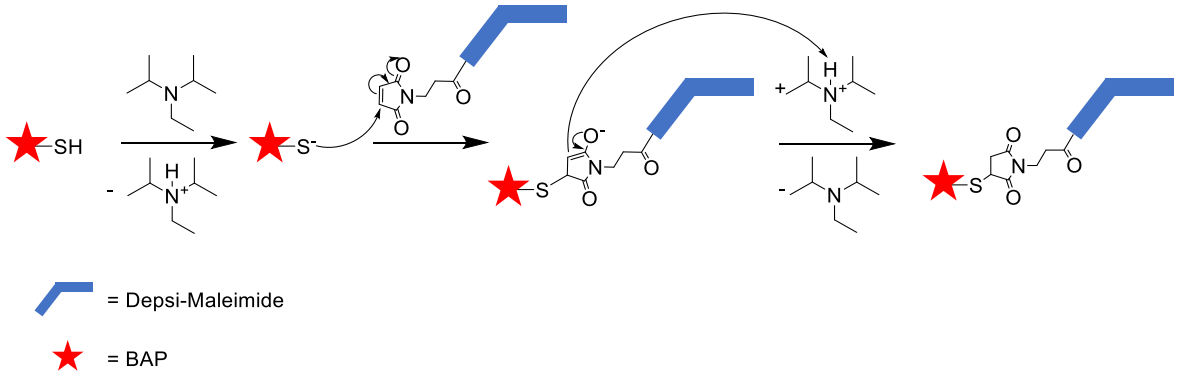

Scheme 8: Coupling reaction of the BAP to the Depsi-Maleimide by thiol-ene Michael addition.

First, a base (DIPEA) abstracts a proton from the thiol group. Then, the activated thiol attacks the Michael acceptor. Finally, protonation and tautomerization results in the Michael product.

The couplings of the self-synthesized BAPs **[1]** to **[5]** to D-Mal were performed according to chapter 6.2.4. Coupling reactions were then repeated using the purchased BAPs, aside from **[5],** which was only coupled with the self-synthesized peptides. The yields are listed in the following Table 4.

Table 4: Yields of the coupling products D_{MAL}-BAP. The first batch (#1) was carried out using the self-synthesized peptide sequences and the second batch (#2) using the purchased ones.

Substance #	Sequence	Yield [mg]	Yield [%]
[7]	IKVAVC-D_{MAL}	1.3 (#1) 2.8 (#2)	86 (#1) 37 (#2)
[8]	VGVAPGC-D_{MAL}	0.8 (#1) 2.7 (#2)	54 (#1) 36 (#2)
[9]	SVVYGLRC-D_{MAL}	1.5 (#1) 1.7 (#2)	87 (#1) 20 (#2)
[10]	D_{MAL}-sGliafin	2.3 (#1) 5.8 (#2)	59 (#1) 59 (#2)
[11]	D_{MAL}-CRKRLQVQLSIRT	2.7	59

The first coupling led to higher yields than the second one, aside from the coupling of D-Mal to sGliafin. The lower yield might be caused by the usage of the purchased peptides, which were harder to dissolve in comparison to the self-synthesized ones, that were yielded as very soft and fluffy powders after lyophilization.

To observe the success of the reaction as well as the purity of the coupling product, MALDI-TOF-MS measurements were performed (see chapter 8.1.). Unexpectedly, some MALDI-TOF-MS spectra showed a high amount of starting material masses indicating an unsuccessful coupling reaction. To investigate whether the reaction did not work entirely, LC-MS measurements (see chapter 6.2.4.) were performed. Exemplarily, the MALDI-TOF-MS spectrum of **[10]**, batch 1 is shown in the following Figure 19, **A**.

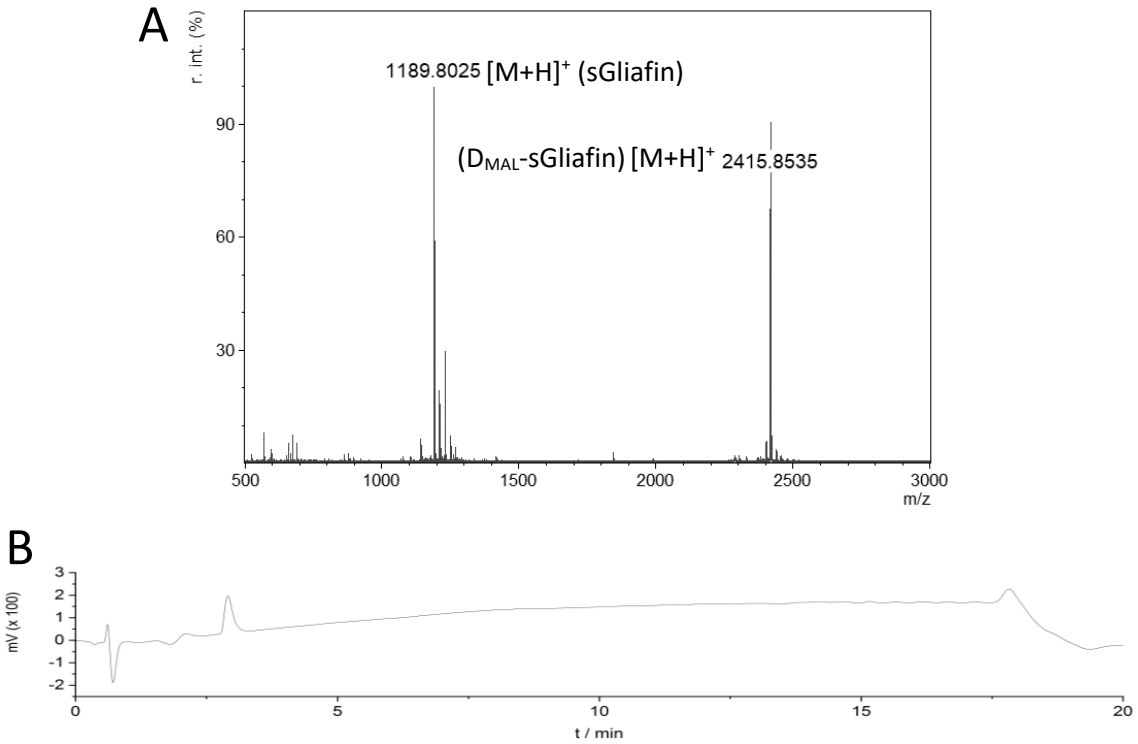

Figure 19: (A) MALDI-TOF-MS spectrum and (B) LC chromatogram of D_{MAL}-sGliafin (D_{MAL}-CILKNLSRSR), batch 1,, after purification via HPLC.

The LC-MS measurement of **[10]** (Figure 19, **B**) confirmed the success of the coupling reaction with a high purity, as well as the LC-MS chromatograms of all coupling products. Therefore, it is possible that the laser intensity of the MALDI was set too high and the product was decomposed during the measurements. Another reason could be differences in the tendency to ionize between educt and product, which may lead to exaggerated signal intensities for the educt. This could be tested by deliberately adding small quantities of the educt to the MALDI sample.

It is known that the Depsi-Maleimide peptide self-assembles in aqueous solution at neutral pH into fibrils[1]. Analogue to chapter 4.1.3.2., ThT assay and TEM measurements were performed to investigate whether the conjugation of BAPs to D-Mal has an impact on fibril formation.

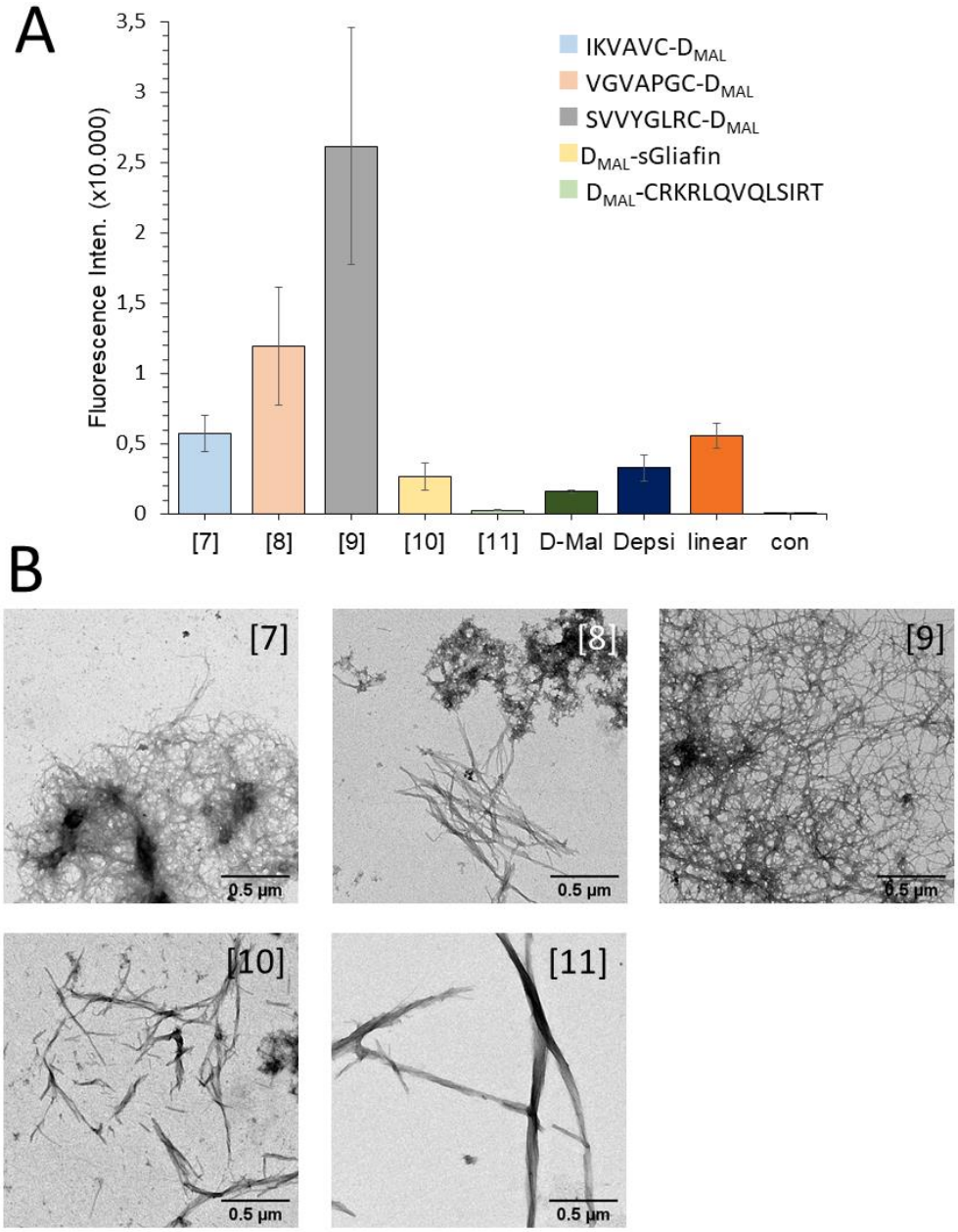

*Figure 20: Results of ThT Assay and TEM micrographs of BAPs coupled to D-Mal (**[7]** – **[11]**). (A) ThT assay, measured after 24 h incubation of the peptides in PBS. In addition, the measurements of D-Mal, Depsi (D-Mal without maleimide functionalization) and the non-kinked linear KIKISQINM from Figure 18 are added to achieve a better comparability. As a negative control (con), only PBS was added. Samples were measured in triplicate and five times per well. (B) Representative TEM pictures after 24 h incubation in PBS of the respective coupled BAPs (**[7]** to **[11]**).*

The results of the ThT-Assay (Figure 20, **A**) show that the functionalization of Depsi-Maleimide with BAPs has an impact on the detected Thioflavin-T fluorescence. Apparently, the coupling of D-Mal with **[3]** results in a strong increase in ThT signal (peptide **[9]**), indicating a strong amyloid fibril formation. Especially compared to the linear KIKISQINM, the average fluorescence signal increases five-fold. A similar, but lower effect occurs at the peptides **[7]** and **[8]**, whereby the intensity measured at peptide **[7]** is similar to the linear KIKISQINM and in comparison, **[8]** is 2.5 times increased. Peptide **[10]** has an identical effect on fluorescence intensity as the Depsi-Maleimide itself. Unexpectedly, **[11]** does not affect Thioflavin-T fluorescence, as it is comparable to the control with PBS. In conclusion, a significant increase in ThT fluorescence signal is observed regarding all BAPs after coupling to D-Mal, except for **[11]**. In many cases, the ThT signal of the conjugates is several times higher than the signal of the D-Mal.

The TEM measurements (Figure 20, **B**) mostly confirm the ThT-Assay results. It is ascertained that the coupling of the bioactive sequences to the Depsi-Maleimide affect amyloid formation. Interestingly, peptide **[11]** assembles into thick and long bundles of fibers that are visible in TEM, despite not showing ThT activity. A possible explanation is that **[11]** does not form amyloid fibrils but other superstructures in which Thioflavin T is not able to intercalate. Alternatively, there is a false negative result in the ThT-Assay. For future comprehensive characterization, IR (infrared) and CD (circular dichroism) spectroscopy should be applied to provide information about the substructure of the fibril and hence, may highlight significance of the ThT assay.

The morphological differences in fibrilization are clarified if the fibril thickness is taken into consideration. Peptides **[7]** to **[9]** are comparable regarding visual fiber formation with an approximate thickness of 30 nm diameter. The fibril bundles of **[10]** are in comparison twice as thick with approximate 60 nm diameter. Remarkably, the peptide **[11]** congregates into large bundles of fibers with a thickness around 100 nm diameter.

In comparison to the BAPs before coupling to D-Mal, structural differences can be observed, often quite substantial. Before coupling, peptides **[2]**, **[3]** and **[4]** did not form fibrils (chapter 4.1.3.2., Figure 18, **B**), but **[2]** and **[4]** formed aggregate-like structures. After coupling, fibril structures are visible (Figure 20, **B, [8]** to **[10])** and the visible morphology of peptides **[8]** and **[10]** has similarities to the pure assembled D-Mal (chapter 4.1.2., Figure 16). In comparison to D-Mal, peptide **[9]** forms more thin and fine fibrils. Furthermore, the morphology of **[11]** is different from the uncoupled peptide. The visible fibrils are much thicker and form bundles of

fibers. Lastly, the only BAP that forms fibrils with comparable morphologies before and after coupling is **[1]** and **[7]**, respectively. In both cases, long and fine networks of fibrils are observed.

In conclusion, coupling of a bioactive peptide sequence to the self-assembling Depsi-Maleimide affects its fibril formation, but does not have an inhibiting effect on fibril formation, even though some of the BAPs did not build fibril structures by themselves.

4.2. *In vitro* Analyses

4.2.1. CellTiter-Glo® Luminescent Cell Viability Assay

To investigate if the bioactive sequences or the coupling products have an impact on cell viability in cell culture, the CellTiter-Glo® Luminescent cell viability assay was performed. Therefore, the assay was performed as described in chapter 6.1.10. using the A549 cell line. The differences in concentration ranges of the peptides arise from the previous uses of these peptides in literature[27,56–58]. BAPs were used by different working groups in various concentrations probably caused by their differences in biological activity.

First, it was analyzed whether the peptides have an adverse effect on the viability of cells. Figure *21* shows that no decrease in cell viability could be observed after 24 h, independent of the concentration and the type of BAP that was added to the culture medium. This indicates that the addition of a cysteine to the bioactive sequences does not affect overall cell survival in normal culture conditions. Peptide **[5]** was not tested due to unexpected insolubility in PBS. In order to reach the final peptide concentration, it was necessary to dissolve the peptide at a higher concentration before addition to the well containing the cells. It should have been able to be dissolved at minimum 200 µg/mL[27] in culture medium, but all attempts to bring the peptide into solution failed. Consequently, the peptide sequence CRKRLQVQLSIRT (**[5]**) was excluded from further experiments.

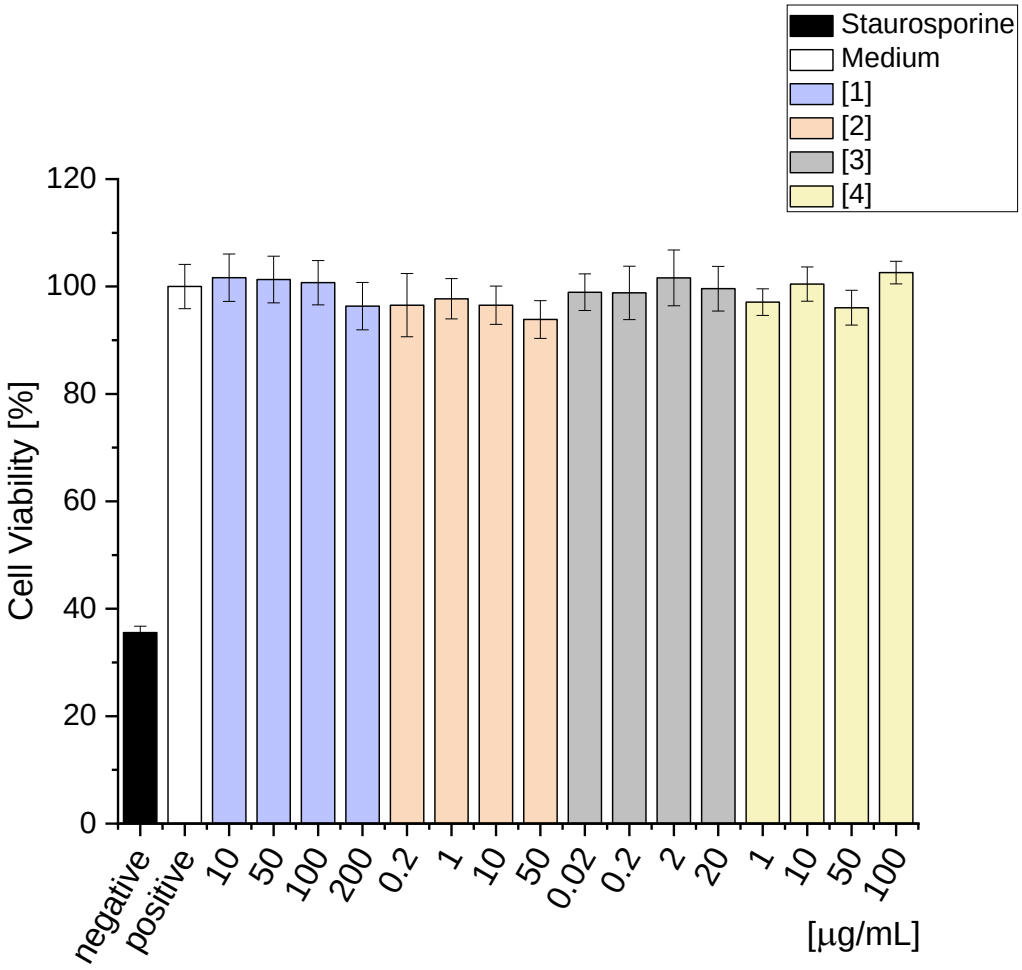

*Figure 21: Results of the CellTiter-Glo Luminescent assay of A549 cells incubated with the pure bioactive sequences (**[1]** to **[4]**). Luminescence detection correlates with cell viability. Staurosporine was added at a concentration of 1 µg/mL. As a positive control medium was added.*

Next, the D-Mal coupled BAPs (**[7]** to **[10]**) were tested on their impacts on cell viability.

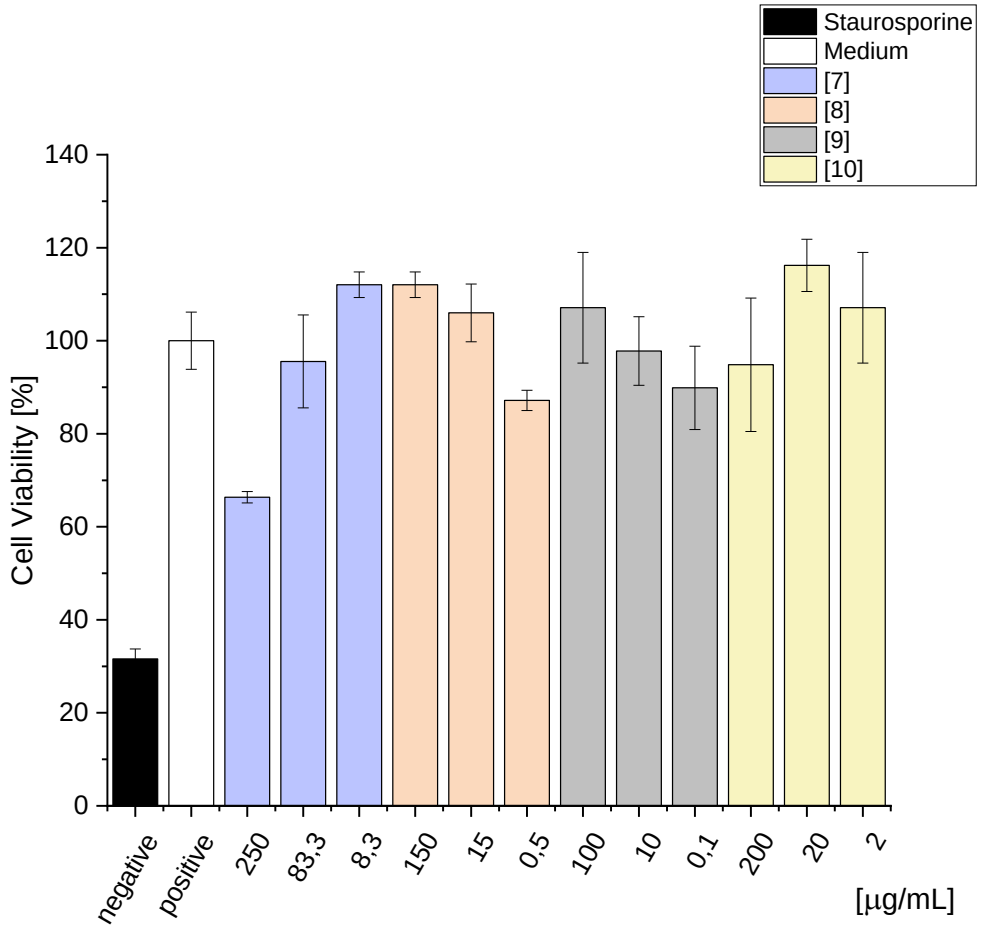

Figure 22: Results of the CellTiter-Glo Luminescent assay of A549 cells incubated with D-Mal coupled bioactive sequences. Luminescence detection correlates with cell viability. Staurosporine was added at a concentration of 1 µg/mL. As a positive control medium was added.

If peptide **[5]** was coupled to D-Mal (**[11]**), it was still not soluble properly and therefore, its effect on cell viability was not tested. Here, the used concentrations were all slightly adjusted to account for the increase of the molecular weight after coupling. Apparently, **[7]** decreases average cell viability after 24 h at high concentrations (250 µg/mL) to approx. 70% (Figure 22). Large gel-like structures of peptide **[7]** were observed in cell culture medium**,** shown in chapter 4.2.2. (Figure 25), which may interfere in the assay. However, it must be taken into consideration, that in the case of **[7]**, the highest overall concentration was used, hence a larger effect on cell viability could also arise from the relatively high peptide concentration. All other tested D_{MAL}-BAPs show different tendencies with increasing concentrations, which is unexpected because it is unusual that lower concentrations of a substance are more toxic than higher ones. In general, the D_{MAL}-BAPs showed higher ThT activity in comparison to single BAPs,

therefore gelling of the conjugates is more likely and may thus correlate with higher toxicity. In addition, differences between the D_{MAL}-BAPs could be ascribed to the large differences in the applied concentration ranges. A comparison with the effects of different concentration D-Mal itself on cell viability would be advantageable because it could be investigated if the decreasing viability correlates with increase of D-Mal concentration.

4.2.2. HUVEC Tube Formation Assay on Matrigel

Next, HUVEC tube formation assays were performed to investigate angiogenic effects of the BAPs.

4.2.2.1. Adjustment of Cell Number

First, an appropriate protocol for HUVEC tube formation assay had to be established. The tube formation of HUVECs can be influenced by many factors, such as cell seeding density, incubation time, presence or absence of serum proteins, underlying matrix, etc. Tubes may not be established properly if the cell number is too low. In comparison, if it is too high, tissue-like monolayers of cells could be formed. Also, the amount present growth factors (GFs) in the medium or Matrigel affects tube formation, whereby an increase in GFs enhances tube formation. At cultivation times above 24 h, HUVECs may undergo apoptosis in tube formation assay, hence the incubation time needs to be adapted.[47]

First, the HUVEC tube formation assay was performed on growth factor reduced Matrigel to identify the appropriate cell number for seeding to be used in later assays. Therefore, an assay was performed as described in 6.1.8. without addition of BAP. Cells were seeded in duplicates on top of Matrigel at concentrations of either 50000 cells/mL or 100000 cells/mL to receive 2500 cells/well or 5000 cells/well by seeding 50 µL of cell suspension, respectively. Pictures of the cells were taken after 4 and 24 h.

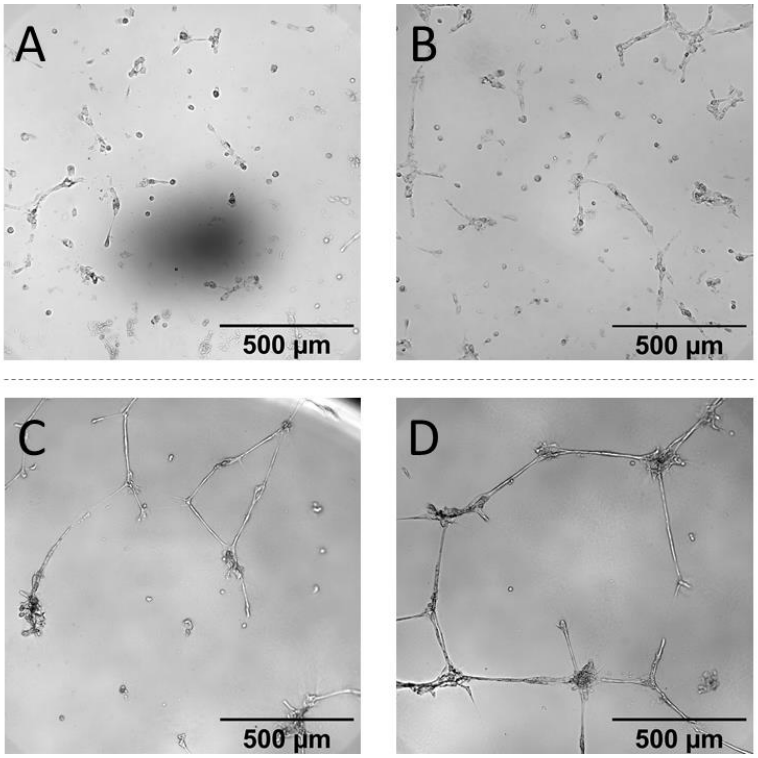

Figure 23: HUVEC tube formation assay for determination of the suitable cell concentration for further assays. (A) 2500 cells/well, after 4 h. (B) 5000 cells/well, after 4 h. (C) 2500 cells/well, after 24 h. (D) 5000 cells/well, after 24 h. Scalebars represent 500 µm.

Figure 23, **A** and **B** illustrate that 4 h of incubation time is too short for HUVECs to differentiate into tube-like structures and change morphology. After 24 h, as can be seen in Figure 23, **C**, just a slight tube formation could be observed after seeding of 2500 cells/well. In comparison, if 5000 cells/well were seeded (Figure 23, **D**), an appropriate amount of tube formation was observed. Thus, in further experiments 5000 cells/well were seeded into the ibidi µ-Slides.

4.2.2.2. Assay with Bioactive Peptides

Next, the HUVEC tube formation assay was performed on Matrigel with addition of the linear BAPs to identify their potential to promote angiogenesis *in vitro* and to optimize the concentration for further assays.

Therefore, a serial dilution of BAPs in PBS to three different concentrations was prepared. The final concentrations cover a wide range of the ones used in literature[27,56–58] and are listed in the following Table 5.

Table 5: Concentrations of the bioactive peptide sequences used in the HUVEC tube formation assay.

	[1]	[2]	[3]	[4]
Concentration [µg/mL]	10	0.2	0.002	1
	100	10	0,2	10
	200	50	20	100

The HUVEC tube formation assay was performed in triplicate, quantified as described in 6.1.8. and pictures of tube formation were taken after 16 h.

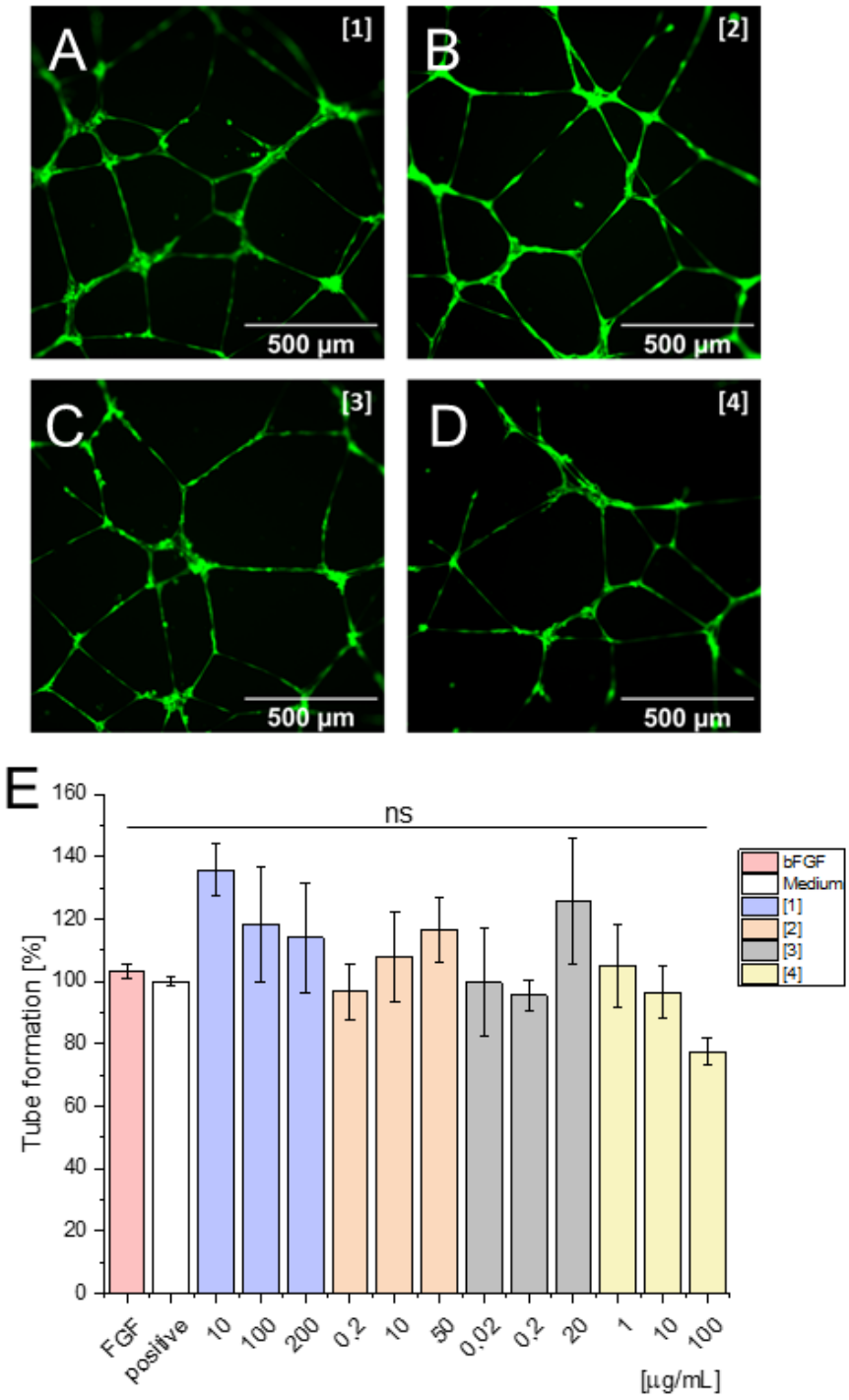

Figure 24: Tube formation of HUVEC cells on growth factor reduced Matrigel after 16 h with addition of different concentrations of bioactive sequences. ***(A - D)*** *Fluorescence photographs of HUVECs after addition of the following peptide concentrations: (A):* ***[1]****, 100 µg/mL; (B):* ***[2]****, 50 µg/mL; (C):* ***[3]****, 0.2 µg/mL; (D):* ***[4]****, 10 µg/mL. Scalebars represent 500 µm. (E) Results of the HUVEC tube formation assay quantified with ImageJ using total tube length as tube formation parameter. Significance was determined using One-way ANOVA with Dunnett. *p<0.05.*

Figure 24 shows the impacts of BAPs on HUVEC tube formation after 16 h. As positive control medium was added. Also, the effect of bFGF (Basic fibroblast growth factor) was tested, but just a slight increase in tube formation was observed. Probably the bFGF concentration was too low with 50 ng/mL to enhance tube formation significantly.

Peptide **[1]** enhanced tube formation the most at the lowest concentration (10 µg/mL). There, tube formation average was increased around 35%. The remaining concentrations increased the tube formation after 16 h around an average of 15 – 20%.

An increase of **[2]** concentration results in enhanced average tube formation, thus showing an opposite trend as IKVAVC. Using **[2]** at a concentration of 50 µg/mL shows the highest effect on tube formation by an average increase of around 18%.

The peptide sequence **[3]** shows the same observable tendency as **[2]** but does also not reach statistical significance. With increasing concentration, the tube formation enhances. The highest impact on tube formation has the concentration of 20 µg/mL, where an average increase of 25% can be observed.

[4] shows an observable tendency to decrease tube formation with increasing concentration. A concentration of 1 µg/mL has almost no impact on the tube formation as well as 10 µg/mL. When using a concentration of 100 µg/mL, the average tube formation decreases around 23%.

In conclusion, the bioactive sequence that seems to enhance tube formation the most is **[1]** (IKVAVC). But in addition, it has to be mentioned that no peptide or concentration enhanced the tube formation statistically significant according to a one-way analysis of variance (*$p<0.05$). However, the results correspond to the expectations, that a tube formation enhancement of the specific pro-angiogenic sequences **[1]** to **[3]** would be observed. Furthermore, the most pro-angiogenic concentration of each BAP could be determined. In addition, the observation that **[4]** does not enhance tube formation of HUVECs is reasonable because it usually affects neuronal cells.[61]

To enhance the possibility of receiving statistically significant differences in the assay, an approach would be to increase the number of tested wells or extend the peptide concentration ranges. It is also possible to test if an increase of added bFGF concentration leads to a significant increase. The change of the quantified parameter from total tube length to number of tubes, nodes, branches or meshes would probably not result in significant results due to high observed correlations of all parameters with each other. Since the lowest possible growth factor presence

was already applied and Matrigel itself seem to enhance tube formation very well, generation of statistically significant trends in tube formation enhancement could be difficult in general. Nevertheless, also the observable tendencies can be used to suggest the most suitable BAP for angiogenesis promotion.

To give a better overview, the concentrations that enhanced average tube formation the most are listed in the following Table 6.

*Table 6: Overview of the peptide concentrations of **[1]** to **[3]** that enhanced tube formation in average to most. **[4]** is not listed due to no observation of considerable enhancement.*

[1] - IKVAVC	[2] - VGVAPGC	[3] - SVVYGLRC
10 mg/mL	50 mg/mL	20 mg/mL

4.2.2.3. Assay with D_{MAL}-BAP

To examine if the coupling of the D-Mal to the BAPs affects the angiogenesis promotion observed in 4.2.2.2., a second HUVEC tube formation test on Matrigel was performed using the peptide conjugates, D_{MAL}-BAPs. Therefore, the peptides were pre-dissolved in PBS to reach the following concentrations in the assay (Table 7).

Table 7: Concentrations of the D-Mal coupled bioactive peptide sequences used in the HUVEC tube formation assay.

	[7] **IKVAVC- D_{MAL}**	**[8]** **VGVAPGC-D_{MAL}**	**[9]** **SVVYGLRC- D_{MAL}**	**[10]** **D_{MAL}-sGliafin**	**[11]** **D_{MAL}-CRKRLQVQLSIRT**
Conc. [µg/mL]	8.3	0.5	0.1	2	2
	83.3	15	10	20	20
	250	150	100	200	-

Again, the sequence **[11]** was much less soluble in PBS than **[7]** to **[10]**. But here, it was first accomplished to dissolve **[11]** at low concentrations (2 and 20 µg/mL) to use them in the following assay.

The HUVEC tube formation assay was again performed in triplicate and quantified as described in 6.1.8. Pictures of tube formation were taken after 16 h.

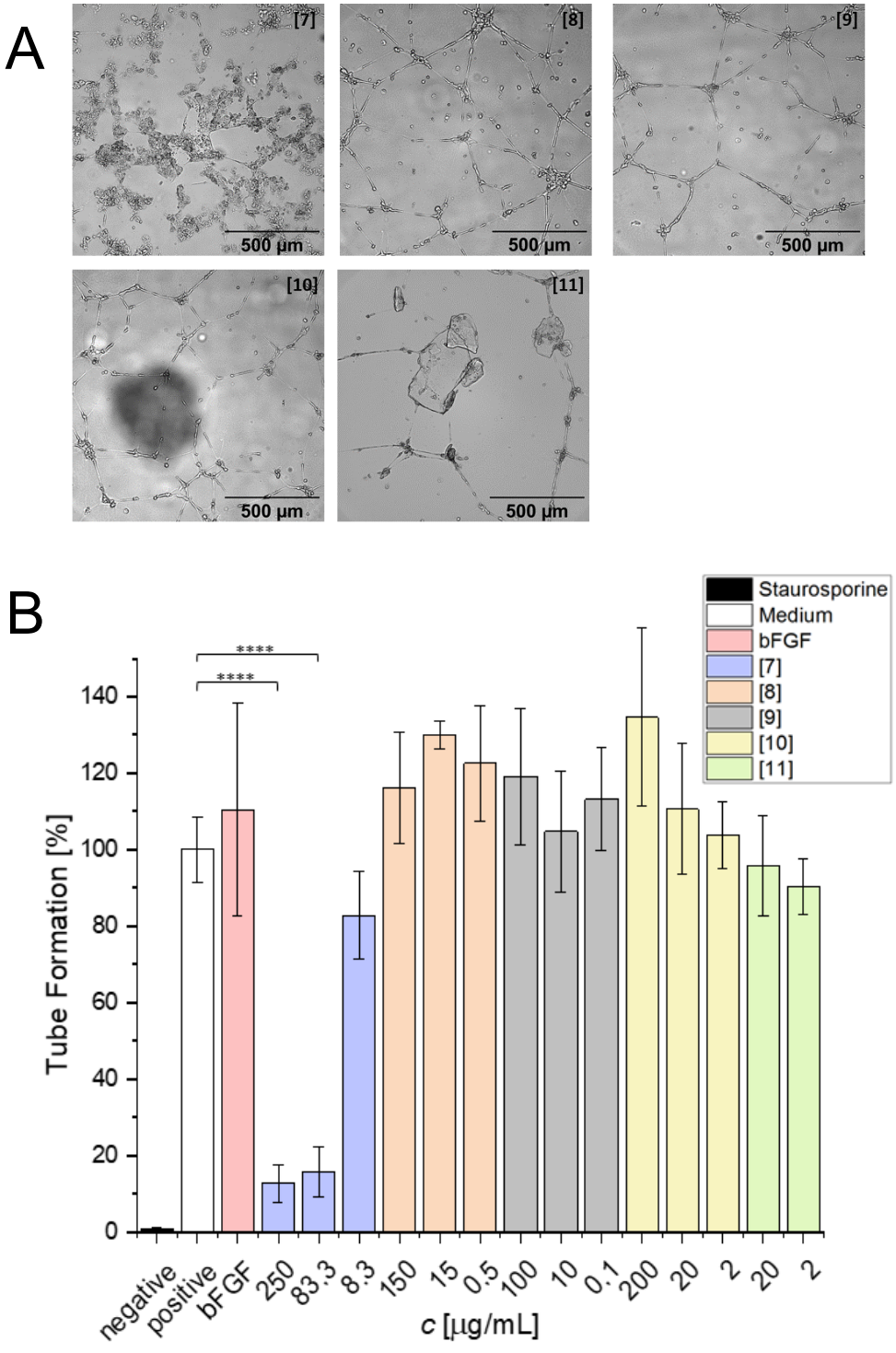

Figure 25: Tube formation of HUVECs on growth factor reduced Matrigel after 16 h with addition of different concentrations of D_{MAL}-BAP. ***(A)*** *Brightfield pictures of tube formation after 16 h on Matrigel after addition of the following D_{Mal}-BAP concentrations:* ***[7]****, 250 µg/mL;* ***[8]****: 0.5 µg/mL;* ***[9]****: 0.1 µg/mL;* ***[10]****: 20 µg/mL;* ***[11]****, 20 µg/mL. Scalebars represent 500 µm.* ***(B)*** *Results of the tube formation assay. ImageJ was used to quantify the tube length as parameter for tube formation. As positive control, medium was added. As negative control, 1 µg/mL staurosporine was used. Significance was determined using One-way ANOVA with Dunnett. *p<0.05, ****p<0.0001).*

This time, an additional negative control was prepared whereby staurosporine, an apoptosis inductor, was used.

The first observation after 16 h of incubation was a gel- or aggregate-like structure formation of some D_{MAL}-BAPs on top of Matrigel accompanied by a decrease in tube formation. This occurred mainly by addition of high concentrations of **[7]** or **[11]** (Figure 25, **A**). An explanation may be the fact that the two BAPs **[1]** and **[5]** also self-assemble without being conjugated to the D-Mal (see Figure 18, chapter 4.1.3.2.). The visible fibril structure of **[11]** varied after coupling where it showed more compact bundles of fibers. Also, the increase of the concentration of **[7]** could have induced the aggregate formation. The HUVECs seem to accumulate close to the aggregate-like structures which is plausible due to promotion of cell adhesion by IKVAV. All in all, the sediments of gels and aggregates, respectively, that were observed for highly concentrated samples, such as **[7]** or changes in fibril formation (**[11]**) could be the reason for the decrease of tube formation by HUVECs.

Unexpectedly, peptide **[10]**, which did not enhance tube formation before coupling (see chapter 4.2.2.2., Figure 24), now seemed to enhance tube formation at high concentrations (200 mg/mL). Possibly, the D-Mal itself has an impact on tube formation at certain concentrations.

The D_{MAL}-BAP that enhanced average tube formation the most was **[8]**, the concentration of 15 µg/mL increased the tube formation in average about 30%. For the rest, different tendencies with high standard deviations were observed. Nevertheless, no statistically significant enhancement of tube formation was observed (statistical analysis, Figure 25) but some observed tendencies were conspicuous.

To give a better overview, the concentrations that enhanced average tube formation the most are listed in the following Table 8.

*Table 8: Overview of the peptide concentrations of **[8]** to **[10]** that enhanced tube formation in average to most. **[7]** and **[11]** are not listed due to no considerable enhancement.*

[8] – VGVAPGC-D_{MAL}	**[8] – SVVYGLRC- D_{MAL}**	**[10] – D_{MAL}-sGliafin**
15 mg/mL	100 mg/mL	200 mg/mL

4.2.3. HUVEC Tube Formation Assay on dcHSA-PD Hydrogel

4.2.3.1. Assay after 24 hours

Due to the ambiguous results of the tube formation assays of chapter 4.2.2.3., the BAPs **[7]** to **[10]** were used for co-assembly with dcHSA in the following assay.

The next step was to co-assemble the D_{MAL}-BAP with dcHSA-PD into the hydrogel (chapter 3., Figure 13). Therefore, two of the D_{MAL}-BAPs (**[9]** and **[10]**) were pre-dissolved in 100 mM phosphate buffer (PB, pH 7.4) at a concentration of 40 µg/mL to be added directly to the solid dcHSA-PD (second batch, dcHSA-PEG(2000)$_{23}$-D-Mal$_{13}$) into an ibidi µ-Slide to form a hydrogel (see chapter 6.1.9.). The other two D_{MAL}-BAPs, **[7]** and **[8],** were added as a solid and dissolved together with the dcHSA-PD in 100 mM PB. Then, the hydrogel was left to assemble for 15 min before 50 µL of cell suspension in medium was seeded on top. After 24 h the cells were stained with Calcein AM. Pictures were taken using a confocal microscope.

While taking pictures of the stained HUVECs, it first occurred that the hydrogel caused high light scattering (Figure 26) or showed autofluorescence. Due to that, besides the brightfield and Calcein AM detection channels, a third detection channel was used set at higher emission and extinction to detect the background light scattering of the hydrogel.

A second difficulty emerged while working at the confocal microscope. Caused by the inhomogeneity and opacity of the hydrogel, it was not possible to detect all cells that were attached to the gel. Therefore, further optimization of the gel preparation was attempted in a next assay (chapter 4.2.3.).

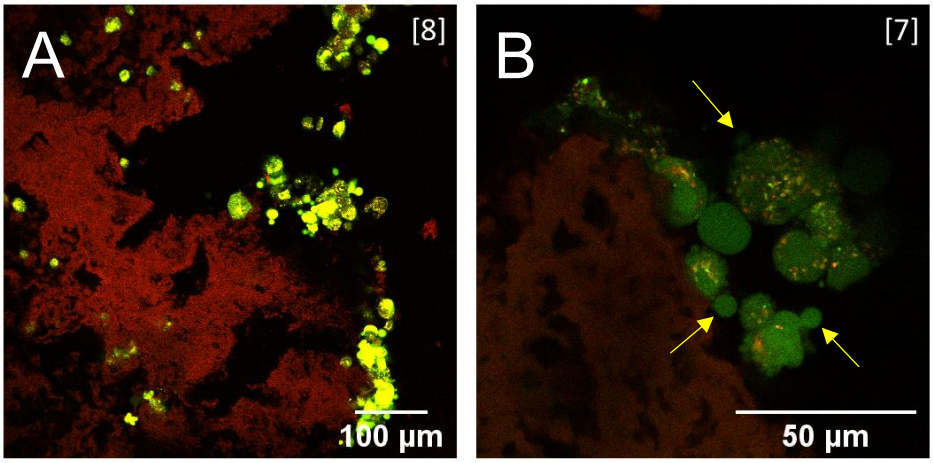

*Figure 26: HUVEC tube formation assay on dcHSA-PD (batch 2) hydrogel co-assembled with (A) **[8]** and (B) **[7]** after 24 h. Green: Calcein AM. Red: Background light scattering. Pictures were taken using a confocal microscope. Scalebars represent 100 µm (A) and 50 µm (B).*

According to the pictures taken after 24 h, no tube formation could be observed (Figure 26). Cells were found in every well, but only **[8]** and **[7]** could be imaged in confocal microscopy properly. In general, cells seem to be attached to the co-assembled hydrogel, but no change in morphology was observed. In addition, the cells did not show the typical HUVEC morphology as it was observed in cell culture (comparable to HUVECs on Matrigel after 4 h, chapter 4.2.2.1., Figure 23, **A** and **B**). Some cells seem to have initiated apoptosis due to observation of blebbing, which is the formation of bulges from the plasma membrane.[65] This can be seen in Figure 26, **B** (arrows) and could have been induced by Calcein AM staining. HUVECs were not fixed after staining and it is known that Calcein AM can induce DNA damage after exposure to blue light, especially by increasing incubation time and longtime exposure.[66] In this experiment, the exposure time and the incubation time were both extended due to the above mentioned difficulties while imaging. Therefore, it is most likely that the apoptosis was induced be the staining solution and long exposure time, because apoptotic cells should not be able to convert non-fluorescent Calcein AM into the fluorescent molecule.

Due to the aforementioned difficulties that arose during the assay, the assumption was made that HUVECs in the hybrid hydrogels need longer incubation times to respond to the bioactive signals and accumulate to form tube-like structures. In addition, possibly the current prepared hydrogels were not perfectly suitable for HUVEC tube formation assay regarding their optical properties. In literature HUVECs remained viable over long periods of 7 days on the dcHSA-PD hydrogel.[1] Due to that, the next attempt was to perform a second assay on co-assembled

hydrogel where cells were incubated for a longer period (8 d) including usage of different batches of dc-HSA.

4.2.3.2. Assay after 8 days

Next, the HUVEC tube formation assay on hydrogel from 4.2.3.1. was repeated, including some changes. First, the hydrogel was left to gel for 24 h at room temperature to enhance the possibility of receiving a more homogeneous gel. Second, three different batches of dcHSA-PD were tested [dcHSA-PEG(2000)$_{23}$-D-Mal$_{13}$ (batch 1, chapter 6.2.5.); dcHSA-PEG(2000)$_{19}$-D-Mal$_{11}$ (chapter 6.2.6., second batch) and dcHSA-PEG(2000)$_{22}$-D-Mal$_{20}$ from *Jasmina Gacanin*[1]]. All three batches were included to investigate if variations to the gel composition (PEGylation degree and number of coupled D-Mal units) affect hydrogel formation and cell response. The co-assembly was confined to the addition of **[7]** to have a better comparability between the dcHSA-PD batches. In addition, 50 µg/mL **[2]** was added to two of the respective three wells per batch, to see if the addition of a BAP to the medium enhances the probability to trigger the HUVECs to undergo changes in morphology.

Every 2 – 3 d, the medium inside the wells was replaced as well as the **[2]** supplement. After 8 d, the cells were stained with Calcein AM and this time, fixed with 4% paraformaldehyde afterwards. Pictures were taken after 8 days using a confocal microscope.

Unfortunately, the opacity of the gels was not improved compared to the previous experiment and the samples were again difficult to image in confocal microscopy. Furthermore, very few cells were found to be attached to the hydrogel.

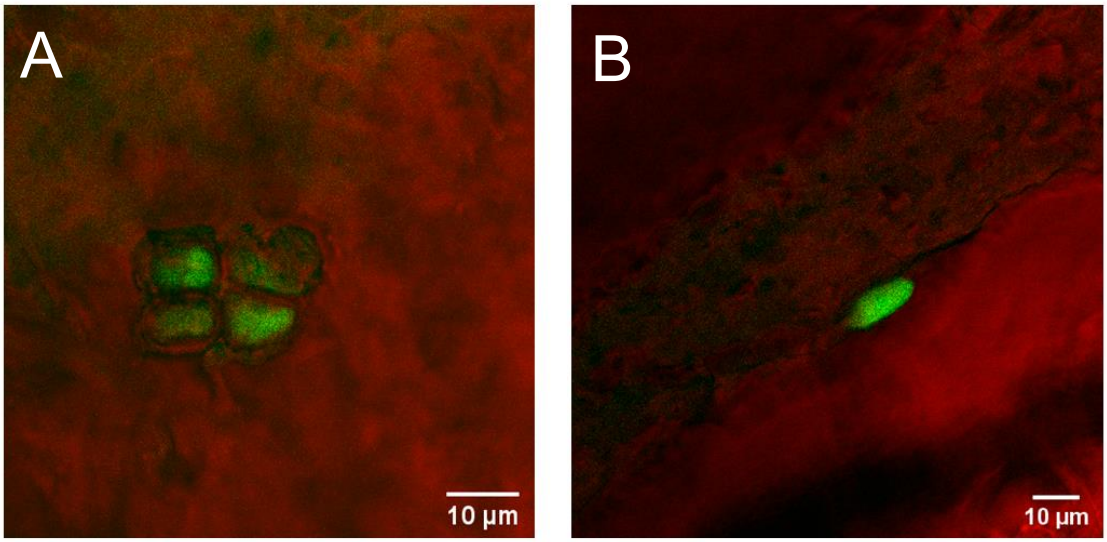

*Figure 27: HUVEC tube formation assay on co-assembled hydrogel after 8 d with addition of 50 µg/mL **[2]** to the medium. (A) dcHSA-PEG(2000)$_{23}$-D-Mal$_{13}$ (batch 2) co-assembled with **[7]**. (B) dcHSA-PEG(2000)$_{22}$-D-Mal$_{20}$ (from Jasmina Gacanin [1]) co-assembled with **[7]**. Scalebars represent 10 µm.*

Nonetheless, some scattered cells were observed embedded in the hydrogel (Figure 27). In Figure 27, **A,** presumably four cells resulting from proliferation of one or two cells can be observed. Regarding **B**, only one isolated cell could be observed. It is possible that cells were removed during the exchange of medium. Perhaps, the cells were not attached properly to the gel and so HUVECs were washed out by the medium change. Furthermore, a change in morphology of HUVECs or tube-like structure formation could again not be observed in this assay. Despite everything, an improvement could be achieved through fixation of cells because in this assay, no apoptotic cells could be observed. Therefore, it is most likely that the apoptotic cells found in the previous assay (chapter 4.2.3.1., Figure 26) induced apoptosis due to Calcein AM staining and the long imaging process.

In future assays, an improvement could be achieved by changing medium more careful or through a solely partly replacement of the medium. In addition, a varying mixture of the bioactive components inside the hydrogel could be applied for a successful assay. The outlook is described more detailed in the next chapter.

5. Conclusion and Outlook

The main aim of the project was to add bioactive components to the previously described peptide-protein hybrid hydrogel[1] to generate a biocompatible material for tissue engineering. Hence, the dcHSA-PD was synthesized after a recently published protocol[1] and purified. The synthesis yielded two slightly different types of dcHSA-PD with either higher or lower PEGylation and a lower D-Mal coupling rate as the reported peptide-protein hybrid (*Gacanin, J. et al., 2019)[1].*

Next, the Depsi-Maleimide (Maleimide-KIKI(COO-)SQINM) was synthesized twice and yielded sufficient amounts of peptide to conduct the subsequent study. Additionally, five angiogenesis promoting sequences from literature were synthesized containing a cysteine either at the N- or C-terminus for coupling to the maleimide function of the D-Mal. Caused by side reactions with the Fmoc-Cys(Trt) Wang resin, four of the five sequences were purchased. The couplings of the BAPs to the D-Mal were successful and showed adequate yields. TEM measurements confirmed fibril formation of all coupled D_{MAL}-BAPs, albeit with significant differences in the fiber diameters and lengths. In addition, results from a ThT assay indicated that most BAP conjugates also form amyloid structures. Furthermore, the bioactive peptides **[1]** and **[5]** self-assembled into fibrous structures without conjugation to D-Mal.

Moreover, *in vitro* assays were performed to investigate the suitability of the BAPs and D_{MAL}-BAPs in promoting angiogenesis and effects on cell viability. Here, it was first observed that peptide **[5]** was insoluble at the desired concentrations. The CellTiter Glo cell viability assay showed that the BAPs have no toxic effect on A549 cells in a time range of 24 h. In comparison, the addition of the coupled D_{MAL}-BAPs affected the cells, especially in the case of peptide **[7]**, but not significantly. A protocol for HUVEC tube formation assay was established and performed first by addition of the BAPs in different concentrations. It was ascertained that **[1]**, IKVAVC, enhanced average tube formation the most. Particularly noteworthy is that all BAPs increased tube formation, aside from high concentrations of **[4].** Furthermore, the test was repeated using D_{MAL}-BAPs instead. Here, high concentrations of the conjugated **[1]** (**[7]**) decreased tube formation dramatically. Especially peptides **[7]** and **[11]** built visible aggregate-/gel-like structures on top of the Matrigel which seem to be the reason for the decrease.

At last, the HUVEC tube formation assay was performed using the dcHSA-PD hydrogel instead of Matrigel. In addition, the hydrogel was co-assembled with D_{MAL}-BAPs. It turned out that the HUVECS attached to the hydrogel but did not change morphology after 24 h as it was observed

in the assays performed on Matrigel. In addition, apoptotic membrane blebbing of HUVECs was observed. Therefore, the incubation time was extended to 8 days and cells fixed after Calcein AM staining. However, still no tube formation of HUVECs could be observed after the increased incubation time and very few cells were still attached to the gel. Additionally, this time no indication of apoptosis was observed.

For future assays, the HUVEC tube formation assay on Matrigel has to be improved to show statistically significant differences regarding angiogenesis promoting. Therefore, a first attempt is to prepare mixtures of the D_{MAL}-BAPs to enhance tube formation more significant. The consideration hereby is to reach a better ECM mimic. It consists of numerous different components and therefore, various stimulation signals could enhance the cell response. Additionally, the mixture could also be co-assembled with dcHSA-PD and applied in further assays. Nevertheless, the hydrogels have to be improved regarding their homogeneity and therefore their optical properties.

Second, another approach is to perform a 3D assay. A suitable assay is the HUVEC spheroid sprouting assay, where HUVECs make up a 3D model. Regarding human physiology, 3D *in vitro* assays are more proximal and the *in vitro* advantages still remain.[67] The 3D HUVEC spheroid sprouting assay is suitable for ECM mimicking materials with more permissive, softer characteristics.[68] Hence, it would be suitable for the here presented co-assembled hydrogel since no homogeneous surface for a 2D assay could have been prepared. In addition, the before mentioned attempt to try a mixture of D_{MAL}-BAPs could also be applied to this assay. Exemplarily, spheroid formation can be seen in Figure 28.

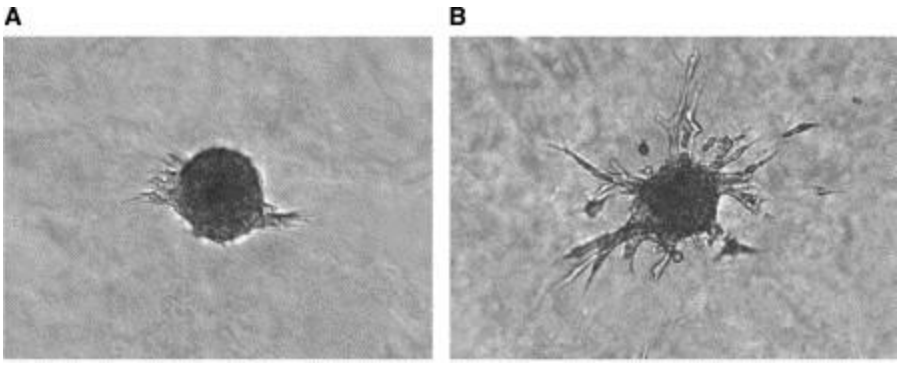

Figure 28: Example of HUVEC spheroid sprouting in collagen gel (by Stahl, A. et al., 2005).[69]

Third, a HET-CAM assay could be performed, which is an *in vitro* assay that is usable to detect angiogenetic activity. If the hydrogel is applied to the CAM, angiogenetic effects can be

visualized by sprouting of new blood vessels in the area of application, whereby this assay simulates a more appropriate *in vivo* application.[70]

Lastly, it would be helpful to integrate a 3D gradient into the hydrogel. Angiogenetic sprouting usually follows a biochemical gradient (chapter 2.1.4.1., Figure 6), whereby vessels sprout into the direction of the highest signal concentration. Due to the dynamics and self-healing properties of the dcHSA-PD hydrogel, a gradient could easily be formed by preparing two dcHSA-PD hydrogels, one co-assembled with D-Mal, one with D_{MAL}-BAPs. If those are brought into contact, the dynamics of the hydrogel could affect the formation of a gradient by exchange of D-Mal and D_{MAL}-BAP between the gels. Through different analysis methods like TCCD (Two Color Coincidence Detection)[71] or FRAP (Fluorescence Recovery After Photobleaching)[72] the dynamics of the co-assembled dcHSA-PD hydrogel could be understood better and the success of gradient formation be verified using fluorescence labeled D-Mals.

6. Experimental Section

6.1. Experimental Procedures

All chemicals used in this work were purchased and used as received.

6.1.1. Solid Phase Peptide Synthesis (SPPS)

All peptide sequences were synthesized using the Fmoc-based strategy of solid-phase peptide synthesis from C to N-terminus. As coupling reagents for amide bonds DIC (activator) and Oxyma (activator base) were used in all syntheses and peptides were purified using reversed-phase HPLC. The following Scheme 9 gives an overview of the respective synthesis steps and the used chemicals.

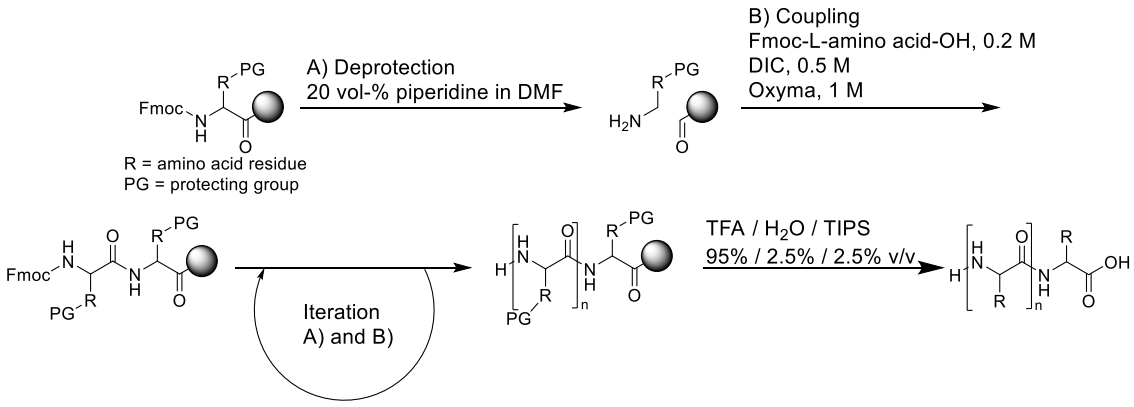

Scheme 9: Scheme of the solid phase peptide synthesis performed by an automated peptide synthesizer.

First, the mass of a preloaded resin was calculated referred to its loading, weighted and left to swell on a shaker in a few mL of DMF for one hour. Afterwards, the resin was introduced into the *Liberty Blue Automated Peptide Synthesizer* from *CEM* as well as the following reagents (Table 9).

Table 9: Reagents and their concentrations used for the automated peptide synthesis.

Batch size	Wash solvent	Deprotection cocktail	Amino acid conc.	Activator conc.	Activator base conc.
0.1 – 0.5 mmol	DMF	20 vol-% Piperidine in DMF	0.2 M	0.5 M DIC in DMF	1.0 M Oxyma in DMF

The first step of the automated peptide synthesis was the washing of the resin with DMF (5 min). Then, the first amino acid was deprotected by injection of 20 vol-% piperidine in DMF to the resin and a temperature / time setting of 75 °C / 15 s followed by 90 °C / 50 s. Then, a single coupling step was set where the respective amino acid dissolved in DMF was injected with a temperature / time setting of 75 °C / 15 s followed by 90 °C / 110 s. A double coupling step was only set for Fmoc-*L*-Arg(Pbf)-OH whereby the single coupling step was repeated. Each coupling step was followed by a deprotection step. After the final deprotection, the resin was removed from the reaction vessel using DCM and dried under an airflow.

For cleavage of the peptide from the resin, a mixture of TFA : H_2O : TIPS (95 : 2.5 : 2.5 %v/v) was prepared. For 0.1 mmol batches, 2 mL of cleavage solution was prepared, which was upscaled for larger batches. Then, the solution was introduced to the resin and shaken for 2 h. Afterwards, the peptide in cleavage solution was added dropwise to 50 mL ice cold diethyl ether to precipitate. It was centrifuged for 10 min at 4000 rpm and 4 °C. Then, the diethyl ether was decanted, and the precipitate was kept under an airflow to dry.

6.1.2. Peptide Coupling

Adapted from the patent from *Balganesh, M. et al. (1999)*[64], the Michael addition of the cysteine thiol to the double bond of the maleimide was performed by adding 1 eq of the respective bioactive peptide dissolved in 30 µL DMF to 1 mg of the D-Mal ($8.2 \cdot 10^{-7}$ mol) dissolved in 30 µL DMF. Immediately, 1 µL of DIPEA ($5.7 \cdot 10^{-6}$ mol, 7 eq) was added to the mixture and incubated on a shaker (1000 rpm) for 24 – 48 h. Then, the solvent was removed with a Schlenk line and the dried coupling product was dissolved in *Milli-Q* H_2O + 0.1 vol-% TFA for purification via reversed-phase HPLC.

6.1.3. High-Performance Liquid Chromatography (HPLC)

The purification of synthesized peptides was carried out via RP-HPLC. Therefore, the dried peptide was dissolved in *Milli-Q* H_2O + 0.1 vol% TFA at a concentration of 1 – 5 mg/mL with the assumption of 100% yield. Then, the solution was filtered using a *Rotilabo® syringe filter nylon, 0.2 µm* and injected into HPLC via manual injection. For purification of all peptides, the following gradient (Table 10) at a flow rate of 10 mL/min was set at the HPLC device from *Shimadzu*

containing the units *DGU-20A5R, LC-20AT, CBM-20A, CTO-20 AC, SPD-M20A, SIL-20AC HT, FRC-10A* with usage of the *Kinetex® 5 µm EVO C18 100 Å Phenomenex* column.

Table 10: Gradient of RP-HPLC used for purification of all peptides.

Time [min]	**0 – 5**	**5 – 35**	**35 – 40**	**40 – 45**	**45 – 50**	**50 – 55**
ACN [%]	0	0 – 40	40 – 100	100	100 – 0	0

6.1.4. Mass Spectrometry

To control the success of the reactions or purifications, mass spectrometric methods were used.

For **MALDI-TOF-MS** (matrix-assisted laser desorption/ionization time-of-flight mass spectrometry) measurements, the peptide sample was dissolved in *Milli-Q* H_2O + 0.1 vol-% TFA. As matrix CHCA (α-Cyano-4-hydroxycinnamic acid) was used. As matrix for dcHSA-PD samples sinapinic acid was used. The device used for measuring samples was *Waters MALDI SYNAPT G2-Si HDMS*.

For **LC-MS** (liquid chromatography – mass spectrometry) measurements, peptide samples were prepared at 1 mg/mL in *Milli-Q* H_2O + 0.1 vol-% TFA. After dilution to 1 µg/mL, the sample was measured using *Milli-Q* water and acetonitrile + 0.1 vol-% formic acid as solvents. The used device was *Shimadzu LCMS-2020 Single Quadrupole MS* using a *Kinetex® 2.6 µm EVO C18 100 Å Phenomenex* column. The gradient was set at 5 - 95% acetonitrile / 20 min.

6.1.5. Transmission electron microscopy (TEM)

The peptides were incubated for 24 h on a shaker (1000 rpm) at a concentration of 1 mg/mL in filtered (*Rotilabo® syringe filter nylon, 0.2 µm*) PBS, diluted from a DMSO stock solution (10 mg/mL).

For TEM measurements, TEM grids from *plano GmbH*, *Item-Nr.: S162-3, Formvar/carbon film on 3.05 mm Cu-nets, 300 mash* were used. The TEM grids were plasma cleaned prior to use. Then, 10 µL of 1% uranyl acetate solution were pipetted onto a piece of parafilm. The TEM grids were covered with the peptide by pipetting 4 µL of the peptide solution on top of the grid and were incubated for 5 min. Afterwards, the solution was removed from the edge of the grid using a

filter paper and the grid was placed upside down on top of the uranyl acetate drop. After an incubation time of 2.5 min, the TEM grid was removed from the drop and washed three times with *Milli-Q* H_2O and left to dry for around 15 min. The measurements were performed using a *JEOL 1400* transmission electron microscope.

6.1.6. Thioflavin-T Assay (ThT Assay)

For ThT assay, the peptides were incubated for 24 h on a shaker (1000 rpm) at a concentration of 1 mg/mL in filtered PBS (*Rotilabo® syringe filter nylon, 0.2 µm*) prepared from a DMSO stock solution (10 mg/mL). Afterwards, 10 µL of 50 µM ThT solution in PBS were placed in a 384 well plate. 2 µL of each peptide solution was introduced in triplicate and incubated for 10 min in the dark. Then, fluorescence was measured using a *Spark® Multimode Microplate Reader* by *Tecan* at an excitation of λ_{ex} = 440 nm and an emission of λ_{em} = 488 nm with a bandwidth of 10 nm, respectively. Each well was measured five times in different positions.

6.1.7. HUVEC cell culture

HUVEC/TERT66 (Human Umbivial Vein Endothelial Cells) were purchased from *EVERCYTE* and cultured according to the manufacturer's instructions. The cells were split 1:2 after reaching 90-95% confluence (every 2-3 d) and were kept in complete supplemented Endopan 3 or Endopan 300 (*PAN-Biotech*). For splitting see chapter 6.1.8.

6.1.8. HUVEC Tube Formation Assay on Matrigel®

The HUVEC tube formation assay was adapted from a protocol by *ibidi GmbH (2018)*[73]. First, 10 µL of Matrigel with reduced growth factors was pipetted into an ibidi µ-Slide on ice and placed inside of a petri dish in a humdified incubator (37 °C, 5% CO_2) for 0.5 – 1 h to gel. In addition, a T-25 flask was covered with 1.5 mL 0.1% gelatine in PBS and incubated for 10 – 60 min. In the meantime, HUVECs were harvested and split. Therefore, the medium was discarded and the flask washed twice with 3 mL PBS. Then, 500 µL trypsin was added and incubated until complete detachment of the cells (3-4 min). 500 µL of trypsin inhibitor was added and subsequently 4 mL of medium. The cells were washed down from the surface by resuspending the solution thoroughly and put into a 15 mL Falcon tube. The tube was centrifugated at 200 × g for 5 min. Then, the supernatant was removed, 1 mL of new medium

added and the cells resuspended. 10 µL of cell suspension were mixed with 10 µL of trypan blue staining solution and pipetted into a chamber slide. The cells were counted using the *Invitrogen™ Countess™ Automated Cell Counter*. Next, the cells were diluted to $1.04 \cdot 10^5$ cells/mL to reach a density of 5000 cells/well. Then, respective 49 µL of the cell suspension was seeded into each well of the with Matrigel covered µ-Slides. Lastly, 1 µL of a peptide dissolved in PBS was added in triplicate. The slides were incubated inside of a petri dish in the incubator. After 16 h, cells were stained with Calcein AM. Therefore, 3.1 µL of a 100 µg/mL Calcein AM solution in PBS was added to each well and incubated in the dark at 37 °C for 30 min. Afterwards, pictures of the stained cells were taken with a *Leica inverted fluorescence microscope DMi8* using a *Leica DFC9000 GT* camera at an extinction of 480 nm (40 nm bandwidth) and emission of 527 nm (30 nm bandwidth). Besides, brightfield photos were taken of each sample. The tube formation was quantified using ImageJ Angiogenesis Analyzer PlugIn[50].

6.1.9. HUVEC Tube Formation Assay on Hydrogel

The tube formation assay on the peptide-protein hybrid hydrogel was performed similar to the assay on Matrigel (6.1.8.), with the exception of the matrix preparation. Therefore, the hydrogel (4 wt% dcHSA-PD, 0.4 mg in 10 µL of 100 mM filtered phosphate buffer, pH 7.4) was prepared directly in an ibidi µ-Slide and was allowed to gel for either 15 min or 24 h. In addition, coassembled hydrogels were also prepared. Therefore the respective D_{MAL}-BAP was either weighted and added as a solid to the dcHSA-PD before addition of phosphate buffer or pre-dissolved in 100 mM phosphate buffer. After incubation time, if cells had to be fixed, the Calcein AM staining solution was discarded and 50 µL of 4% paraformaldehyde was added to the well and incubated for 30 min at room temperature. Then, the fixing solution was discarded, PBS added and pictures were taken using a confocal laser scanning microscope (*Leica TCS SP5, Wetzlar, Germany*) containing a *HCX IRAPO L 25.0x0.95 WATER objective*. Pictures were taken at an extinction wavelenght of 458 nm for Calcein AM detection and 561 nm for background detection, as well as detection of emission in the range of 479 nm – 541 nm for Calcein AM and 575 nm – 648 nm for background detection.

6.1.10. CellTiter-Glo® Luminescent Cell Viability Assay

For this assay, the cell line A549 was used and cultivated in DMEM according to the manufacturer's instructions. A cell suspension of 180000 cells/mL was prepared to seed 50 µL (9000 cells/well) in a 96 well plate. The plate was incubated for 24 h in a humdified incubator (37 °C, 5% CO_2). Then, the medium was discarded and the wells washed with 50 µL of medium. 49 µL of fresh medium was added to the wells and 1 µL of the respective peptide solution in DPBS was added in triplicate. As a negative control, 5 µL of a 10 µM staurosporine solution and as a positive control medium was added in triplicate. After 24 h in the incubator, the supernatant was discarded, the wells washed with 50 µL PBS and 50 µL of medium was added. Three additional empty wells were filled with 50 µL of medium to measure the background luminescence. Lastly, 50 µL of CellTiter-Glo® reagent was added to each well and luminescence was measured with a luminometer (*GloMax®-Multi Detection System by Promega*) after 10 min incubation time.

6.2. Syntheses and Yields

6.2.1. Synthesis of Depsi-Maleimide [KIKI-(COO)SQINM]

The synthesis of Depsi-Maleimide was performed in four steps that are consecutively listed in the following.

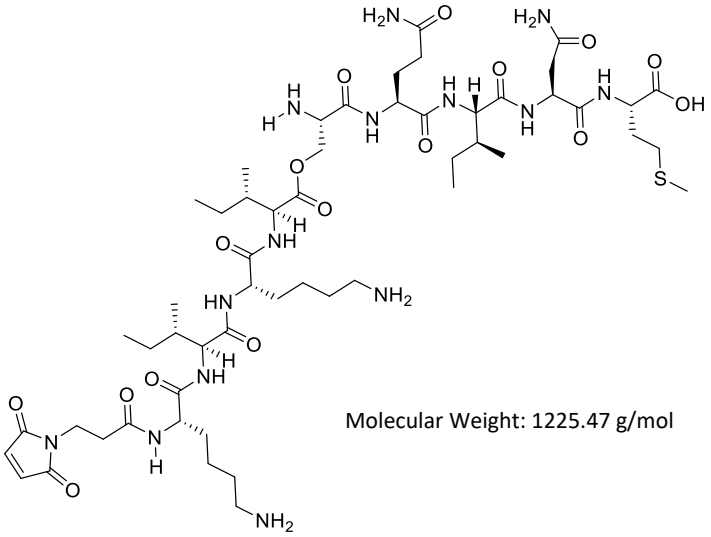

Figure 29: Chemical structure of D-Mal.

6.2.1.1. Synthesis of SQINM

First, the C-terminal sequence (SQINM) was synthesized. Therefore, preloaded Fmoc-Met-Wang resin (100-200 mesh, loading: 0.68 mmol/g, 0.37 g, 0.25 mmol) was left to swell on a shaker (200 rpm) in 2 - 3 mL DMF for one hour. Afterwards, the resin was introduced into the *Liberty Blue Automated Peptide Synthesizer* as well as the following reagents dissolved in DMF. The synthesis was performed according to chapter 6.1.1.

Fmoc-*L*-Asn(Trt)-OH (0.72 g, 0.5 mmol, 2 eq, dissolved in 6 mL DMF), Fmoc-*L*-Ile-OH (0.42 g, 1 mmol, 2 eq, dissolved in 6 mL DMF), Fmoc-*L*-Gln(Trt)-OH (0.73 g, 1 mmol, 2 eq, dissolved in 6 mL DMF), Boc-Ser-OH (0.25 g, 1 mmol, 2 eq, dissolved in 6 mL DMF), DIC (0.81 g, 6.5 mmol, 26 eq, diluted in 12 mL DMF), Oxyma (1.00 g, 7 mmol, 28 eq, dissolved in 7 mL DMF).

After each coupling step a deprotection with 20 vol-% piperidine in DMF was carried out. Finally, the resin was removed from the reaction vessel with DCM and dried under an air flow.

6.2.1.2. Synthesis of I(COO-)SQINM

Next, the ester coupling of the OH-protected Serine of the SQINM with Fmoc-*L*-Ile-OH was performed to receive the Depsi sequence I-(COO)SQINM. Therefore, the dried SQINM peptide was mixed with 4-DMAP (30.55 mg, 0.25 mmol, 1 eq), DIC (77.25 µL, 0.5 mmol, 2 eq) and Fmoc-*L*-Ile-OH (883.53 mg, 2.5 mmol, 10 eq) in 2-3 mL DMF and was incubated on a shaker for 2 h. Then, the reaction solution was removed, and the resin washed several times with DMF. The reaction mixture was renewed and shaken for another 24 h. At last, the reaction solution was removed, and the resin again washed several times with DMF.

6.2.1.3. Synthesis of KIKI(COO-)SQINM

To complete the peptide synthesis, the remaining three amino acids (KIK) were coupled to the I-(COO)SQINM peptide using the peptide synthesizer. The synthesis was performed according to chapter 6.1.1. Therefore, Fmoc-*L*-Lys(Boc)-OH (2.25 g, 2 mmol, 4 eq, dissolved in 24 mL DMF), Fmoc-*L*-Ile-OH (0.85 g, 1 mmol, 2 eq, dissolved in 12 mL DMF), DIC (1.05 g, 8.5 mmol, 17 eq, diluted in 17 mL DMF), Oxyma (1.42 g, 10 mmol, 20 eq, dissolved in 10 mL DMF) were introduced into the automated peptide synthesizer. After the synthesis, the resin was removed from the reaction vessel with DCM and again dried under an air flow.

6.2.1.4. Synthesis of Mal-KIKI(COO-)SQINM

The last step was the N-terminal functionalization of the Depsi peptide with a maleimide group. Therefore, 3-maleimidopropionic acid *N*-hydroxysuccinimide ester (133.11 mg, 0.5 mmol, 2 eq) and DIPEA (217.70 µL, 1.25 mmol, 5 eq) were dissolved in 2 – 3 mL DMF and introduced to the dried KIKI-(COO)SQINM resin. The reaction mixture was left on a shaker for 72 h, then washed twice with DMF and DCM, respectively and dried under an airflow.

The synthesis yielded 37.3 mg (0.03 mmol, 12%).

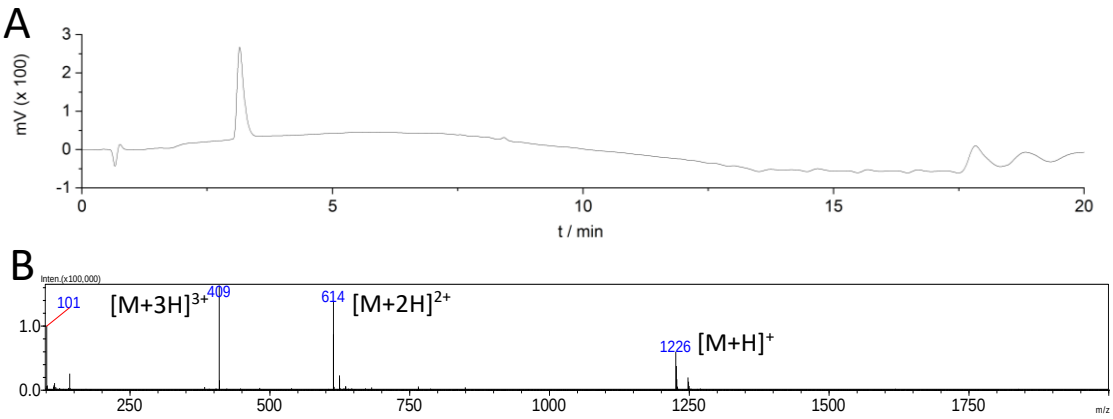

Figure 30: (A) LC chromatogram and (B) positive ion mode mass spectrum of integrated LC peak of D-Mal.

6.2.2. Synthesis of Depsi-Maleimide – Second Batch

A second batch of D-Mal was synthesized. Thereby, the procedure from chapter 6.2.1. was applied. In the following, solely the used chemicals and concentrations for the synthesis are listed as well as the yield.

6.2.2.1. Synthesis of SQINM

Fmoc-Met-Wang resin (100-200 mesh, loading: 0.68 mmol/g, 0.74 g, 0.5 mmol), Fmoc-*L*-Asn(Trt)-OH (1.44 g, 1 mmol, 2 eq, dissolved in 12 mL DMF), Fmoc-*L*-Ile-OH (0.85 g, 1 mmol, 2 eq, dissolved in 12 mL DMF), Fmoc-*L*-Gln(Trt)-OH (1.47 g, 1 mmol, 2 eq, dissolved in 12 mL DMF), Boc-Ser-OH (0.49 g, 1 mmol, 2 eq, dissolved in 12 mL DMF), DIC (1.37 g, 11 mmol, 22 eq, diluted in 22 mL DMF), Oxyma (1.71 g, 12 mmol, 24 eq, dissolved in 12 mL DMF).

6.2.2.2. Synthesis of I(COO-)SQINM

Fmoc-*L*-Ile-OH (1.77 g, 5 mmol, 10 eq, dissolved in 5 mL DMF), 4-DMAP (61.10 mg, 0.5 mmol, 1 eq), DIC (154.50 µL, 0.5 mmol, 2 eq).

6.2.2.3. Synthesis of KIKI(COO-)SQINM

Fmoc-*L*-Lys(Boc)-OH (2.25 g, 2 mmol, 4 eq, dissolved in 24 mL DMF), Fmoc-*L*-Ile-OH (0.85 g, 1 mmol, 2 eq, dissolved in 12 mL DMF), DIC (1.05 g, 8.5 mmol, 17 eq, diluted in 17 mL DMF), Oxyma (1.42 g, 10 mmol, 20 eq, dissolved in 10 mL DMF).

6.2.2.4. Synthesis of Mal-KIKI(COO-)SQINM

3-Maleimidopropionic acid *N*-hydroxysuccinimide ester (266.22 mg, 1 mmol, 2 eq, dissolved in 5 mL DMF), DIPEA (435.0 µL, 2.5 mmol, 5 eq).

The synthesis yielded 98.7 mg (0.08 mmol, 16%).

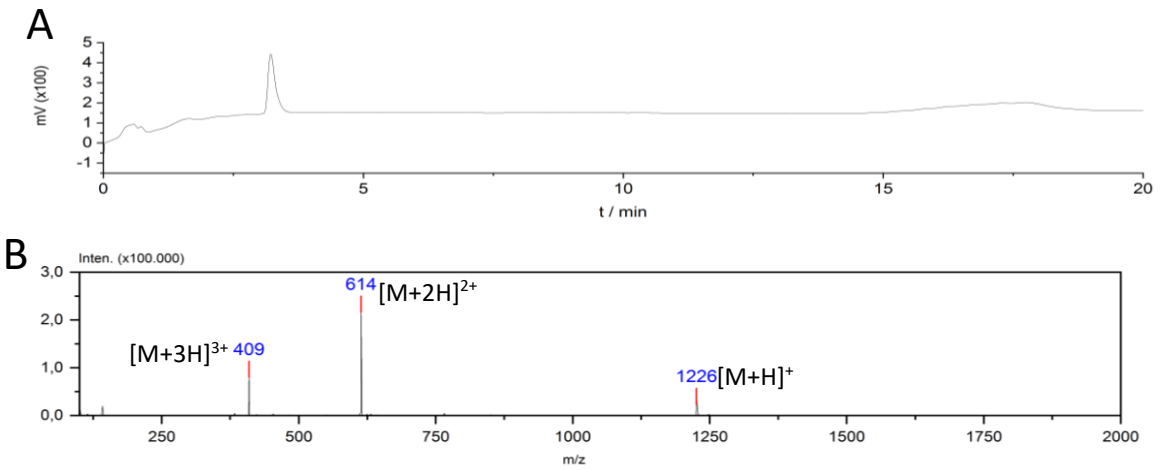

Figure 31: (A) LC chromatogram and (B) positive ion mode mass spectrum of integrated LC peak of D-Mal (second batch).

6.2.3. Synthesis of BAP (Bioactive Peptides)

In the following, all peptide sequences were synthesized via SPPS according to the procedure of chapter 6.1.1. Only the concentrations and chemicals are listed, as well as the respective LC-MS spectra.

*6.2.3.2. Synthesis of **[1]** (IKVAVC)*

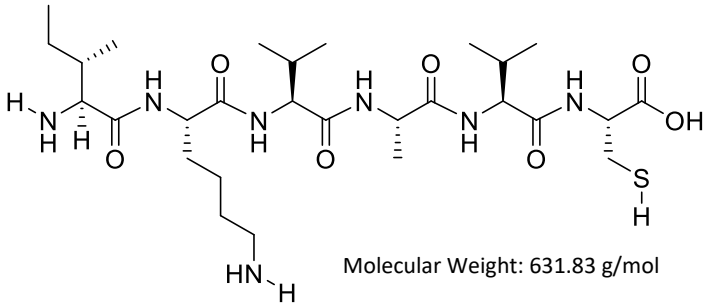

Figure 32: Chemical structure of IKVAVC.

Fmoc-Cys(Trt)-Wang resin (100-200 mesh, loading: 0.60 mmol/g, 0.83 g, 0.5 mmol), Fmoc-*L*-Ala-OH (0.75 g, 1 mmol, 2 eq, dissolved in 12 mL DMF), Fmoc-*L*-Ile-OH (0.85 g, 1 mmol, 2 eq, dissolved in 12 mL DMF), Fmoc-*L*-Lys(Boc)-OH (1.13 g, 1 mmol, 2 eq, dissolved in 12 mL DMF), Fmoc-*L*-Val-OH (1.63 g, 2 mmol, 4 eq, dissolved in 24 mL DMF), DIC (1.62 g, 13 mmol, 26 eq, diluted in 24 mL DMF), Oxyma (1.99 g, 14 mmol, 28 eq, dissolved in 14 mL DMF).

The synthesis yielded 5.0 mg (0.008 mmol, 2%) after purification and lyophilization.

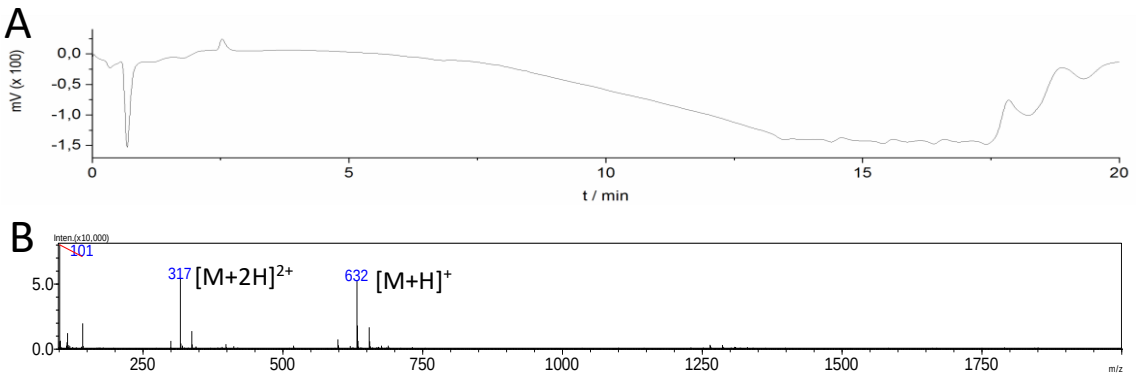

Figure 33: (A) LC chromatogram and (B) positive ion mode mass spectrum of integrated LC peak of IKVAVC.

*6.2.3.3. Synthesis of **[2]** (VGVAPGC)*

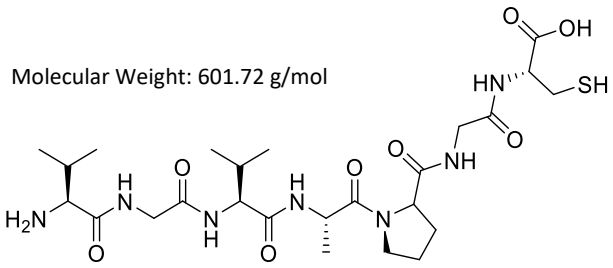

Figure 34: Chemical structure of VGVAPGC.

Fmoc-Cys(Trt)-Wang resin (100-200 mesh, loading: 0.60 mmol/g, 0.42 g, 0.25 mmol), Fmoc-*L*-Val-OH (0.82 g, 1 mmol, 4 eq, dissolved in 12 mL DMF), Fmoc-*L*-Pro-OH (0.41 g, 0.5 mmol, 2 eq, dissolved in 6 mL DMF), Fmoc-*L*-Gly-OH (0.72 g, 0.5 mmol, 4 eq, dissolved in 12 mL DMF), Fmoc-*L*-Ala-OH (0.38 g, 0.5 mmol, 2 eq, dissolved in 6 mL DMF), DIC (1.06 g, 8 mmol, 32 eq, diluted in 17 mL DMF), Oxyma (1.42 g, 10 mmol, 40 eq, dissolved in 10 mL DMF).

The synthesis yielded 13.7 mg (0.02 mmol, 9%) after purification and lyophilization.

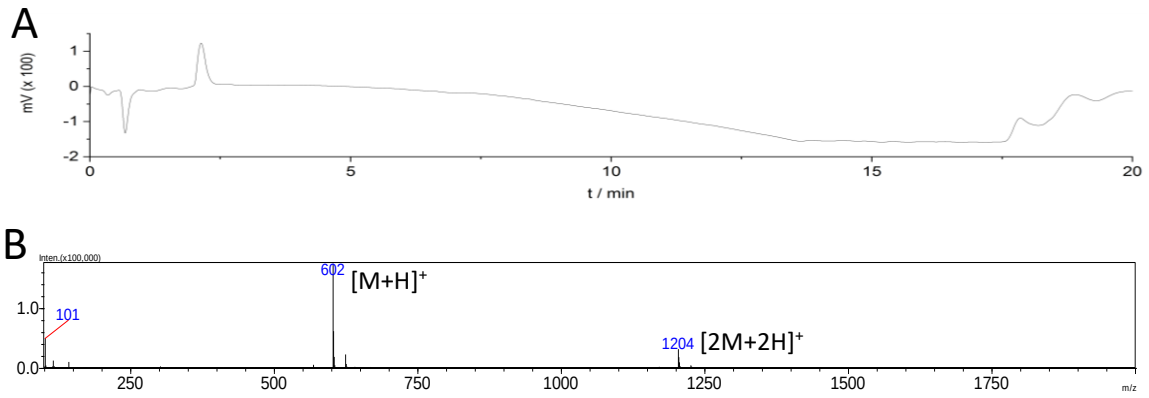

Figure 35: (A) LC chromatogram and (B) positive ion mode mass spectrum of integrated LC peak of VGVAPGC.

*6.2.3.3. Synthesis of **[3]** (SVVYGLRC)*

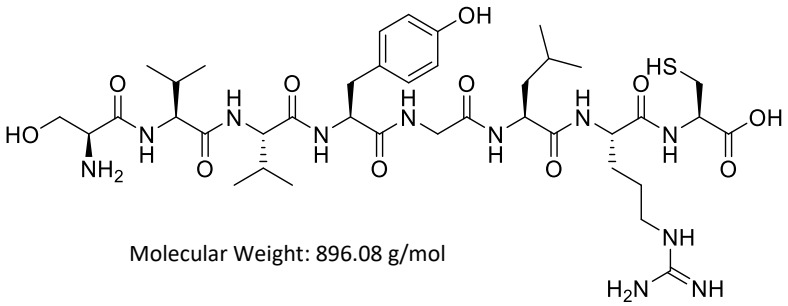

Molecular Weight: 896.08 g/mol

Figure 36: Chemical structure of SVVYGLRC.

Fmoc-Cys(Trt)-Wang resin (100-200 mesh, loading: 0.60 mmol/g, 0.42 g, 0.25 mmol), Fmoc-*L*-Ser(tBu)-OH (0.47 g, 0.5 mmol, 2 eq, dissolved in 6 mL DMF), Fmoc-*L*-Val-OH (0.82 g, 1 mmol, 4 eq, dissolved in 12 mL DMF), Fmoc-*L*-Tyr(tBu)-OH (0.56 g, 0.5 mmol, 2 eq, dissolved in 6 mL DMF), Fmoc-*L*-Gly-OH (0.36 g, 0.5 mmol, 2 eq, dissolved in 6 mL DMF), Fmoc-*L*-Leu-OH (0.43 g, 0.5 mmol, 2 eq, dissolved in 6 mL DMF), Fmoc-*L*-Arg(Pbf)-OH (1.56 g, 1 mmol, 4 eq, dissolved in 12 mL DMF), DIC (1.39 g, 11.0 mmol, 45 eq, diluted in 22 mL DMF), Oxyma (1.71 g, 12 mmol, 48 eq, dissolved in 12 mL DMF).

The synthesis yielded 4.0 mg (0.005 mmol, 2%) after purification and lyophilization.

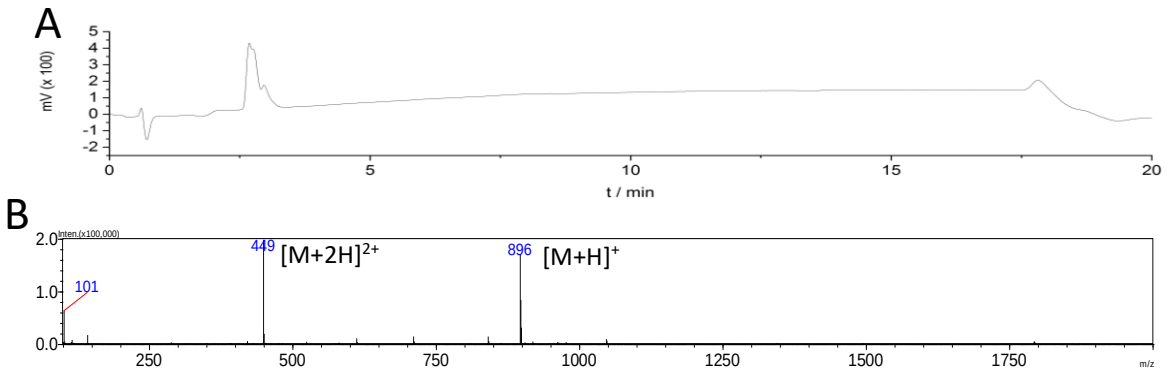

Figure 37: (A) LC chromatogram and (B) positive ion mode mass spectrum of integrated LC peak of SVVYGLRC.

Regarding Figure 37, **A**, the entire peak was integrated, including the bulge.

*6.2.3.4. Synthesis of **[4]** (sGliafin / CILKNLSRSR)*

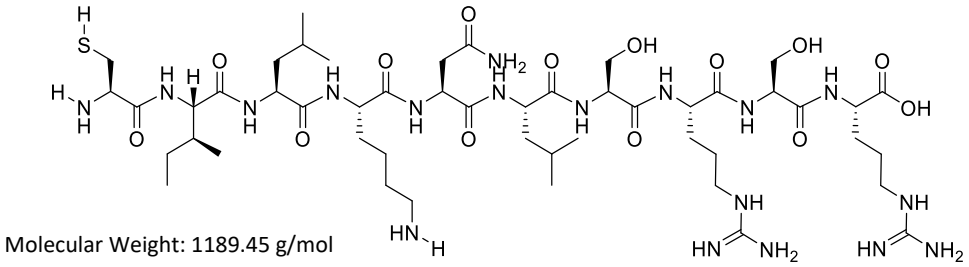

Figure 38: Chemical structure of sGliafin.

Fmoc-*L*-Arg(Pbf)-Wang resin (100-200 mesh, loading: 0.71 mmol/g, 0.14 g, 0.1 mmol), Fmoc-*L*-Cys(Trt)-OH (0.36 g, 0.2 mmol, 2 eq, dissolved in 3 mL DMF), Fmoc-*L*-Ile-OH (0.22 g, 0.2 mmol, 2 eq, dissolved in 3 mL DMF), Fmoc-*L*-Leu-OH (0.43 g, 0.4 mmol, 4 eq, dissolved in 6 mL DMF), Fmoc-*L*-Lys(Boc)-OH (0.29 g, 0.2 mmol, 2 eq, dissolved in 3 mL DMF), Fmoc-*L*-Asn(Trt)-OH (0.36 g, 0.2 mmol, 2 eq, dissolved in 3 mL DMF), Fmoc-*L*-Ser(tBu)-OH (0.47 g, 0.4 mmol, 4 eq, dissolved in 6 mL DMF), Fmoc-*L*-Arg(Pbf)-OH (0.78 g, 0.4 mmol, 4 eq, dissolved in 6 mL DMF), DIC (0.90 g, 7.1 mmol, 71 eq, diluted in 14 mL DMF), Oxyma (1.14 g, 8 mmol, 80 eq, dissolved in 8 mL DMF).

The synthesis yielded 29.2 mg (0.025 mmol, 25%) after purification and lyophilization.

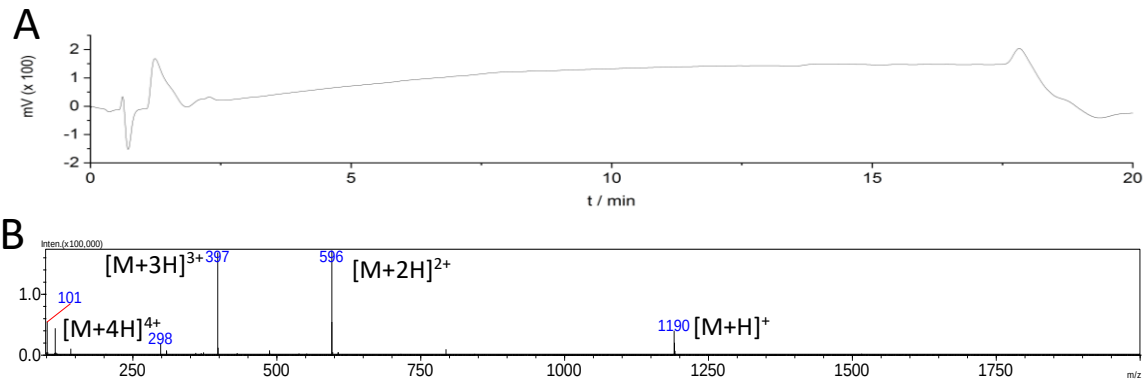

Figure 39: (A) LC chromatogram and (B) positive ion mode mass spectrum of integrated LC peak of sGliafin.

*6.2.3.5. Synthesis of **[5]** (CRKRLQVQLSIRT)*

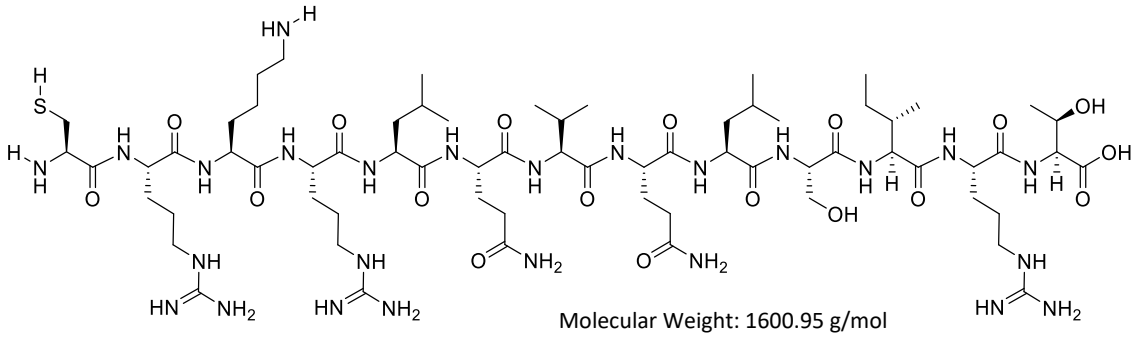

Figure 40: Chemical structure of CRKRLQVQLSIRT.

Fmoc-Thr(tBu)-Wang resin (100-200 mesh, loading: 0.53 mmol/g, 0.19 g, 0.1 mmol), Fmoc-*L*-Arg(Pbf)-OH (2.34 g, 1.2 mmol, 12 eq, dissolved in 18 mL DMF), Fmoc-*L*-Cys(Trt)-OH (0.36 g, 0.2 mmol, 2 eq, dissolved in 3 mL DMF), Fmoc-*L*-Gln(Trt)-OH (0.74 g, 0.4 mmol, 4 eq, dissolved in 6 mL DMF), Fmoc-*L*-Ile-OH (0.29 g, 0.2 mmol, 2 eq, dissolved in 3 mL DMF), Fmoc-*L*-Leu-OH (0.43 g, 0.4 mmol, 4 eq, dissolved in 6 mL DMF), Fmoc-*L*-Lys(Boc)-OH (0.29 g, 0.2 mmol, 2 eq, dissolved in 3 mL DMF), Fmoc-*L*-Ser(tBu)-OH (0.24 g, 0.2 mmol, 2 eq, dissolved in 3 mL DMF), Fmoc-*L*-Val-OH (0.21 g, 0.2 mmol, 2 eq, dissolved in 3 mL DMF), DIC (1.29 g, 10 mmol, 100 eq, diluted in 20 mL DMF), Oxyma (1.56 g, 11 mmol, 110 eq, dissolved in 11 mL DMF).

The synthesis yielded 40.8 mg (0.026 mmol, 26%) after purification and lyophilization.

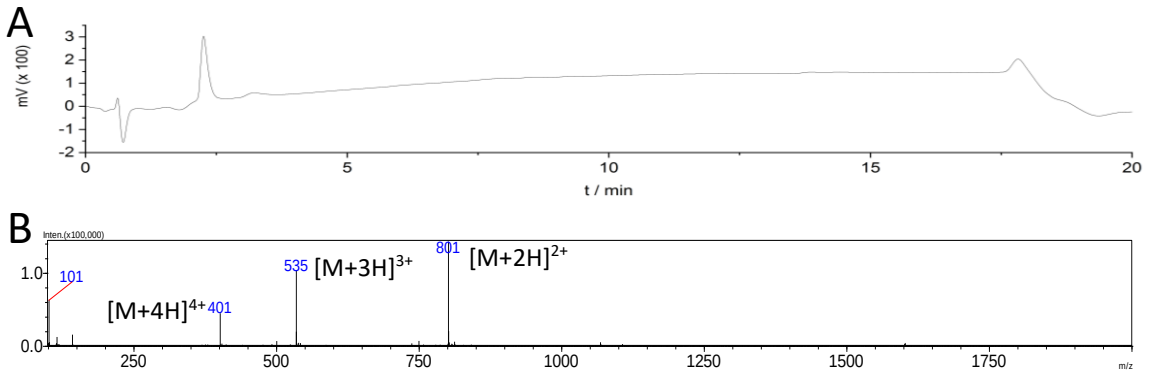

Figure 41: (A) LC chromatogram and (B) positive ion mode mass spectrum of integrated LC peak of CRKRLQVQLSIRT.

6.2.4. Coupling of Bioactive Peptides to D-Mal

The experimental performance of the coupling of a BAP to D-Mal (Scheme 10) is described in chapter 6.1.2. In the following, solely the chemicals and concentrations of the different BAPs are shown.

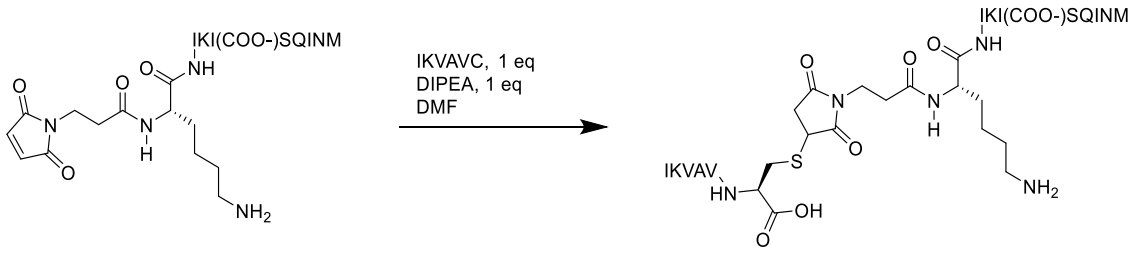

Scheme 10: Coupling of IKVAVC to D-Mal yielding IKVAVC-D_{MAL}, exemplarily for every BAP used in this work.

*6.2.4.1. Synthesis of **[7]** (IKVAVC-D_{MAL})*

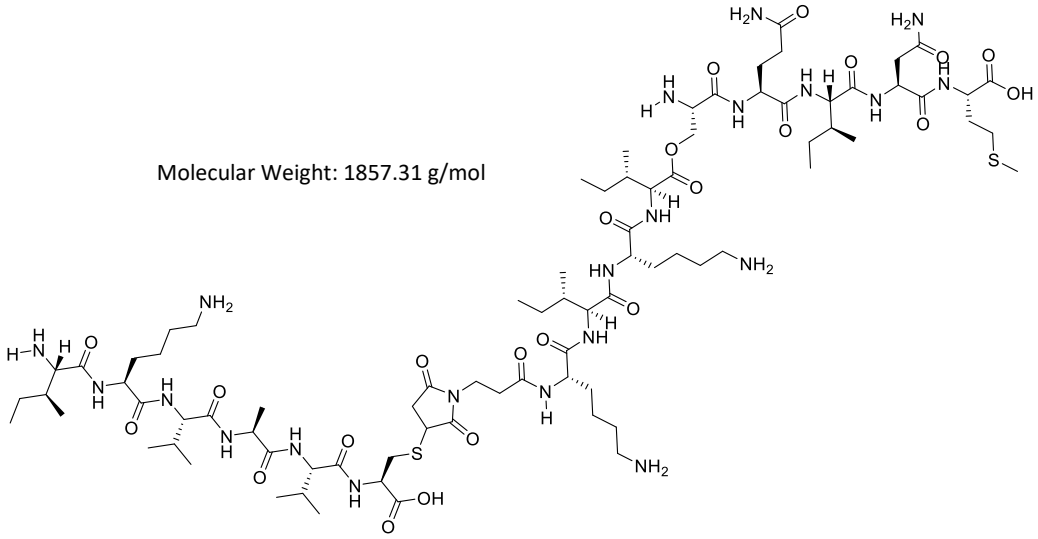

Figure 42: Chemical structure of IKVAVC-D_{MAL}.

First batch:

Mal-KIKI(COO)SQINM (1 mg, $8.2 \cdot 10^{-4}$ mmol, dissolved in 30 µL DMF), IKVAVC (0.52 mg, $8.2 \cdot 10^{-4}$ mmol, 1 eq, dissolved in 30 µL DMF), DIPEA (1 µL, $5.74 \cdot 10^{-6}$ mmol, 0.007 eq).

The synthesis yielded 1.3 mg ($7.0 \cdot 10^{-4}$ mmol, 86%) after purification and lyophilization.

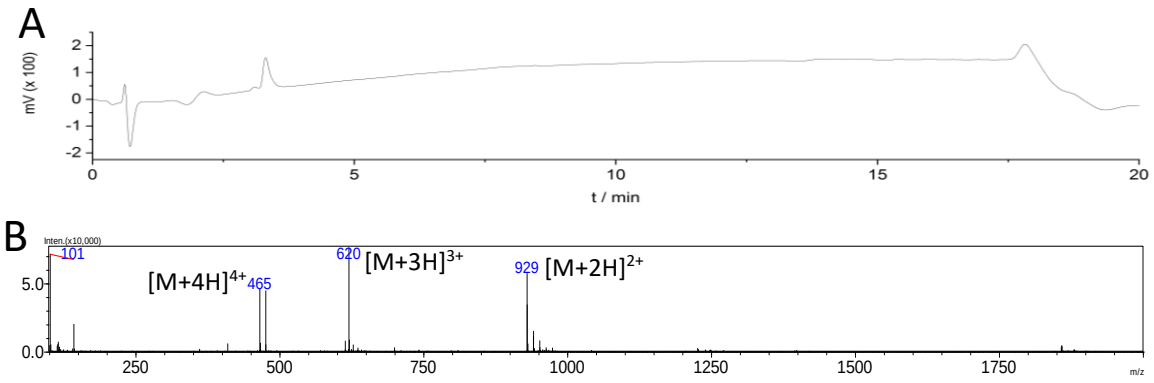

Figure 43: (A) LC chromatogram and (B) positive ion mode mass spectrum of integrated LC peak of IKVAVC-D_{MAL} (first batch).

Second batch:

Mal-KIKI(COO)SQINM (5 mg, 4.1 · 10^{-3} mmol, dissolved in 150 µL DMF), IKVAVC (2.60 mg, 4.1 · 10^{-3} mmol, 1 eq, dissolved in 150 µL DMF), DIPEA (5 µL, 2.87 · 10^{-5} mmol, 0.007 eq).

The synthesis yielded 2.8 mg (1.5 · 10^{-3} mmol, 37%) after purification and lyophilization.

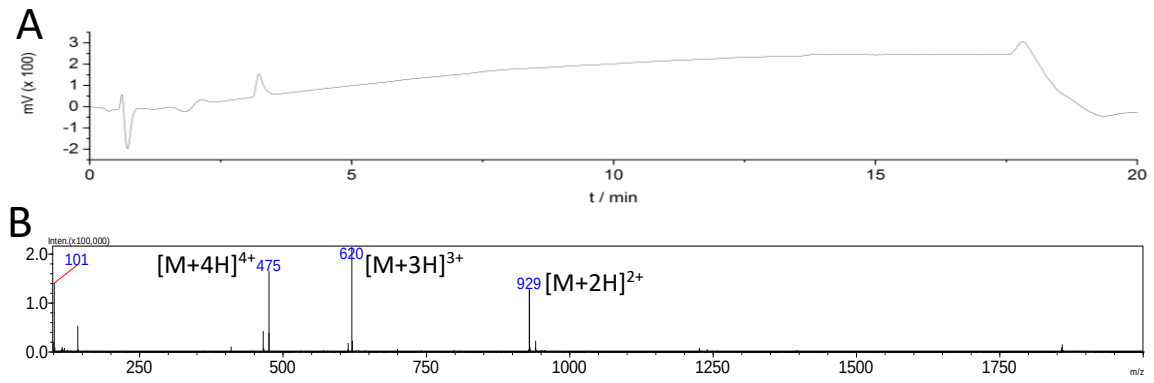

Figure 44: (A) LC chromatogram and (B) positive ion mode mass spectrum of integrated LC peak of IKVAVC-D_{MAL} (second batch).

*6.2.4.2. Synthesis of **[8]** (VGVAPGC-D_{MAL})*

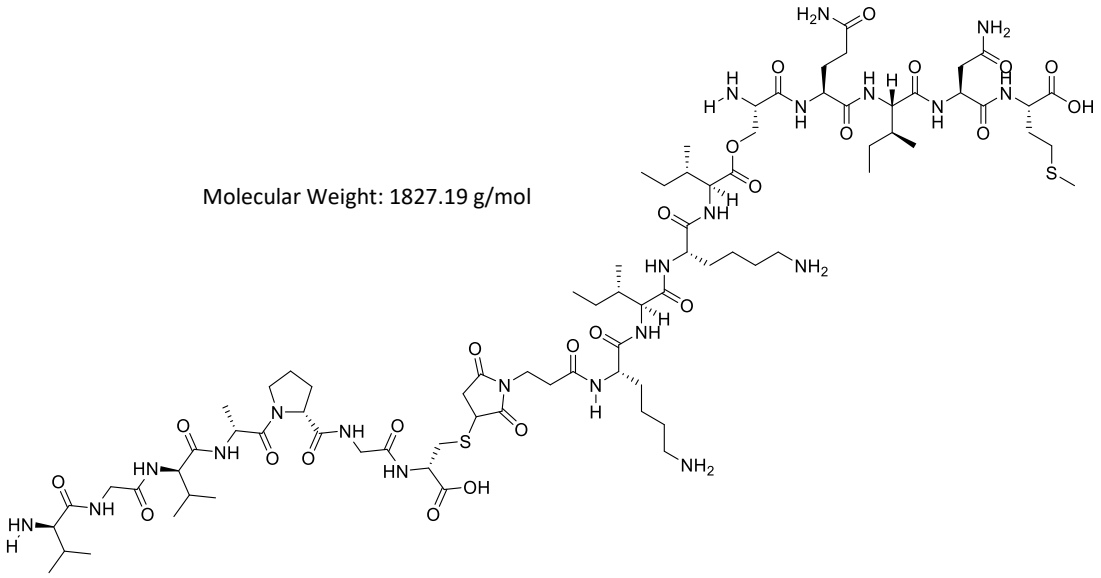

Figure 45: Chemical structure of VGVAPGC-D_{MAL}.

First Batch:

Mal-KIKI(COO)SQINM (2 mg, $1.6 \cdot 10^{-3}$ mmol, dissolved in 60 µL DMF), VGVAPGC (0.98 mg, $1.6 \cdot 10^{-3}$ mmol, 1 eq, dissolved in 60 µL DMF), DIPEA (2 µL, $1.2 \cdot 10^{-5}$ mmol, 0.007 eq).

The synthesis yielded 0.8 mg ($8.7 \cdot 10^{-4}$ mmol, 54%) after purification and lyophilization.

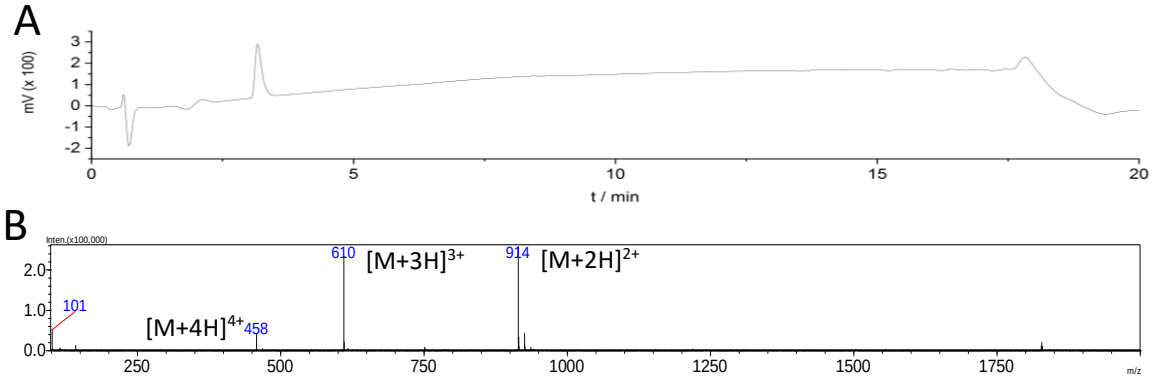

Figure 46: (A) LC chromatogram and (B) positive ion mode mass spectrum of integrated LC peak of VGVAPGC-D_{MAL} (first batch).

Second batch:

Mal-KIKI(COO)SQINM (5 mg, $4.1 \cdot 10^{-3}$ mmol, dissolved in 150 µL DMF), VGVAPGC (2.45 mg, $4.1 \cdot 10^{-3}$ mmol, 1 eq, dissolved in 150 µL DMF), DIPEA (5 µL, $2.9 \cdot 10^{-5}$ mmol, 0.007 eq).

The synthesis yielded 2.7 mg ($1.5 \cdot 10^{-3}$ mmol, 36%) after purification and lyophilization.

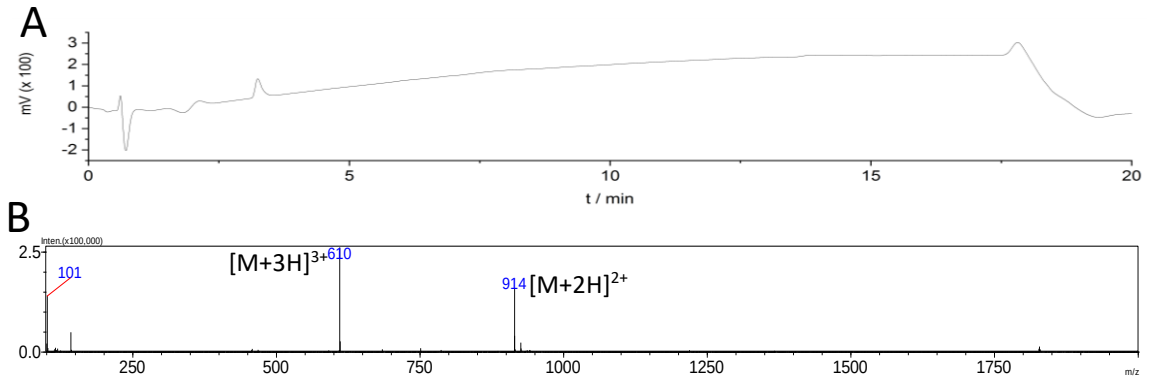

Figure 47: (A) LC chromatogram and (B) positive ion mode mass spectrum of integrated LC peak of VGVAPGC-D_{MAL} (second batch).

*6.2.4.3. Synthesis of **[9]** (SVVYGLRC -D_{MAL})*

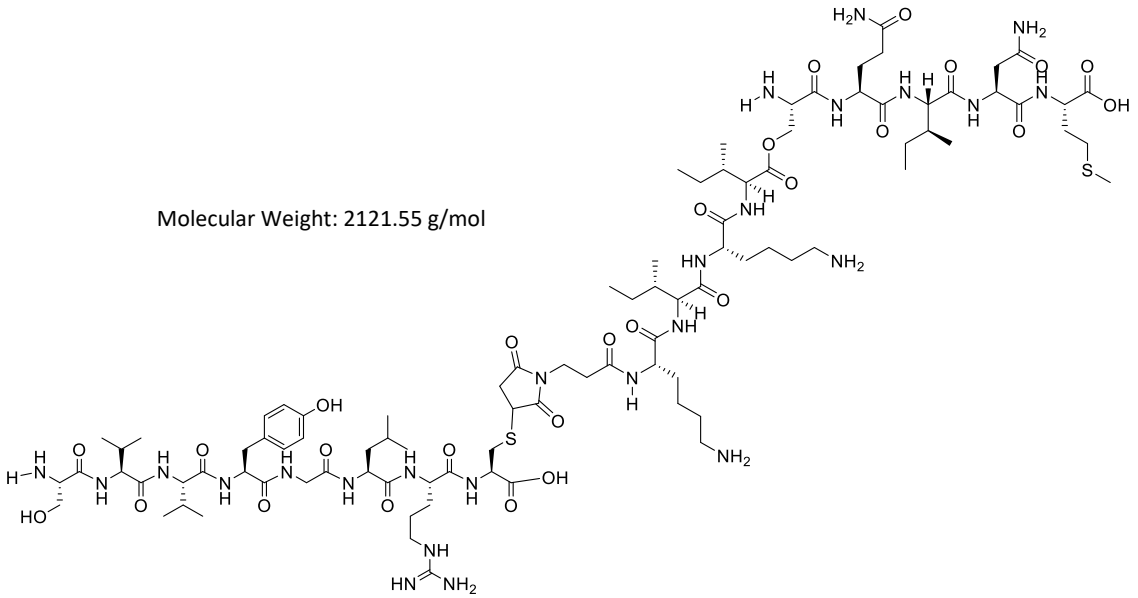

Figure 48: Chemical structure of SVVYGLRC-D_{MAL}.

First batch:

Mal-KIKI(COO)SQINM (1 mg, 8.2 · 10^{-4} mmol, dissolved in 30 µL DMF), SVVYGLRC (0.73 mg, 8.2· 10^{-4} mmol, 1 eq, dissolved in 30 µL DMF), DIPEA (1 µL, 5.7 · 10^{-6} mmol, 0.007 eq)

The synthesis yielded 1.5 mg (7.1 · 10^{-4} mmol, 87%) after purification and lyophilization.

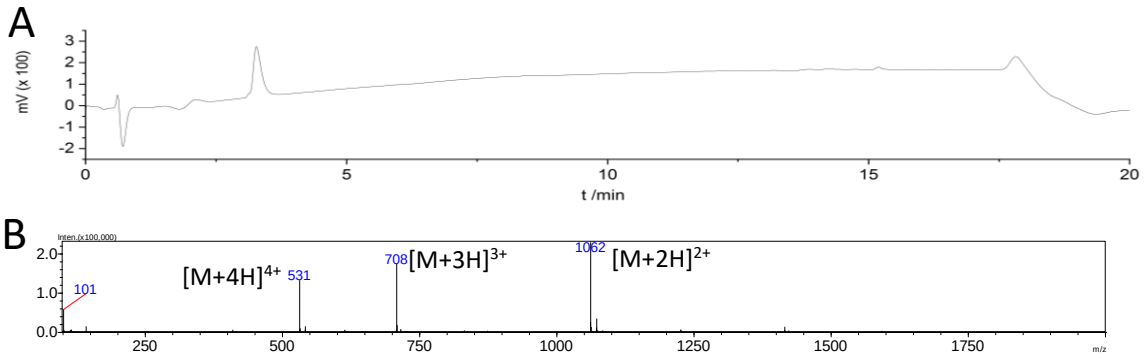

Figure 49: (A) LC chromatogram and positive ion mode (B) positive ion mode mass spectrum of integrated LC peak of SVVYGLRC-D_{MAL} (first batch).

Second batch:

Mal-KIKI(COO)SQINM (5 mg, $4.1 \cdot 10^{-3}$ mmol, dissolved in 150 µL DMF), SVVYGLRC (3.65 mg, $4.08 \cdot 10^{-3}$ mmol, 1 eq, dissolved in 150 µL DMF), DIPEA (5 µL, $2.87 \cdot 10^{-5}$ mmol, 0.007 eq).

The synthesis yielded 1.7 mg ($8.0 \cdot 10^{-4}$ mmol, 20%) after purification and lyophilization.

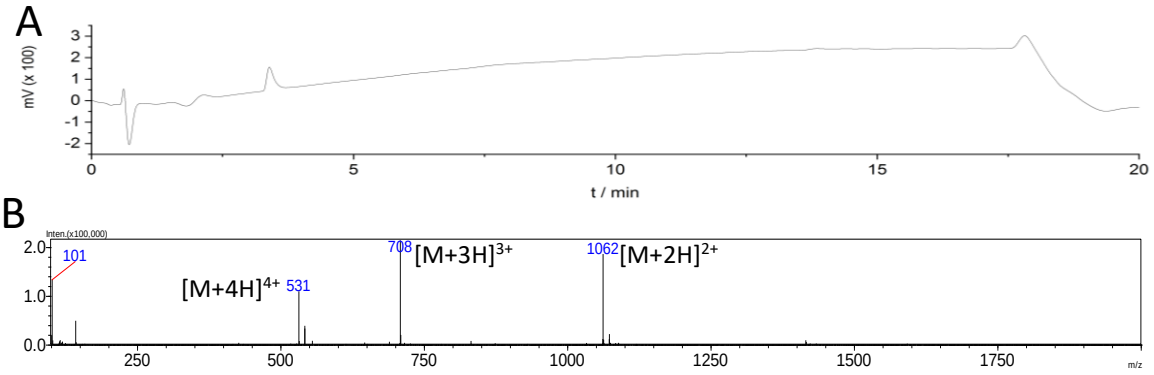

Figure 50: (A) LC chromatogram and (B) positive ion mode mass spectrum of integrated LC peak of SVVYGLRC-D_{MAL} (second batch).

*6.2.4.4. Synthesis of **[10]** (D_{MAL}-sGliafin)*

Molecular Weight: 2414.92 g/mol

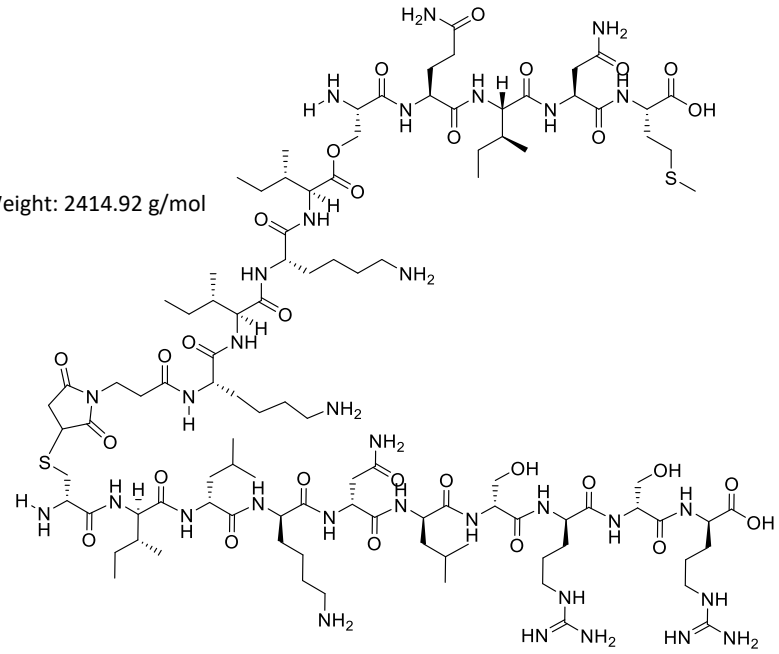

Figure 51: Chemical structure of D_{MAL}-s Gliafin.

First batch:

Mal-KIKI(COO)SQINM (2 mg, 1.6 · 10^{-3} mmol, dissolved in 60 µL DMF), sGliafin (1.94 mg, 1.6 · 10^{-3} mmol, 1 eq, dissolved in 60 µL DMF), DIPEA (2 µL, 1.2 · 10^{-5} mmol, 0.007 eq).

The synthesis yielded 2.3 mg (9.5 · 10^{-4} mmol, 59%) after purification and lyophilization.

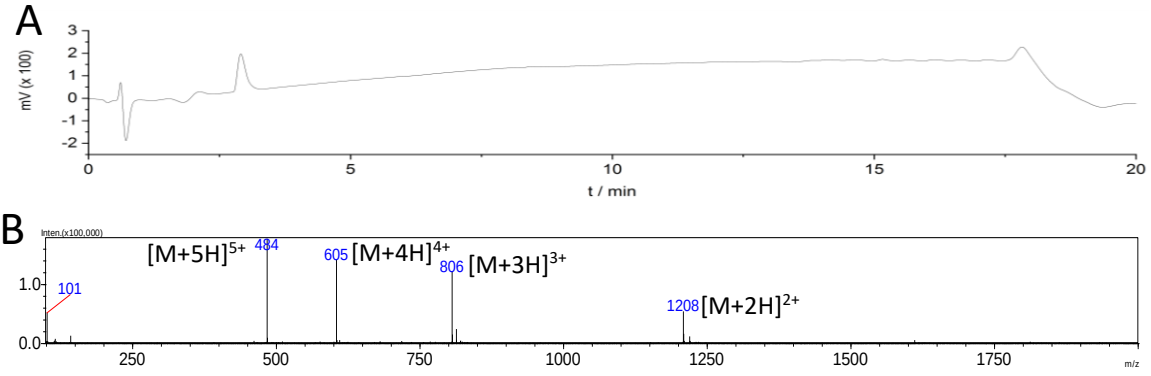

Figure 52: (A) LC chromatogram and (B) positive ion mode mass spectrum of integrated LC peak of D_{MAL}-sGliafin (first batch).

Second batch:

Mal-KIKI(COO)SQINM (5 mg, 4.1 · 10^{-3} mmol, dissolved in 150 µL DMF), sGliafin (4.85 mg, 4.1 · 10^{-3} mmol, 1 eq, dissolved in 150 µL DMF), DIPEA (5 µL, 2.9 · 10^{-5} mmol, 0.007 eq).

The synthesis yielded 5.8 mg (2.4 · 10^{-3} mmol, 59%) after purification and lyophilization.

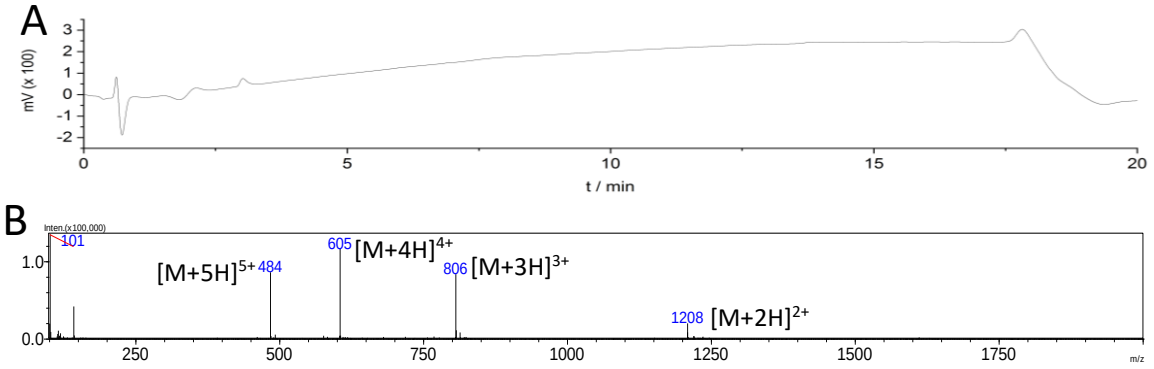

Figure 53: (A) LC chromatogram and (B) positive ion mode mass spectrum of integrated LC peak of D_{MAL}-sGliafin (second batch).

*6.2.4.5. Synthesis of **[11]** (D_{MAL}-CRKRLQVQLSIRT)*

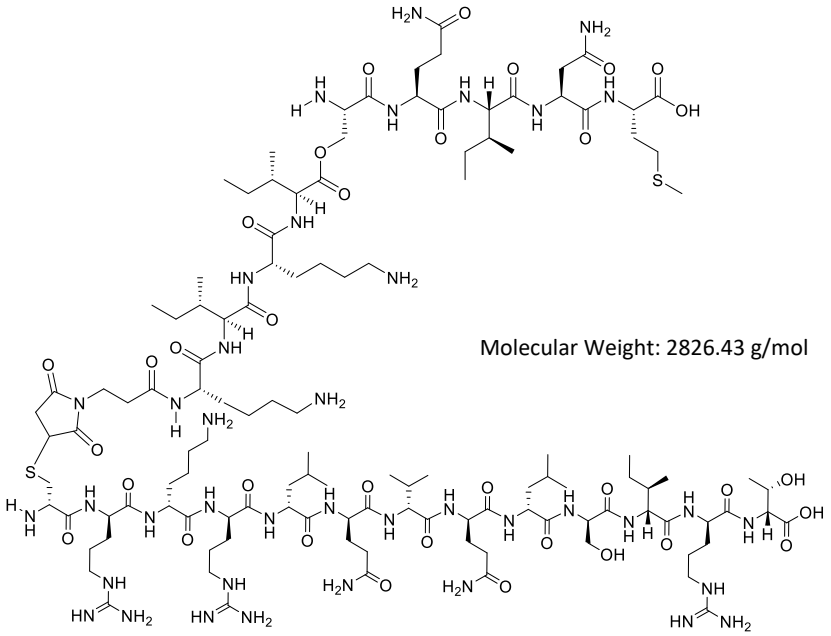

Figure 54: Chemical structure of D_{MAL}-CRKRLQVQLSIRT.

Mal-KIKI(COO)SQINM (2 mg, $1.6 \cdot 10^{-3}$ mmol, dissolved in 60 µL DMF), CRKRLQVQLSIRT (2.6 mg, $1.63 \cdot 10^{-3}$ mmol, 1 eq, dissolved in 60 µL DMF), DIPEA (2 µL, $1.2 \cdot 10^{-5}$ mmol, 0.007 eq).

The synthesis yielded 2.7 mg ($9.5 \cdot 10^{-4}$ mmol, 59%) after purification and lyophilization.

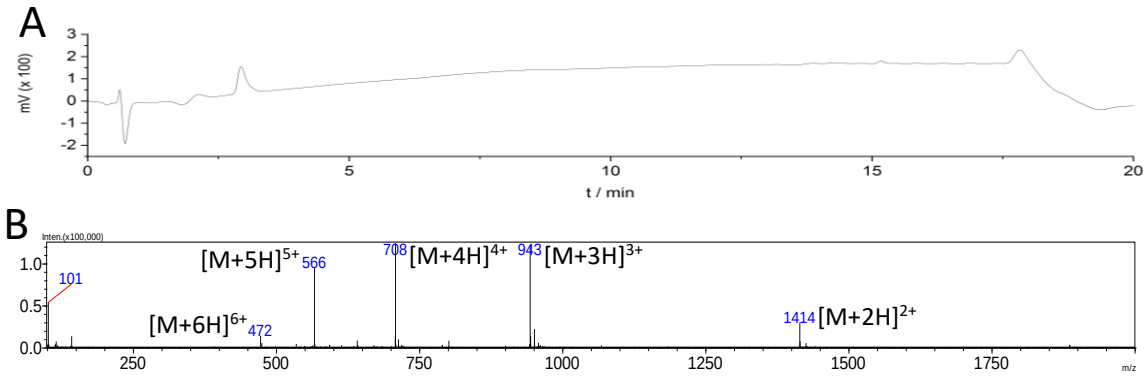

Figure 55: (A) LC chromatogram and (B) positive ion mode mass spectrum of integrated LC peak of D_{MAL}-CRKRLQVQLSIRT.

6.2.5. Synthesis of dcHSA-PD [dcHSA-PEG(2000)$_n$-D-Mal$_m$]

The Depsi-brush was synthesized according to the protocol by *Gacanin, J. et al.*[1]. It is a 4-step synthesis, though in this work the synthesis either started at step two (see 6.2.5.1.) or step three (see 6.2.6.1.).

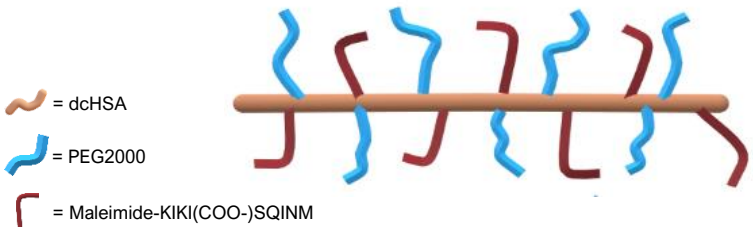

Figure 56: Schematic illustration of the peptide-protein hybrid dcHSA-PD.

6.2.5.1. Synthesis of cHSA-PEG(2000)$_n$

Cationized HSA [cHSA] (50 mg, 0.69 µmol) was dissolved in 28.8 mL degassed phosphate buffer (50 mM, pH 8.0). In addition, MEO-PEG(2000)-NHS ester (50.6 mg, 39 eq) was dissolved in 193 µL DMSO, introduced to the cHSA solution and stirred for 135 min. The solution was first concentrated and then washed eight times with *Milli-Q* water using a *Sartorius VS2092 VivaSpin 20* centrifugal concentrator, 3000 MWCO PES. Lastly, the remaining solution was lyophilized for 2 d to yield a white solid (40.3 mg, 0.37 µmol, 54%). The amount of PEG(2000) chains coupled to the cHSA and the purity were verified using MALDI-TOF-MS (see chapter 4.1.1., Figure 14).

6.2.5.2. Synthesis of dcHSA-PEG(2000)$_n$

To denaturate the cHSA, Urea-phosphate buffer [5M Urea (7.51 g), 50 mM Na_2HPO_4 (0.34 g) in 25 mL *Milli-Q* water, pH 7.4] was degassed 20 min through an argon flow. Then, cHSA-PEG(2000)$_{19}$ (40.3 mg, 0.37 µmol) was added and stirred for 15 min under argon athmosphere. Afterwards, TCEP (Tris(2-carboxyethyl)phosphine hydrochloride, 9.27 mg, 32.4 µmol) was added in a counter-current of argon and stirred under argon athmosphere over night. The reaction mixture was then concentrated using a VivaSpin 20, 3000 MWCO PES tube and washed five times with *Milli-Q* water. At last, the product was lyophilized for four days and a white solid was obtained (33.8 mg, 0.31 µmol, 84%)

6.2.5.3. Synthesis of dcHSA-PD [dcHSA-PEG(2000)$_n$-D-Mal$_m$]

To couple the cysteine residues of the dcHSA-PEG(2000)$_n$ with the Maleimide group of the Depsi peptide, dcHSA-PEG(2000)$_{19}$ (33.8 mg, 0.31 µmol) was dissolved in 333 µL DMSO. In addition, D-Mal [KIKI(COO-)SQINM, 7.5 mg, 6.12 µmol, 20 eq) was dissolved in 75 µL DMSO and introduced to the protein solution. The reaction mixture was vortexed and incubated on a shaker (1150 rpm) for 24 h at room temperature. Finally, the product was concentrated with a VivaSpin 20, 3000 MWCO PES tube and washed 5 times with *Milli-Q* water + 0.1 vol% TFA. The product was observed as a white solid (20.1 mg, 0.17 µmol, 55%) and the D-Mal coupling rate determined by MALDI-TOF-MS (chapter 4.1.1., Figure 15)

6.2.6. Synthesis of dcHSA-PD -Second Batch

In addition, a second bath was synthesized starting with cHSA-PEG(2000)$_{23}$. Therefore, the following chemicals were used, and the reactions performed according to the protocol above (chapter 6.2.5.).

6.2.6.1. Synthesis of dcHSA-PEG(2000)$_n$

cHSA-PEG(2000)$_{23}$ (59.10 mg, 0.50 µmol dissolved in 27.65 mL Urea phosphate buffer), TCEP (13.65 mg, 47.4 µmol).

Yield: 56.30 mg, 0.48 µmol, 96%

6.2.6.2. Synthesis of dcHSA-PD [dcHSA-PEG(2000)$_n$-D-Mal$_m$]

dcHSA-PEG(2000)$_{23}$ (56.30 mg, 0.48 µmol, dissolved in 714 µL DMSO), D-Mal (16.33 mg, 11.76 µmol, 20 eq dissolved in 167 µL DMSO).

Hereby, the reaction time was increased to 48 h.

Yield: 60.1 mg, 0.44 µmol, 92%

7. List of References

(1) Gačanin, J., Hedrich, J., Sieste, S., Glaßer, G., Lieberwirth, I., Schilling, C., Fischer, S., Barth, H., Knöll, B., Synatschke, C. V., Weil, T. Autonomous Ultrafast Self-Healing Hydrogels by pH-Responsive Functional Nanofiber Gelators as Cell Matrices. *Advanced Materials* **2019**, *31*.

(2) Nilsson, B. L.; Doran, T. M., Eds. *Peptide Self-Assembly: Methods and Protocols*; Methods in Molecular Biology 1777; Springer New York; Imprint; Humana Press: New York, NY, 2018.

(3) Berg, J. M.; Tymoczko, J. L.; Gatto, G. J.; Stryer, L. *Stryer Biochemie*; Springer Berlin Heidelberg: Berlin, Heidelberg, 2018.

(4) Chen, J.; Zou, X. Self-assemble peptide biomaterials and their biomedical applications. *Bioactive Materials* **2019**, *4*, 120–131.

(5) Arosio, P.; Owczarz, M.; Wu, H.; Butté, A.; Morbidelli, M. End-to-end self-assembly of RADA 16-I nanofibrils in aqueous solutions. *Biophysical journal* **2012**, *102*, 1617–1626.

(6) Gene Expression *. *Cell Biology*; Elsevier, 2017; pp 165–187.

(7) Wu, Y.; Collier, J. H. α-Helical coiled-coil peptide materials for biomedical applications. *Wiley interdisciplinary reviews. Nanomedicine and nanobiotechnology* **2017**, *9*.

(8) Hendricks, M. P.; Sato, K.; Palmer, L. C.; Stupp, S. I. Supramolecular Assembly of Peptide Amphiphiles. *Accounts of chemical research* **2017**, *50*, 2440–2448.

(9) Jayawarna, V.; Smith, A.; Gough, J. E.; Ulijn, R. V. Three-dimensional cell culture of chondrocytes on modified di-phenylalanine scaffolds. *Biochemical Society transactions* **2007**, *35*, 535–537.

(10) Garcia, A. M.; Iglesias, D.; Parisi, E.; Styan, K. E.; Waddington, L. J.; Deganutti, C.; Zorzi, R. de; Grassi, M.; Melchionna, M.; Vargiu, A. V.*; et al.* Chirality Effects on Peptide Self-Assembly Unraveled from Molecules to Materials. *Chem* **2018**, *4*, 1862–1876.

(11) M. Pieszka; A.M. Sobota; J. Gačanin; T. Weil; D.Y.W. Ng. Orthogonally Stimulated Assembly/Disassembly of Depsipeptides by Rational Chemical Design. *ChemBioChem* **2019**, *20*.

(12) Murphy, M. P.; LeVine, H. Alzheimer's disease and the amyloid-beta peptide. *Journal of Alzheimer's disease : JAD* **2010**, *19*, 311–323.

(13) Ahmed, E. M. Hydrogel: Preparation, characterization, and applications: A review. *Journal of advanced research* **2015**, *6*, 105–121.

(14) Pasqui, D.; Cagna, M. de; Barbucci, R. Polysaccharide-Based Hydrogels: The Key Role of Water in Affecting Mechanical Properties. *Polymers* **2012**, *4*, 1517–1534.

(15) Rivas, M.; Del Valle, L. J.; Alemán, C.; Puiggalí, J. Peptide Self-Assembly into Hydrogels for Biomedical Applications Related to Hydroxyapatite. *Gels (Basel, Switzerland)* **2019**, *5*.

(16) Liu, T.; Jiao, C.; Peng, X.; Chen, Y.-N.; Chen, Y.; He, C.; Liu, R.; Wang, H. Super-strong and tough poly(vinyl alcohol)/poly(acrylic acid) hydrogels reinforced by hydrogen bonding. *J. Mater. Chem. B* **2018**, *6*, 8105–8114.

(17) Clarke, D. E.; Pashuck, E. T.; Bertazzo, S.; Weaver, J. V. M.; Stevens, M. M. Self-Healing, Self-Assembled β-Sheet Peptide-Poly(γ-glutamic acid) Hybrid Hydrogels. *Journal of the American Chemical Society* **2017**, *139*, 7250–7255.

(18) Wu, Y.; Li, C.; Boldt, F.; Wang, Y.; Kuan, S. L.; Tran, T. T.; Mikhalevich, V.; Förtsch, C.; Barth, H.; Yang, Z.*; et al.* Programmable protein-DNA hybrid hydrogels for the immobilization and release of functional proteins. *Chemical communications (Cambridge, England)* **2014**, *50*, 14620–14622.

(19) Brian J. Bennion; Valerie Daggett. The molecular basis for the chemical denaturation of proteins by urea. *Proceedings of the National Academy of Sciences of the United States of America* **2003**, *100*, 5142–5147.

(20) Swanson, K. I.; Schlieve, C. R.; Lieven, C. J.; Levin, L. A. Neuroprotective effect of sulfhydryl reduction in a rat optic nerve crush model. *Investigative ophthalmology & visual science* **2005**, *46*, 3737–3741.

(21) Kuan, S. L.; Wu, Y.; Weil, T. Precision biopolymers from protein precursors for biomedical applications. *Macromolecular rapid communications* **2013**, *34*, 380–392.

(22) Joussen, A. M.; Kirchhof, B.; Gottstein, C. Molekulare Mechanismen der Vaskulogenese und Angiogenese. Möglichkeiten antiangiogener Therapie. *Der Ophthalmologe : Zeitschrift der Deutschen Ophthalmologischen Gesellschaft* **2003**, *100*, 284–291.

(23) Sarkar, B.; Nguyen, P. K.; Gao, W.; Dondapati, A.; Siddiqui, Z.; Kumar, V. A. Angiogenic Self-Assembling Peptide Scaffolds for Functional Tissue Regeneration. *Biomacromolecules* **2018**, *19*, 3597–3611.

(24) James D. Tang; Cameron Mura; Kyle J. Lampe. Stimuli-Responsive, Pentapeptide, Nanofiber Hydrogel for Tissue Engineering. *Journal of the American Chemical Society* **2019**, *141*, 4886–4899.

(25) Wang, T.-W.; Chang, K.-C.; Chen, L.-H.; Liao, S.-Y.; Yeh, C.-W.; Chuang, Y.-J. Effects of an injectable functionalized self-assembling nanopeptide hydrogel on angiogenesis and neurogenesis for regeneration of the central nervous system. *Nanoscale* **2017**, *9*, 16281–16292.

(26) Chen, S.; Zhang, M.; Shao, X.; Wang, X.; Zhang, L.; Xu, P.; Zhong, W.; Zhang, L.; Xing, M.; Zhang, L. A laminin mimetic peptide SIKVAV-conjugated chitosan hydrogel promoting wound healing by enhancing angiogenesis, re-epithelialization and collagen deposition. *J. Mater. Chem. B* **2015**, *3*, 6798–6804.

(27) Mochizuki, M.; Philp, D.; Hozumi, K.; Suzuki, N.; Yamada, Y.; Kleinman, H. K.; Nomizu, M. Angiogenic activity of syndecan-binding laminin peptide AG73 (RKRLQVQLSIRT). *Archives of biochemistry and biophysics* **2007**, *459*, 249–255.

(28) Storgard, C.; Mikolon, D.; Stupack, D. G. Angiogenesis assays in the chick CAM. *Methods in molecular biology (Clifton, N.J.)* **2005**, *294*, 123–136.

(29) Merrifield, R. B. Solid Phase Peptide Synthesis. I. The Synthesis of a Tetrapeptide. *J. Am. Chem. Soc.* **1963**, *85*, 2149–2154.

(30) Hussein, W. M.; Skwarczynski, M.; Toth, I. *Peptide Synthesis* 2103; Springer US: New York, NY, 2020.

(31) Pearson, D. A.; Blanchette, M.; Baker, M. L.; Guindon, C. A. Trialkylsilanes as scavengers for the trifluoroacetic acid deblocking of protecting groups in peptide synthesis. *Tetrahedron Letters* **1989**, *30*, 2739–2742.

(32) Bacsa, B.; Kappe, C. O. Rapid solid-phase synthesis of a calmodulin-binding peptide using controlled microwave irradiation. *Nature Protocols* **2007**, *2*, 2222–2227.

(33) Malviya R., Bansal V., Pal O.P., Sharma P.K. High Performance Liquid Chromatographie: A Short Review. *Journal of Global Pharma Technology* **2010**, *2*, 22–26.

(34) Kraus, L.; Koch, A.; Hoffstetter-Kuhn, S. *Dünnschichtchromatographie*; Springer Berlin Heidelberg: Berlin, Heidelberg, 1996.

(35) Gey, M. H. *Instrumentelle Analytik und Bioanalytik*; Springer Berlin Heidelberg: Berlin, Heidelberg, 2015.

(36) Pitt, J. J. Principles and Applications of Liquid Chromatography-Mass Spectrometry in Clinical Biochemistry. *The Clinical Biochemist Reviews* **2009**, *30*, 19–34.

(37) Biancalana, M.; Koide, S. Molecular mechanism of Thioflavin-T binding to amyloid fibrils. *Biochimica et biophysica acta* **2010**, *1804*, 1405–1412.

(38) Stsiapura, V. I.; Maskevich, A. A.; Kuzmitsky, V. A.; Turoverov, K. K.; Kuznetsova, I. M. Computational study of thioflavin T torsional relaxation in the excited state. *The journal of physical chemistry. A* **2007**, *111*, 4829–4835.

(39) Khurana, R.; Coleman, C.; Ionescu-Zanetti, C.; Carter, S. A.; Krishna, V.; Grover, R. K.; Roy, R.; Singh, S. Mechanism of thioflavin T binding to amyloid fibrils. *Journal of structural biology* **2005**, *151*, 229–238.

(40) Xue, C.; Lin, T. Y.; Chang, D.; Guo, Z. Thioflavin T as an amyloid dye: fibril quantification, optimal concentration and effect on aggregation. *Royal Society open science* **2017**, *4*, 160696.

(41) Michler, G. H. Richtungen der Elektronenmikroskopie. *Kompakte Einführung in die Elektronenmikroskopie: Techniken, Stand, Anwendungen, Perspektiven*; Springer Fachmedien Wiesbaden: Wiesbaden, 2019; pp 7–31.

(42) Bauch, J.; Rosenkranz, R. TEM - Transmissionselektronenmikroskopie. In *Physikalische Werkstoffdiagnostik*; Bauch, J., Rosenkranz, R., Eds.; Springer Berlin Heidelberg: Berlin, Heidelberg, 2017; pp 8–9.

(43) Schmitz, S.; Desel, C. Fluoreszenzmikroskopie. In *Der Experimentator Zellbiologie*; Schmitz, S., Desel, C., Eds.; Springer Berlin Heidelberg: Berlin, Heidelberg, 2018; pp 81–112.

(44) Lichtman, J. W.; Conchello, J.-A. Fluorescence microscopy. *Nature methods* **2005**, *2*, 910–919.

(45) Jüstel, T.; Schwung, S. J. *Leuchtstoffe, Lichtquellen, Laser, Lumineszenz*; Springer Berlin Heidelberg: Berlin, Heidelberg, 2019; pp 89–90.

(46) Schier, J.; Kovář, B.; Kočárek, E.; Kuneš, M. Image Processing for Automated Analysis of the Fluorescence In-Situ Hybridization (FISH) Microscopic Images. In *Convergence and Hybrid Information Technology*; Lee, G., Howard, D., Ślęzak, D., Eds.; Lecture Notes in Computer Science; Springer Berlin Heidelberg: Berlin, Heidelberg, 2011; pp 622–633.

(47) Irina Arnaoutova; Hynda K. Kleinman. In vitro angiogenesis: Endothelial cell tube formation on gelled basement membrane extract. *Nature Protocols* **2010**, *5*, 628–635.

(48) Elias Horn, ibidi GmbH. Product Information: µ-Slide Angiogenesis. Version 1.0. https:// slideplayer.com/slide/13514645/ (accessed April 8, 2020).

(49) ibidi GmbH. Application Note 27: Experimental Setup Optimization and Data Analysis of Tube Formation Assays. Version 1.9. https://ibidi.com/img/cms/support/AN/AN27_Tube_ Formation_Data_Analysis.pdf (accessed April 8, 2020).

(50) Carpentier, G. ImageJ contribution: Angiogenesis Analyzer. *ImageJ News* **2012**, *5*.

(51) Promega Corporation. *CellTiter-Glo® Luminescent Cell Viability Assay*, #TB288; Technical Bulletin, 2015.

(52) Seitz, W. R.; Neary, M. P. Chemiluminescence and Bioluminescence Analysis. In *Contemporary Topics in Analytical and Clinical Chemistry: Volume 1*; Hercules, D. M., Hieftje, G. M., Snyder, L. R., Evenson, M. A., Eds.; Springer US: Boston, MA, 1977; pp 49–125.

(53) Koutsopoulos, S.; Zhang, S. Long-term three-dimensional neural tissue cultures in functionalized self-assembling peptide hydrogels, matrigel and collagen I. *Acta Biomaterialia* **2013**, *9*, 5162–5169.

(54) Tashiro, K.; Sephel, G. C.; Weeks, B.; Sasakig, M.; Martin, G. R.; Kleinman, H. K.; Yamada, Y. A Synthetic Peptide Containing the IKVAV Sequence from the A Chain of Laminin Mediates Cell Attachment, Migration, and Neurite Outgrowth. *Journal of Biological Chemistry* **1989**, *27*, 16174–16182.

(55) Grant, D. S.; Kinsella, J. L.; Fridman, R.; Auerbach, R.; Piasecki, B. A.; Yamada, Y.; Zain, M.; Kleinman, H. K. Interaction of endothelial cells with a laminin A chain peptide (SIKVAV) in vitro and induction of angiogenic behavior in vivo. *Journal of Cellular Physiology* **1992**, *153*, 614–625.

(56) Katherine M. Malinda; Motoyoshi Nomizu; Melissa Chung; Mucio Delgado; Yuchiro Kuratomi; Yoshihiko Yamada; Hynda K. Kleinman; M. Lourdes Ponce. Identification of laminin α1 and β1 chain peptides active for endothelial cell adhesion, tube formation, and aortic sprouting. *FASEB Journal* **1999**, *13*, 53–62.

(57) Robinet, A.; Fahem, A.; Cauchard, J.-H.; Huet, E.; Vincent, L.; Lorimier, S.; Antonicelli, F.; Soria, C.; Crepin, M.; Hornebeck, W.*; et al.* Elastin-derived peptides enhance angiogenesis by promoting endothelial cell migration and tubulogenesis through upregulation of MT1-MMP. *Journal of cell science* **2005**, *118*, 343–356.

(58) Yoshinosuke Hamada; Kiyoshi Nokihara; Masayuki Okazaki; Wataru Fujitani; Takuya Matsumoto; Mitsuyoshi Matsuo; Yukichi Umakoshi; Junzou Takahashi; Nariaki Matsuura. Angiogenic activity of osteopontin-derived peptide SVVYGLR. *Biochemical and biophysical research communications* **2003**, *310*, 153–157.

(59) Uchinaka, A.; Hamada, Y.; Mori, S.; Miyagawa, S.; Saito, A.; Sawa, Y.; Matsuura, N.; Kawaguchi, N. Cardioprotective effects on ischemic myocardium induced by SVVYGLR peptide via its angiogenic-promoting activity. *Tissue Eng Regen Med* **2015**, *12*, 162–171.

(60) Kyung Min Park; Yunki Lee; Joo Young Son; Jin Woo Bae; Ki Dong Park. In situ SVVYGLR peptide conjugation into injectable gelatin-poly(ethylene glycol)-tyramine hydrogel via enzyme-mediated reaction for enhancement of endothelial cell activity and neo-vascularization. *Bioconjugate chemistry* **2012**, *23*, 2042–2050.

(61) Nielsen, J.; Gotfryd, K.; Li, S.; Kulahin, N.; Soroka, V.; Rasmussen, K. K.; Bock, E.; Berezin, V. Role of glial cell line-derived neurotrophic factor (GDNF)-neural cell adhesion molecule (NCAM) interactions in induction of neurite outgrowth and identification of a binding site for NCAM in the heel region of GDNF. *The Journal of neuroscience : the official journal of the Society for Neuroscience* **2009**, *29*, 11360–11376.

(62) Stathopoulos, P.; Papas, S.; Pappas, C.; Mousis, V.; Sayyad, N.; Theodorou, V.; Tzakos, A. G.; Tsikaris, V. Side reactions in the SPPS of Cys-containing peptides. *Amino acids* **2013**, *44*, 1357–1363.

(63) Niece, K. L.; Hartgerink, J. D.; Donners, J. J. J. M.; Stupp, S. I. Self-assembly combining two bioactive peptide-amphiphile molecules into nanofibers by electrostatic attraction. *J. Am. Chem. Soc.* **2003**, *125*, 7146–7147.

(64) Balganesh, M.; Ethirajulu, K.; Ganguly, B. S.; Janakiraman, R.; Kaur, P.; Kajipala, R.; Nandan, S.; Murugappan, R. P.; Ramamurthy, N.; Venkatamaran, B. Mycobacterial Inhibitors. WO 99/65483, 1999.

(65) Heinrich, P. C.; Koch, H.-G.; Brix, J. Apoptose – Der programmierte Zelltod. In *Löffler/Petrides Biochemie und Pathobiochemie*; Heinrich, P. C., Müller, M., Graeve, L., Eds.; Springer-Lehrbuch; Springer Berlin Heidelberg: Berlin, Heidelberg, 2014; pp 633–637.

(66) Ge, J.; Wood, D. K.; Weingeist, D. M.; Prasongtanakij, S.; Navasumrit, P.; Ruchirawat, M.; Engelward, B. P. Standard fluorescent imaging of live cells is highly genotoxic. *Cytometry. Part A : the journal of the International Society for Analytical Cytology* **2013**, *83*, 552–560.

(67) Zahra, F. T.; Choleva, E.; Sajib, M. S.; Papadimitriou, E.; Mikelis, C. M. In Vitro Spheroid Sprouting Assay of Angiogenesis. *Methods in molecular biology (Clifton, N.J.)* **2019**, *1952*, 211–218.

(68) Chokoza, C.; Gustafsson, C. A.; Goetsch, K. P.; Zilla, P.; Thierfelder, N.; Pisano, F.; Mura, M.; Gnecchi, M.; Bezuidenhout, D.; Davies, N. H. Tuning Tissue Ingrowth into Proangiogenic Hydrogels via Dual Modality Degradation. *ACS Biomater. Sci. Eng.* **2019**, *5*, 5430–5438.

(69) Stahl, A.; Wu, X.; Wenger, A.; Klagsbrun, M.; Kurschat, P. Endothelial progenitor cell sprouting in spheroid cultures is resistant to inhibition by osteoblasts: a model for bone replacement grafts. *FEBS letters* **2005**, *579*, 5338–5342.

(70) Auerbach, R.; Akhtar, N.; Lewis, R. L.; Shinners, B. L. Angiogenesis assays: problems and pitfalls. *Cancer metastasis reviews* **2000**, *19*, 167–172.

(71) Angel Orte; Neil R. Birkett; Richard W. Clarke; Glyn L. Devlin; Christopher M. Dobson; David Klenerman. Direct characterization of amyloidogenic oligomers by single-molecule fluorescence.

Proceedings of the National Academy of Sciences of the United States of America **2008**, *105*, 14424–14429.

(72) Rapp, P. B.; Omar, A. K.; Shen, J. J.; Buck, M. E.; Wang, Z.-G.; Tirrell, D. A. Analysis and Control of Chain Mobility in Protein Hydrogels. *Journal of the American Chemical Society* **2017**, *139*, 3796–3804.

(73) ibidi GmbH. Application Note 19: Tube Formation Assays in µ-Slide Angiogenesis. Version 1.5. https://ibidi.com/img/cms/support/AN/AN19_Tube_Formation.pdf (accessed April 1, 2020).

8. Appendix

8.1. MALDI-TOF-MS

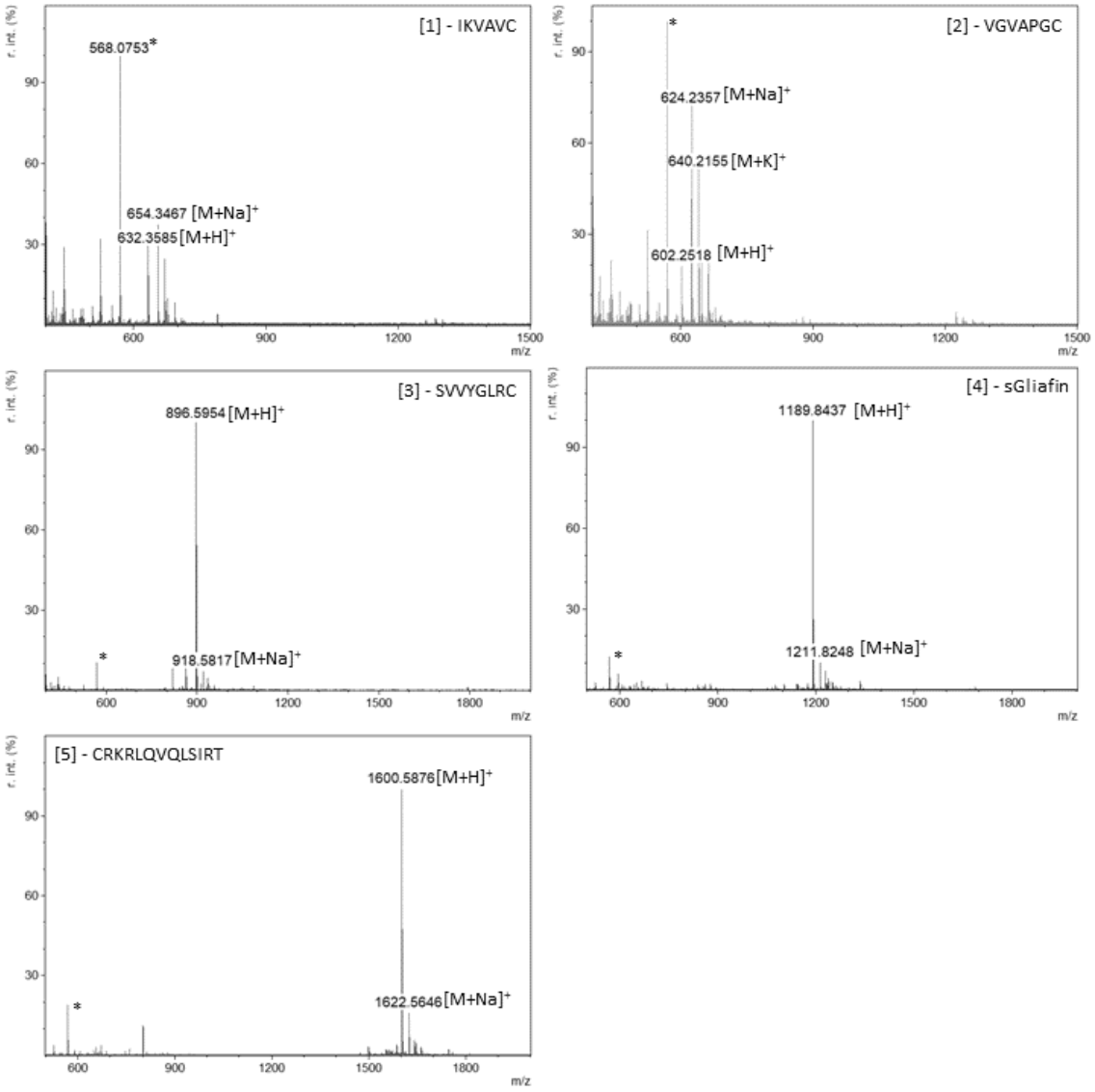

Figure 57: MALDI-TOF-MS spectra of the bioactive sequences **[1]** to **[5]** after purification. * = occurs in every measurement, possibly a constant contamination due to sample preparation.

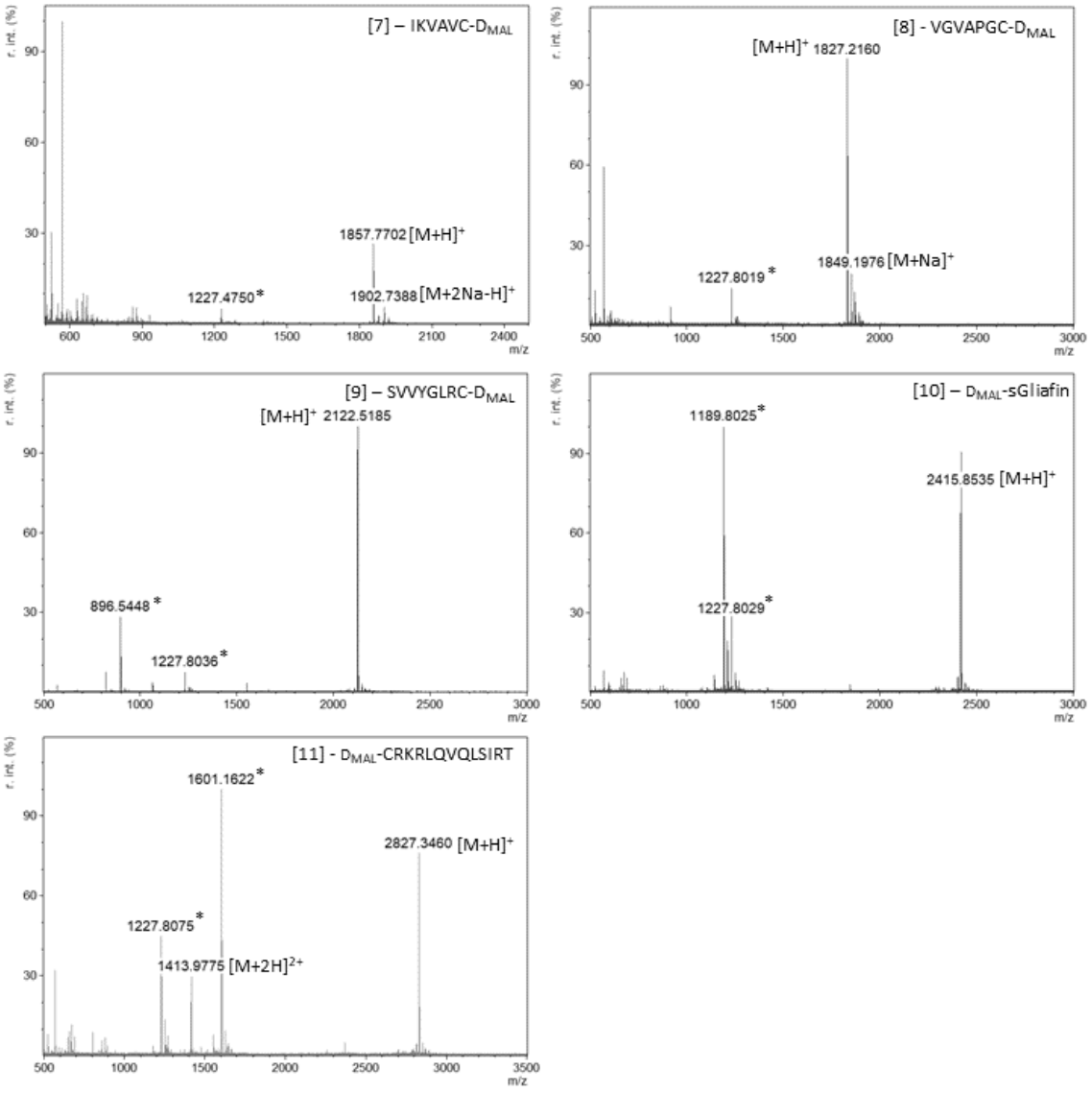

*Figure 58: MALDI-TOF-MS spectra of the D-Mal coupled bioactive sequences **[7]** to **[11]** after purification. First batches, self-synthesized BAPs were used in coupling. * = Starting material.*

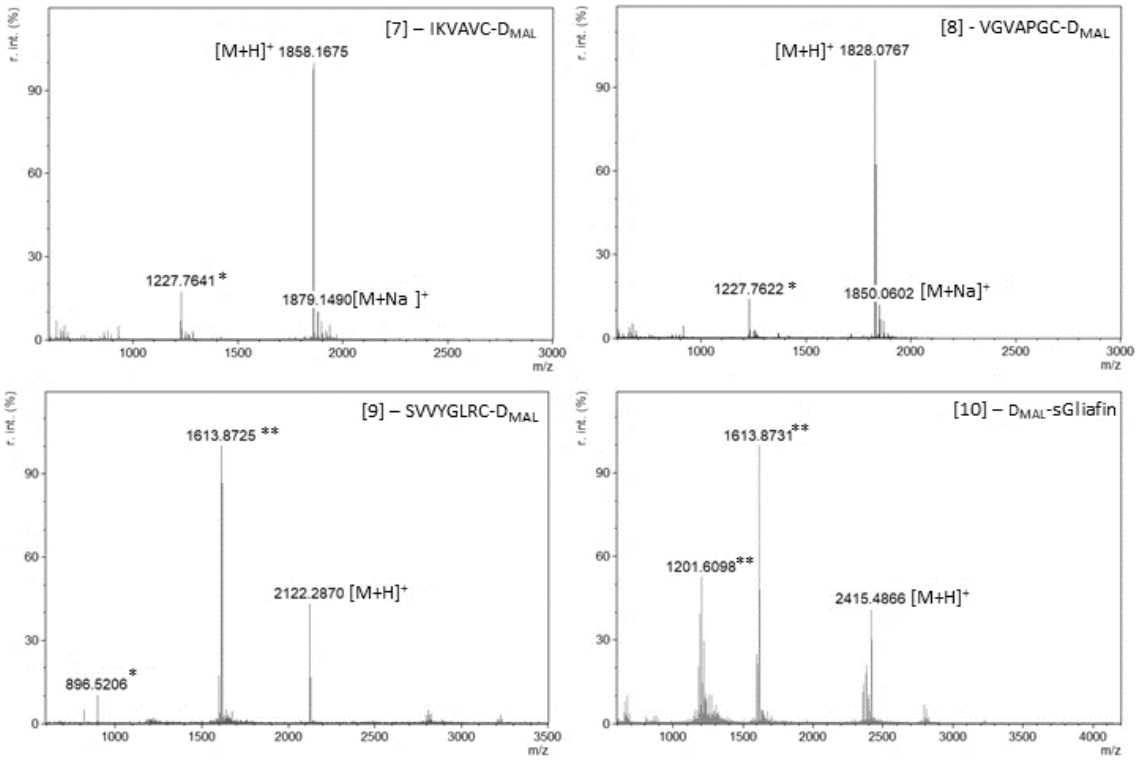

*Figure 59: MALDI-TOF-MS spectra of the D-Mal coupled bioactive sequences [7] to [11] after purification. Second batches, purchased BAPs were used in coupling. * = Starting material, ** = contaminations, probably occurred due to MALDI sample preparation.*

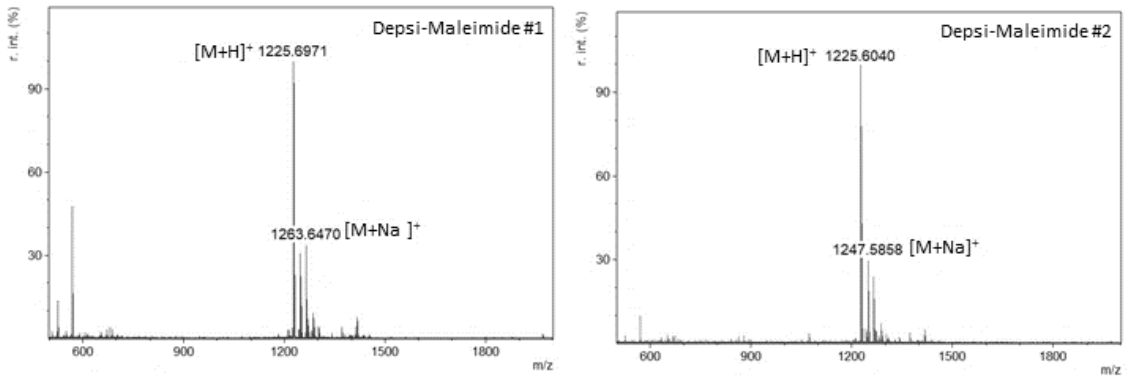

Figure 60: MALDI-TOF-MS spectra of Depsi-Maleimide [KIKI(COO-)SQINM] after purification. Left: first batch. Right: second batch.

8.2. HPLC Chromatograms

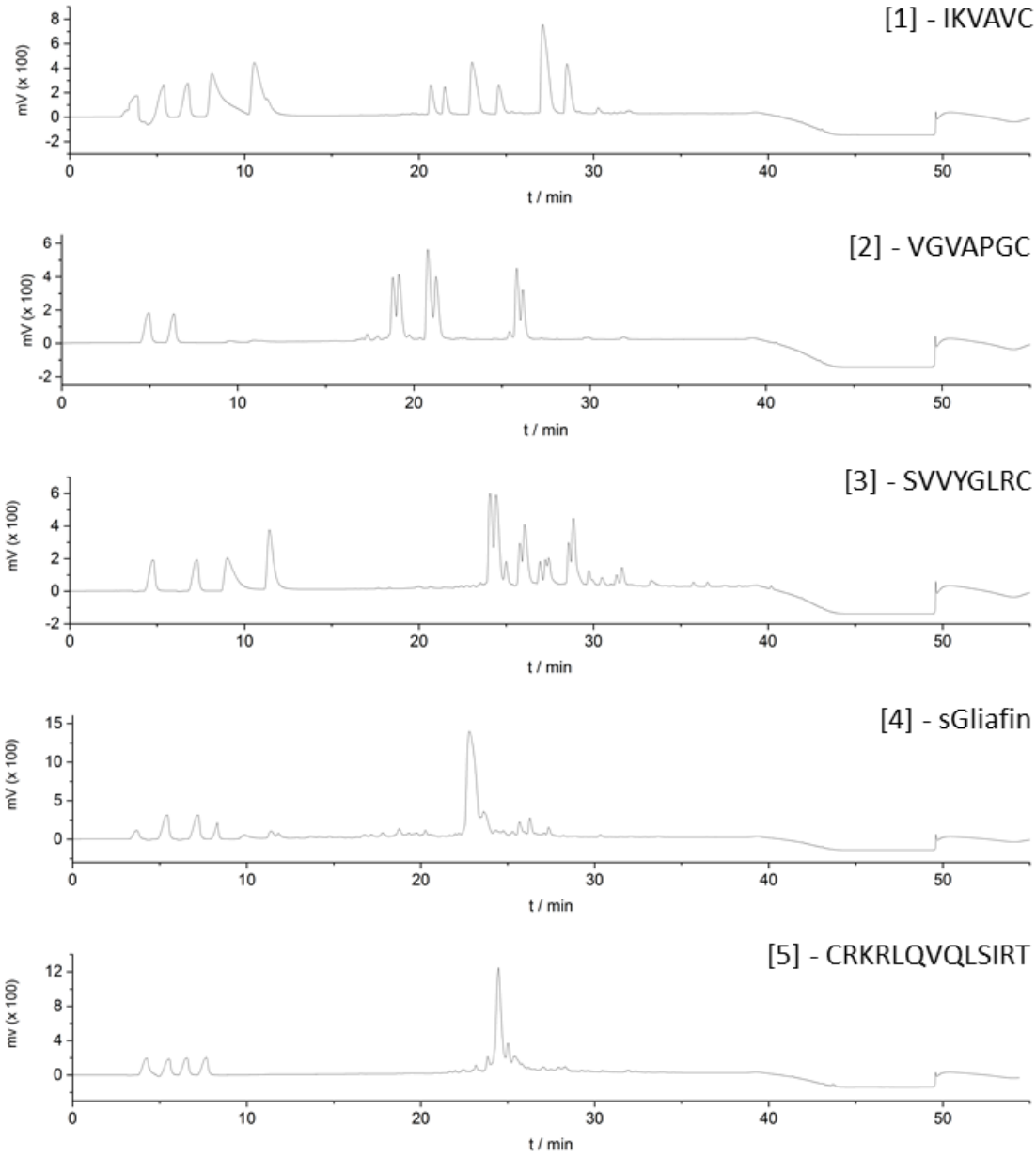

*Figure 61: HPLC chromatograms of the purification of the BAPs **[1]** to **[5]**.*

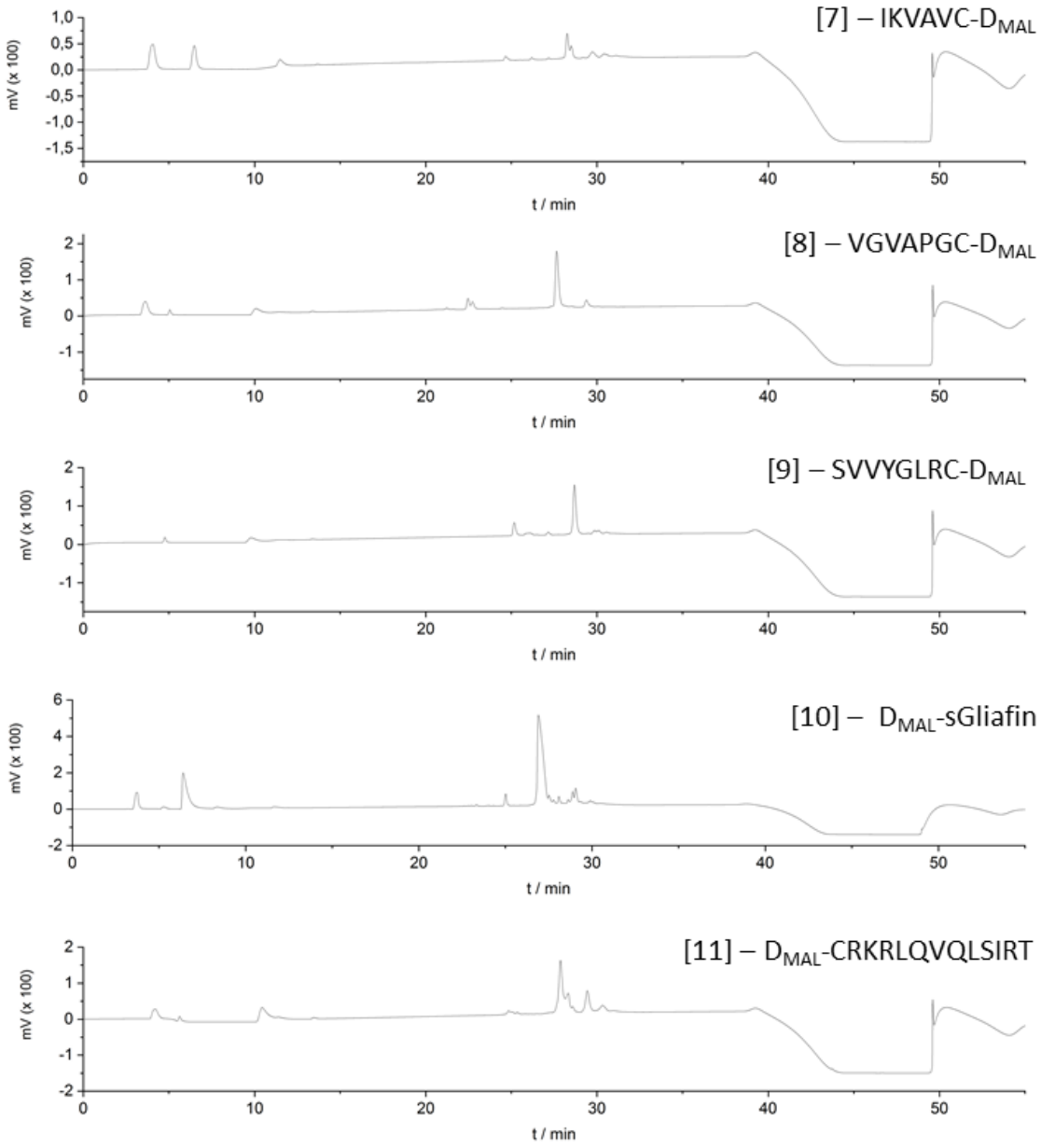

*Figure 62: HPLC chromatograms of the purification of the D_{MAL}-BAPs **[7]** to **[11]**. First batches, self-synthesized BAPs were used in coupling.*

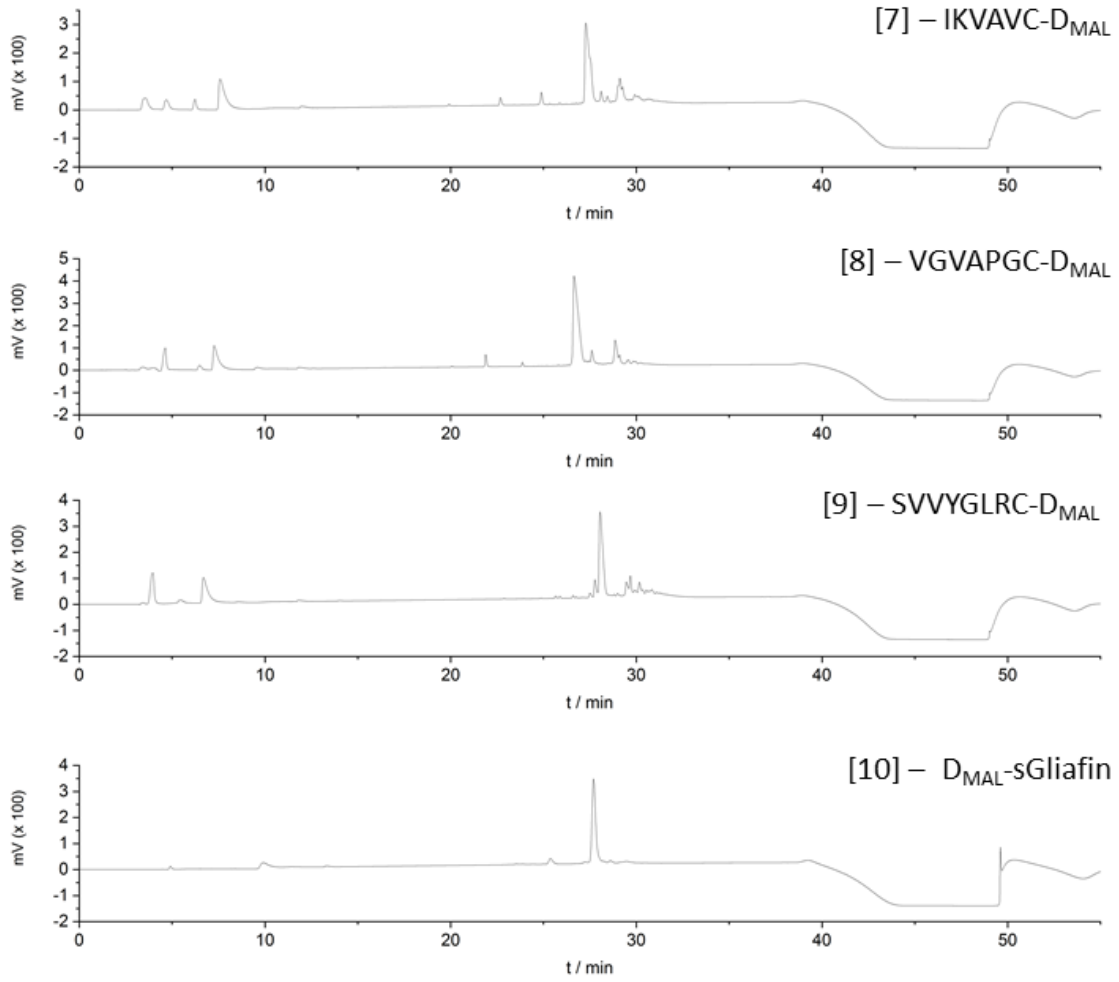

*Figure 63: HPLC chromatograms of the purification of the DMAL-BAPs **[7]** to **[10]**. Second batches, purchased BAPs were used in coupling.*

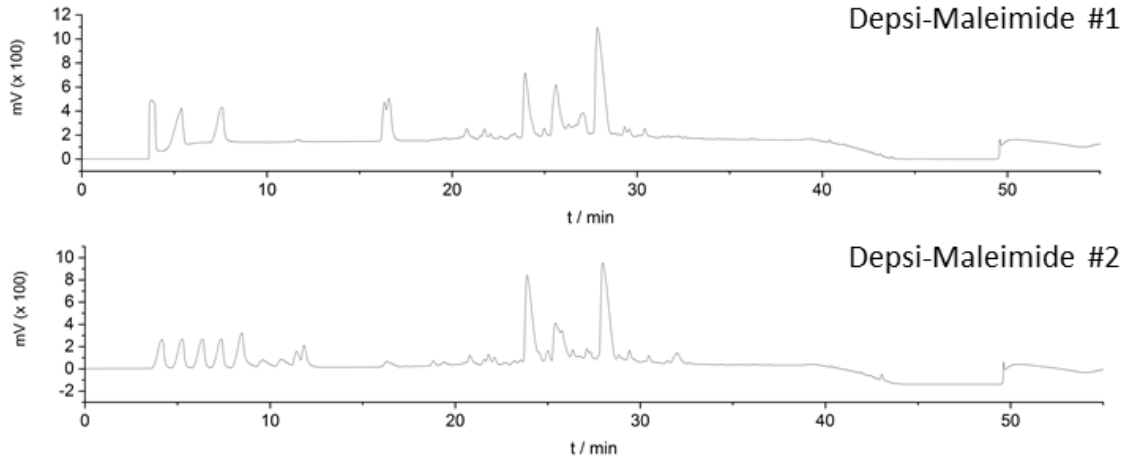

Figure 64: HPLC chromatograms of the purification of Depsi-Maleimide [KIKI(COO-)SQINM]. Top: First batch. Bottom: Second batch.

8.3. Rheology

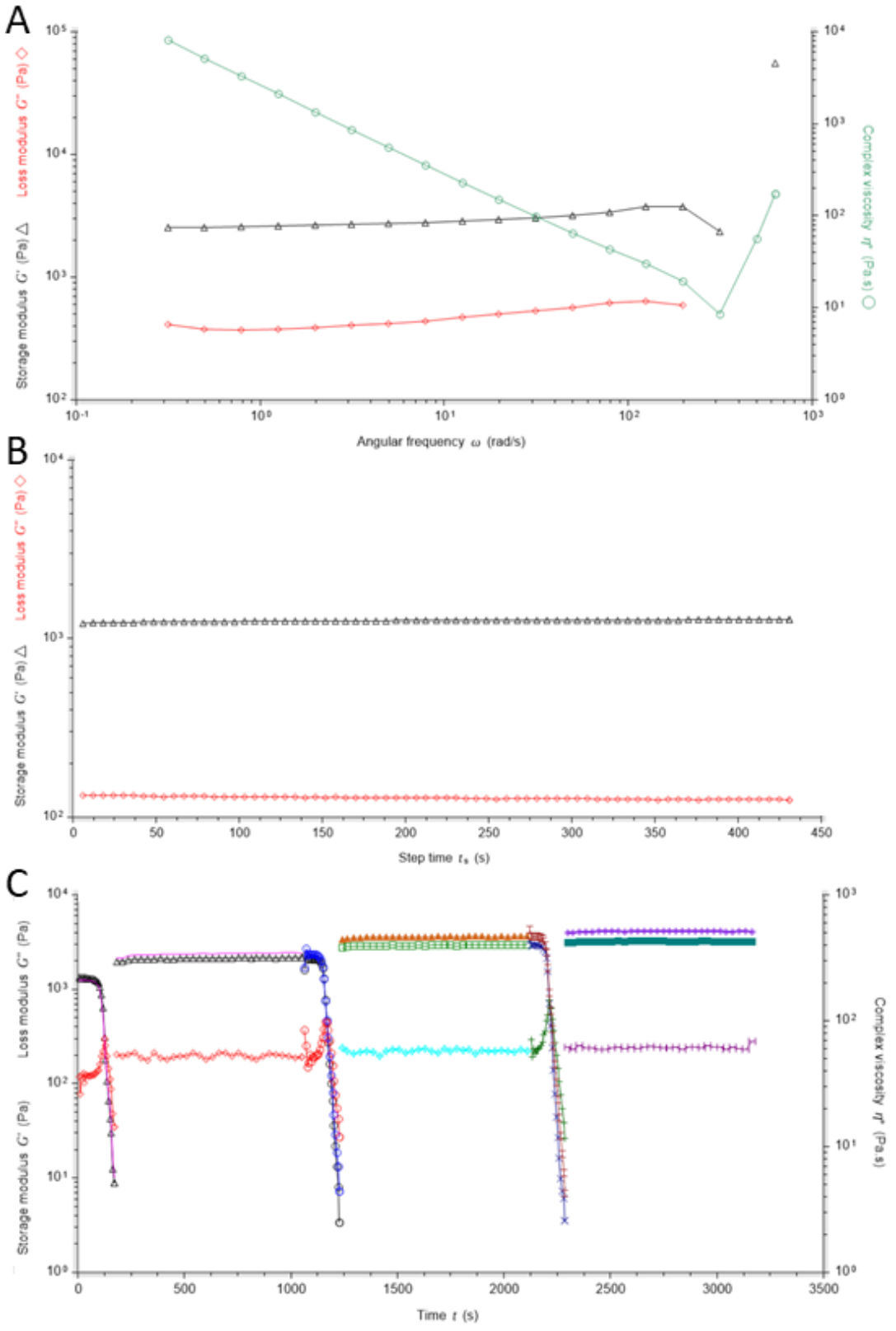

Figure 65: Rheological analyses of dcHSA-PEG(2000)$_{23}$-D-Mal$_{13}$ (batch 2). (A) Frequency sweep. (B) Time sweep. (C) Amplitude sweep.